Computer Simulation Model of Oxygen Transport in Mechanically Ventilated Preterm Infants for the Development and Evaluation of Automated Oxygen Controllers

Technical Medicine
MSc thesis report
Fenne van der Zwaard

Computer Simulation Model of Oxygen Transport in Mechanically Ventilated Preterm Infants for the Development and Evaluation of Automated Oxygen Controllers

by

Fenne van der Zwaard

A thesis in partial fulfilment of the requirements for the joint degree of

Master of Science
in Technical Medicine

at Delft University of Technology, Leiden University and Erasmus University Rotterdam,
to be defended publicly on Thursday May 4, 2023 at 14:15h.

Erasmus MC, Sophia Children's Hospital, Department of Neonatology
Hamilton Medical, Department of Research and New Technology

Student number:	4434978
Master track:	Sensing and Stimulation
Course code:	TM30004 (35 ECTS)
Project duration:	July 2022 - April 2023

Supervisors:	Dr. André Kroon	Erasmus MC
	Dr. Jan M. Zimmermann	Hamilton Medical
	Ir. Tom Goos	Erasmus MC

Thesis committee:	Prof. Dr. Jenny Dankelman	TU Delft, chair
	Prof. Dr. Irwin K.M. Reiss	Erasmus MC
	Dr. Jan M. Zimmermann	Hamilton Medical
	Ir. Tom Goos	Erasmus MC

An electronic version of this thesis is available at `https://repository.tudelft.nl/`.

Preface and Acknowledgements

With this graduation project, my years of studying at the TU Delft, Erasmus University and Leiden University have come to an end. At the start of my studies Clinical Technology I was excited to learn about the technical possibilities for clinical problems. These years of studying have taught me about the great amount of technological developments in the medical field and has made me curious about the developments that will follow. This graduation project is an ideal fit for this studies, as it aimed to translate neonatal respiratory and cardiovascular physiology into a computational model with the goal to enhance oxygen therapy.

I was excited when the opportunity arose to complete my graduation thesis in collaboration with the NICU of the Sophia Children's Hospital and Hamilton Medical. The project suited my wishes well, as it involved a direct connection to the clinic, a challenging subject, and the necessity to construct something. Now, months later, I have learned a lot about the complexity and versatility of the neonatal respiratory system. I was given the opportunity to spend three months in Switzerland to experience working in a mechanical ventilator company, but also to indulge the beautiful mountains and culture Switzerland has to offer. Acknowledging the gaps in the literature and the necessity for assumptions was difficult at times. Even though it has been tough at times, working on this project was also enjoyable I am extremely proud of the final result.

I would like to thank my supervisors, Tom, Jan and André, for their valuable insights, critical view and enthusiasm for the project. Tom, thank you for the initial idea for the project and direction at moments when I lost overview. Jan, thank you for inviting me to Switzerland and with that giving me the opportunity to get an impression of the company Hamilton Medical and Swiss life in the midst of the mountains. You welcomed me warmly and were always available whenever I had questions. André, thank you for introducing me to the NICU of the Sophia Children's Hospital and for the useful medical feedback you provided. In addition, a special acknowledgement must be extended to Peter for his contribution. The insightful discussions we had, and the information you provided regarding computer simulation of the adult respiratory and cardiovascular systems, served as a great foundation for the thesis. I also would like to thank both the departments of Research and New Technology from Hamilton Medical and Neonatology from the Sophia Children's Hospital for making me feel welcome in their teams.

Last but definitely not least, I want to thank my parents, Casper, family and friends for their support and belief in me. They have been there to lend a listening ear and offer invaluable perspective when I needed it most.

Fenne van der Zwaard
Rotterdam, April 2023

Contents

List of Abbreviations

Ao1	first part of the aortic arch
Ao2	second part of the aortic arch
AOC	automated oxygen controller
AOP	apnea of prematurity
BPD	bronchopulmonary dysplasia
bpm	beats per minute
BW	birth weight
C	compliance
CO_2	carbon dioxide
D	diffusion coefficient
dO_2	oxygen delivery
dt_{art}	arterial time delay
dt_{ven}	venous time delay
E	elastance
EHR	electronic health record
FDA	Food and Drug Administration
$FiCO_2$	fraction of inspired carbon dioxide
FiO_2	fraction of inspired oxygen
GA	gestational age
Hb	haemoglobin
HR	heart rate
I:E	inspiratory to expiratory ratio
kPa	kilopascal
MERC	medical ethics review committee
mmHg	millimetre mercury
MOTP	model of oxygen transport in preterm infants
MR	metabolic rate
NICU	neonatal intensive care unit
O_2	oxygen
ODC	oxygen dissociation curve
OFO	open foramen ovale
P	pressure
p	partial pressure
P_{insp}	inspiratory pressure
$P_{support}$	support pressure
P_{vent}	ventilatory pressure

PA	pulmonary arteries
PC	pulmonary capillaries
pCO_2	partial pressure of carbon dioxide
PDA	patent ductus arteriosus
PEEP	positive end-expiratory pressure
PH	pulmonary hypertension
PMA	postmenstrual age
pO_2	partial pressure of oxygen
Q'_{CO}	cardiac output
Q_{tot}	total blood volume
R	resistance
RDS	respiratory distress syndrome
RR	respiratory rate
s1	intrapulmonary shunt fraction
s2	open foramen ovale shunt fraction
s3	ductus arteriosus shunt fraction
SA	systemic arteries
SaO_2	arterial oxygen saturation
SC	systemic capillaries
SD	standard deviation
SO_2	oxygen saturation
SpO_2	peripheral oxygen saturation
V	volume
V/Q	ventilation-perfusion ratio
Vt	tidal volume
xHbF	fraction of fetal haemoglobin

Computer Simulation Model of Oxygen Transport in Mechanically Ventilated Preterm Infants for the Development and Evaluation of Automated Oxygen Controllers

van der Zwaard, F.[1]
Under supervision of: Kroon, A.[2] & Zimmermann, J.M.[3] & Goos, T.[2]

[1] *MSc Technical Medicine, Delft University of Technology; Erasmus MC; Leiden University MC, the Netherlands*
[2] *Department of Neonatology, Sophia Children's Hospital, Erasmus MC, the Netherlands*
[3] *Department of Research and New Technology, Hamilton Medical, Switzerland*

Abstract

Models for oxygen transport in preterm infants can aid the development and evaluation of automated oxygen controllers by providing insight into the FiO_2-SpO_2 response and enabling virtual trials. A computer simulation model of oxygen transport in preterm infants is developed and FiO_2-SpO_2 responses in preterm infants are investigated. The model consists of a respiration and circulation part, interconnected by a pulmonary gas exchange part. Literature-based parameter ranges are provided. The model's ability to reproduce a patient's FiO_2-SpO_2 response, be generalised to different FiO_2-SpO_2 responses, and replicate physiological shunting and apnea scenarios is investigated. FiO_2-SpO_2 responses in preterm infants exhibit high variability and few responses are found stable. The model could be calibrated to specific FiO_2-SpO_2 responses using literature-based parameter ranges and could replicate physiologically expected shunting and apnea scenarios. The calibrated model could not be generalised to another FiO_2-SpO_2 response. The developed model for oxygen transport in preterm infants is a useful, modular, well-documented framework that can be used to develop and evaluate automated oxygen controllers.

1 Introduction

Preterm infants often require respiratory support, including positive pressure and oxygen (O_2) therapy, to maintain adequate oxygenation. The fraction of inspired O_2 (FiO_2) can be adjusted to maintain the peripheral O_2 saturation (SpO_2) in the target range. This typically ranges between 85% - 96%, but varies between different hospitals [1]. The goal is to limit episodes of hypoxia and hyperoxia because these are associated with injuries such as brain injury, bronchopulmonary dysplasia, and retinopathy of prematurity [2–10]. Achieving this goal is challenged by the underdeveloped lungs and respiratory instability of the preterm infant.

Manual adjustment of FiO_2 levels is challenging and time-consuming. Nurses cannot constantly be at the bedside of every patient. Therefore, FiO_2 adjustments are never an instant reaction to a change in SpO_2. Currently, preterm infants on respiratory support spend only approximately half of the time within the SpO_2 target range [11–14].

Automated oxygen controllers (AOCs) have been developed to increase the time spent in the SpO_2 target range. AOCs aim to improve clinical outcomes by reducing periods of hypoxia and hyperoxia. Furthermore, AOCs aim to reduce workload. AOCs continuously compare the measured SpO_2 to the desired SpO_2, adjusting the FiO_2 to minimise the difference [15]. Their fast reaction to a change in SpO_2 leads to an increase in time spent within the target range and a reduction of the workload for nurses [1, 16].

While having advantages over manual O_2 management, AOCs continue to have several drawbacks. For instance, the time delay between a change in FiO_2 and a corresponding change in SpO_2 is highly variable

between and within patients [17]. To mitigate this, many AOCs implement a lock-out period, where the controller waits for a specified duration before another FiO_2 change can be made [18]. Clinical validation studies in critical care settings like the neonatal intensive care unit (NICU) involve a high patient burden. As a result, setting up these studies requires compliance with laws and regulations, a significant amount of paperwork, and long waiting times for the medical ethics review committee (MERC). Comparing the effectiveness of different AOC systems is challenging due to significant variations in the target range, patient populations, and respiratory support modes [18, 19]. One way to minimise these variations is to use a cross-over design study, where subjects receive a sequence of different exposures. However, it may not be feasible to test more than two algorithms at a time due to changes in patients' respiratory condition [18].

Models for oxygen transport in preterm infants (MOTPs) can aid the development and evaluation of AOCs, e.g. by providing insight into the FiO_2-SpO_2 response. MOTPs could optimise the lock-out period by giving more insight in the time delay between a change in FiO_2 and a corresponding change in SpO_2. MOTPs can be used to set up a virtual trial including virtual patients on which the effects of AOCs can be tested. By doing so, MOTPs complement clinical studies and assist in achieving improved outcomes with minimal patient burden [20]. According to the Food and Drug Administration (FDA), computer simulation modelling can increase efficiency, reduce costs, and prevent errors during physiologic closed-loop control technology development [21]. MOTPs can also provide a standardised environment, e.g. for comparison of different AOCs [18, 22].

Computer modelling of the respiratory and circulatory systems is not a new concept. The first (adult) work in this field was published by Gray in 1945 [23]. However, computer modelling of O_2 transport in preterm infants is limited. Creating an MOTP is more complex than creating an O_2 transport model for adults due to the lack of reference data [24, 25]. The development of an MOTP is further complicated by the variability in gestational ages, and corresponding patient weights and developmental phases.

The primary objective of this study is to create an MOTP for the development and evaluation of an AOC. The secondary objective is to use patient data to provide insight into the FiO_2-SpO_2 response in preterm infants. The aim is to investigate the model's ability to reproduce a patient's FiO_2-SpO_2 response, the model's ability to be generalised to different FiO_2-SpO_2 responses, and the model's ability to reproduce physiological shunting and apnea scenarios. Additionally, the model must be designed in a modular fashion, allowing for future enhancements and improvements to be made.

2 Methods

2.1 Development environment

Simulink and Matlab were chosen as the development environments for the MOTP [26, 27]. Simulink was used for model development. Matlab was used for preprocessing the patient data and initialising and postprocessing the simulations executed in Simulink. Numerous publications exist that also used Simulink [25, 28–31]. A model for adult oxygen transport that served as the foundation for the MOTP was also created in Simulink [32]. Simulink is specifically designed for simulation procedures, and includes a visual representation of the functions, submodules and their relations. Simulink gives the user a common structure to which they can add and adjust building components, and, hence, supports the model's demand for modularity. In addition, Simulink enabled the implementation of the MOTP's requirement of real-time adjustable parameters.

2.2 Full model description

AOCs use the measured SpO_2 to alter the administrated FiO_2. Therefore, FiO_2 and SpO_2 were chosen as the input and output data of the full model. For the rest of the report, the full model represents all model elements between the defined input to the output. This includes the patient model (MOTP) and the models of the devices included in the FiO_2-SpO_2 response (mechanical ventilator and SpO_2 sensor) (Figure 2.1). The mechanical

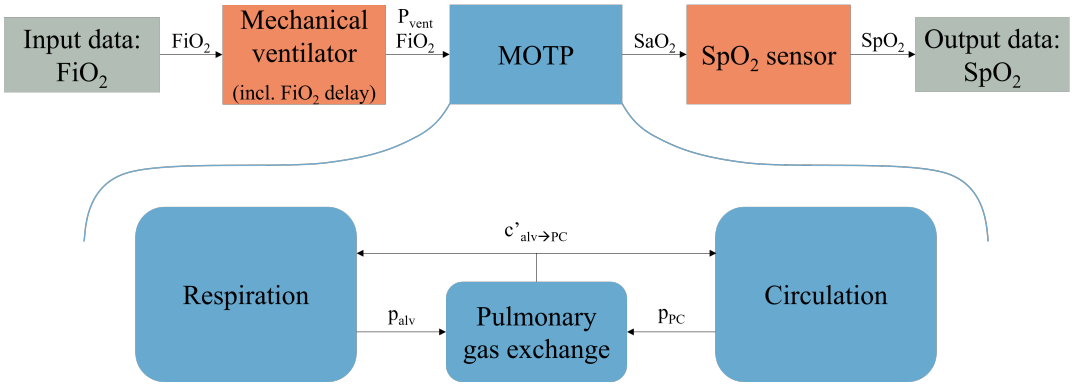

Figure 2.1: Schematic overview of the full oxygen transport model between the input and output data (grey). The full model includes the model for oxygen transport in preterm infants (MOTP) (blue) and the two device models within the FiO_2-SpO_2 response (mechanical ventilator and SpO_2 sensor) (orange). The mechanical ventilator includes the ventilatory pressure (P_{vent}) and an FiO_2 delay block. The MOTP consists of the respiration, pulmonary gas exchange and circulation submodules and produces the arterial O_2 saturation (SaO_2).

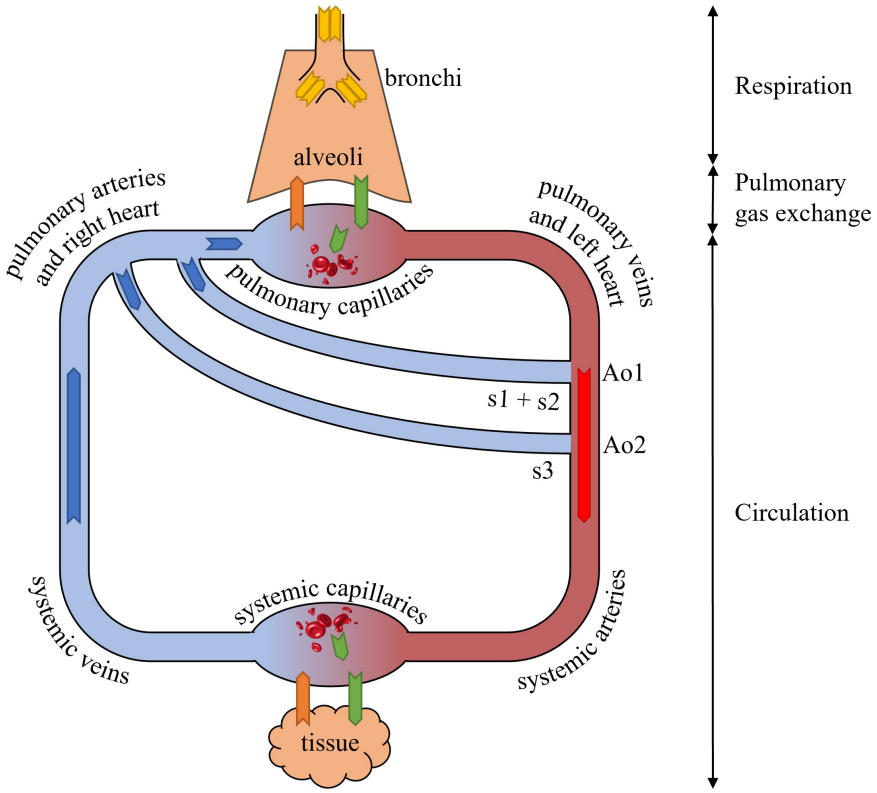

Figure 2.2: A schematic representation of the respiratory and cardiovascular systems of preterm infants. The bronchi are the passageways through which outside air enters and exits the alveoli (yellow arrows). O_2 diffuses from the lungs to the pulmonary capillaries (PC) and into erythrocytes where it binds to haemoglobin (Hb) (green arrows). CO_2 diffuses from the PC to the alveoli (orange arrow). Blood, including the erythrocytes, dissolved O_2 and dissolved CO_2, flows from the PC via the pulmonary vein, the left half of the heart, the first (Ao1) and second (Ao2) part of the aortic arch and the systemic arteries to the systemic capillaries (SC) (red arrow). Ao1 contains pre-ductal blood and Ao2 contains post-ductal blood. The major process in the SC is O_2 dissociation from Hb, wherein O_2 diffuses out of the erythrocytes. This is caused by the O_2 consumption of organs and tissues and combines with CO_2 production. Deoxygenated blood flows from the SC through the systemic veins, the right half of the heart and the pulmonary artery back to the PC, Ao1 and Ao2 (blue arrows). The amount of blood content flowing through each route depends on the three shunting fractions, $s1$, $s2$ and $s3$, which represent shunts caused by intrapulmonary shunting, an open foramen ovale (OFO) and a patent ductus arteriosus (PDA), respectively. Altered from Somhorst [32].

ventilator and SpO_2 sensor were designed to separate the involved devices from the MOTP. The mechanical ventilator system includes the administered ventilatory pressure (P_{vent}) and the FiO_2 time delay block. The MOTP is the true patient model and contains all relations and reactions happening inside the patient's body. The MOTP consists of respiration, pulmonary gas exchange, and circulation submodules (Figure 2.2). The SpO_2 sensor contains the calculation of the SpO_2 based on the arterial O_2 saturation (SaO_2) from the MOTP by the pulse oximeter. A more thorough description of the full model, including equations and references, can be found in Appendix A. The full model will be discussed in the order of the FiO_2-SpO_2 response, from the mechanical ventilator, through the MOTP, to the SpO_2 sensor.

2.2.1 Mechanical ventilator

Preterm infants are often mechanically ventilated. The mechanical ventilator simulates mandatory pressure ventilation based on the support pressure ($P_{support}$), positive end-expiratory pressure ($PEEP$), respiratory rate (RR) and inspiratory to expiratory ratio ($I{:}E$). In addition, the influence of the ventilator circuit, the tubing and humidifier, on the FiO_2 delay was modelled (see Figure 2.1). FiO_2 delay is the time delay from the moment of change in FiO_2 setting on the mechanical ventilator and the moment of the corresponding change in FiO_2 flowing into the patient through the Y-piece. The time delay is derived from the Fabian ventilator (Acutronic Medical Systems AG, Hirzel, Switzerland), the mechanical ventilator used to acquire patient data (see Section 2.5). The time delay was based on measurements and was separately defined for flow rates of 2 to 12 L/min in steps of 1 L/min with a filled and an empty humidifier. A humidifier in the ventilator circuit is connected to a bag of distilled water that constantly replenishes the humidifier to the desired level. The model's option of an empty humidifier was incorporated to address the scenario in which the water container is empty and not promptly replaced, resulting in a humidifier that runs out of water.

2.2.2 Respiration submodule

O_2-rich air enters the lungs through the endotracheal tube of the mechanical ventilator. The respiration submodule of the MOTP consists of two compartments: the bronchi and the alveoli. The bronchi represent the anatomical dead space of the lungs, while the alveoli represent the compartment in which gas exchange occurs.

The respiration submodule consists of the respiratory mechanics and the gas transfer of O_2 and CO_2 within the lungs. The respiratory mechanics have been modelled as an electric circuit analogy. The model includes pressure (P), flow (V'), resistance (R) and compliance (C) as analogies of voltage, current, resistance and capacitance, respectively. Elastance (E) is defined as the inverse of compliance. Given the assumption of perfect mixing, the model does not include any inertial effects [30, 33, 34]. The respiratory mechanics have been modelled as a double-balloon model [32, 35] (Figure 2.3). The inner balloon represents the lung and the outer balloon represents the chest wall. The air starts to flow as a result of a difference in pressure, proportional to Ohm's law. The elasticity of the lung and chest wall exhibits non-linear behaviour [35]. Unfortunately, there is insufficient literature on the characteristics of non-linear elasticity in preterm infants. Consequently, linear elastances were incorporated into the model.

The gas transfer models the transfer of O_2 and CO_2 through the different compartments of the lungs. The fractions of O_2 and CO_2 are described per compartment. The effect of air humidification by the mechanical ventilator on the inspiratory fractions of O_2 and CO_2, FiO_2 and $FiCO_2$, respectively, is implemented.

The respiration submodule eventually combines the alveolar gas fractions and absolute pressure into partial pressures of O_2 and CO_2 in the alveoli. Furthermore, the pressure unit is converted from centimetre water (cmH_2O) to kilopascal (kPa). Pressures in the respiratory system are often expressed in cmH_2O, while pressures in the circulatory system are often expressed in mmHg or kPa. The latter has a more direct relationship to barometric pressure, whereas the former has a more direct relationship to blood pressure. Therefore, the unit kPa was chosen for the circulatory submodule.

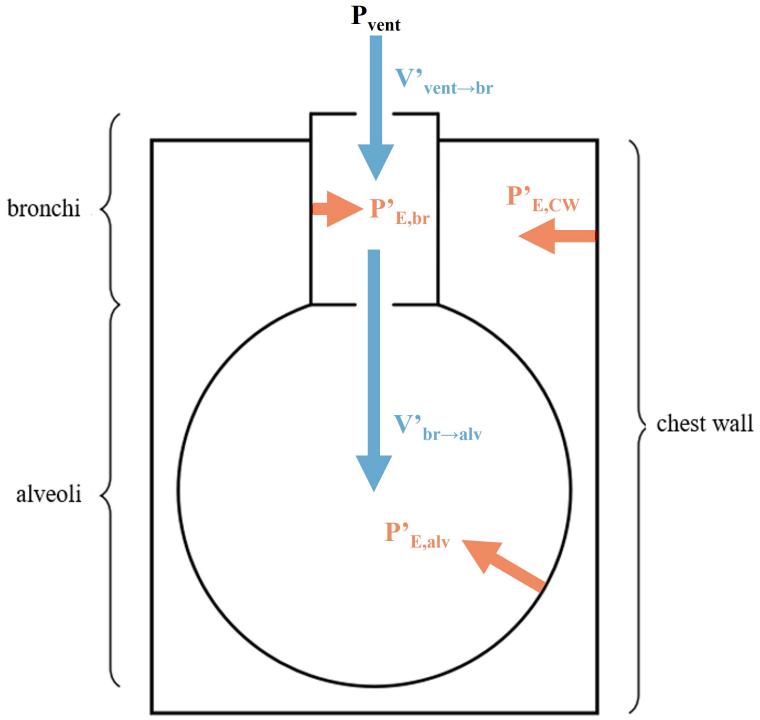

Figure 2.3: The respiratory mechanics can be modelled as a double-balloon model. The inner balloon represents the lung and the outer balloon represents the chest wall (CW). The separation between the alveoli (alv) and bronchi (br) and between the lung and the chest wall are indicated. The blue arrows represent the air currents between the alveoli and bronchi, while the red arrows show the elastic pressures of the tissue [32].

2.2.3 Pulmonary gas exchange submodule

The diffusion of gases over the alveolar membrane is driven by a difference in partial pressures between both sides of the membrane. The diffusion rate between the two compartments is determined by a simplified version of Fick's law [36]. The diffusion coefficient (D) can be influenced by the area and thickness of the diffusion membrane.

2.2.4 Circulation submodule

The circulation submodule describes the transportation of O_2 and CO_2 through the circulatory system. The output of the submodule is the SaO_2. The circulation submodule consists of multiple compartments (Figure 2.2). Diffusion occurs between the alveoli and the pulmonary capillaries (PC). Blood flows from the PC, through the aorta and systemic arteries (SA) to the systemic capillaries (SC). The metabolic rate (MR) affects the gas exchange between the SC and the tissue. Next, blood flows to the pulmonary arteries (PA) and back to the PC. The circulation module is elaborated with the ability to simulate right-to-left shunting. This kind of shunting bypasses the lungs and contributes to the mixture of deoxygenated blood in the arterial system. Intrapulmonary shunting ($s1$), shunting through the OFO ($s2$), and shunting over the PDA ($s3$) were implemented in the model. Blood from $s1$ and $s2$ mixes with non-shunted blood before entering the aorta, while blood from $s3$ enters the aortic arch. Therefore, two mixing compartments between PC and SA were introduced. These compartments are defined as the first and second parts of the aortic branch, Ao1 and Ao2, respectively. The implementation of two separate aortic compartments enables the distinction between pre-ductal and post-ductal SaO_2 values. This is pertinent to the SpO_2 measurements by pulse oximetry, which are pre-ductal for the right hand and post-ductal for both feet. The SpO_2 saturation in the left hand can be influenced by both the pre-ductal and post-ductal SaO_2 [37]. The MOTP allows for selecting pre- or post-ductal SpO_2 sensor placement.

The circulation submodule is described in terms of partial pressures of O_2 and CO_2, pO_2 and pCO_2, respec-

tively. The pO_2 and pCO_2 in the PC and SC change due to diffusion and metabolism, and are based on Henry's law [36]. The pCO_2 is only affected by gas exchange. The pO_2 influences the O_2 buffering, the binding of O_2 to haemoglobin (Hb). O_2 buffering occurs in compartments PC, Ao1, Ao2, and SC. It describes the relationship between the pO_2 and the O_2 saturation (SO_2) and is also known as the oxygen dissociation curve (ODC). The implemented ODC is based on the work of Severinghaus and a simplification of the inverse ODC by Nickalls et al. [38, 39]. The ODC is influenced by multiple factors, e.g. temperature, pH, pCO_2, fraction of fetal Hb (xHbF) and 2,3-diphosphoglycerate. The influence of xHbF on the ODC has been incorporated into the MOTP. The other factors are assumed to be constant.

The pO_2, SO_2 and pCO_2 in the SA and PA compartments are equal to those in Ao2 and SC, respectively, but with a delay. An arterial and venous time delay (dt_{art} and dt_{ven}) have been implemented in the model. The time delays were based on the fraction of blood volume in the arterial and venous system in relation to the cardiac output. SA is reached by application of dt_{art} to the pO_2, pCO_2 and SO_2 in Ao2. PA is reached by application of dt_{ven} to the pO_2, pCO_2 and SO_2 in SC.

The cardiac output was simplified as a multiplication of the heart rate and stroke volume, two parameters defined as constants in the MOTP. Section 2.3 elaborates on how the parameter values were chosen. The computation of O_2 delivery (dO_2) was finally performed. While SaO_2 indicates the proportion of oxygen-bound Hb, it does not provide an accurate measure of the quantity of oxygen that reaches the tissues. On the other hand, dO_2 represents the oxygen amount delivered to the tissues per minute. dO_2 depends on both oxygen content and cardiac output [40].

2.2.5 SpO_2 sensor

An SpO_2 sensor is expected to accurately measure the SaO_2. However, this assumption is not always upheld and SpO_2 obtained by pulse oximetry is limited in accuracy [18, 41, 42]. Therefore, a separate simulation of the SpO_2 sensor has been performed. The SpO_2 sensor simulates the dynamic system of an SpO_2 sensor. This dynamic system was based on data acquired by step tests on the real hardware of a Masimo RD SET Neo sensor. Tests were performed for different SpO_2 averaging times. The measured data on the test bench was fit to a first-order plus deadtime model. This representation of the SpO_2 is fully differentiable and was implemented in the MOTP.

2.3 Neonatal parameters

The full model consists of various formulas in which numerous parameters are involved (Appendix A). The widely-used formulas were tailored using parameters to the particular population that is being modelled. Parameter choice is more challenging in a preterm infant than in an adult, as fewer reference data exist [24, 25]. In addition, accounting for the variation in preterm infants, it is crucial to incorporate weight dependency in the parameter values within the MOTP. There is no "one type of preterm infant". For example, take two newborns, one born with a gestational age (GA) of 24 weeks and a birth weight (BW) of 500 grams, the other with a GA of 36 weeks and a BW of 2750 grams. The weights of these two neonates vary by a factor of 5.5, and their various organ systems are in different fetal developmental stages. Hence, parameters were made weight dependent to account for the variety between preterm infants. Parameters were either fixed or variable [43]. Variable parameters of the model can be further divided into measured or non-measured parameters [20].

2.3.1 Fixed parameters

The fixed parameters were set in the model and automatically calculated for the input weight and Vt. The fixed parameters were based on literature and can be found in Table 2.1. Cardiac output was computed by multiplying the heart rate and stroke volume. One of the range borders was used as cardiac output value when the result of this multiplication exceeded the physiological range of 181 - 317 mL/min [36, 44, 45]. Q_{Ao1}

and Q_{Ao2} were set small enough to avoid a mixing delay, but not too small to prevent a slow model. The binding rate of O_2 to Hb is determined by $k_{O_2\text{-binding}}$. If $k_{O_2\text{-binding}}$ is too low, the equilibrium between pO_2 and SO_2 may not be attained before the blood flow moves to the next compartment. $k_{O_2\text{-binding}}$ was set large enough to avoid binding delay in the model.

2.3.2 Measured variable parameters

The measured variable parameters used in the MOTP were extracted from continuously measured patient data (Section 2.5). Literature-based physiological ranges of the measured variable parameters can be found in Table 2.2. Measured variable parameters can be found in Table 2.2. *I:E* should be set to allow for complete gas inflow and outflow to occur [46]. $P_{support}$ should be sufficient to produce adequate Vt, but the addition of $P_{support}$ and $PEEP$ should not exceed 25 cmH_2O [46]. Fetal Hb has a high affinity for O_2, hence, the O_2-unloading capacity of fetal Hb is lower than that of adult Hb. The Hb concentration depends on the gestational age, is relatively high for recent newborns and decreases over time after birth. The Hb threshold for erythrocyte transfusion differs between different international guidelines. An article comparing different approaches suggests that for patients undergoing invasive ventilation, the transfusion threshold for Hb should be set at 12, 10, and 9 g_{Hb}/dL_{blood} at 1, 2, and 3 weeks of age, respectively [47]. These values are reasonably consistent with the guidelines established by the NICU at the Sophia Children's Hospital, Erasmus MC. xHbF is present in high levels (0.6 - 0.9) at birth and has dropped to less than 0.02 at 6 to 12 months of age [48, 49].

2.3.3 Non-measured variable parameters

The non-measured variable parameters were parameters which could not be extracted from the acquired patient data and hence had to be estimated. The estimated values were aimed to be within the literature-based physiological ranges (Table 2.3). Non-measured variable parameters can be found in Table 2.3. Weight-dependent lung compliance differs for different neonates. Lung compliance is 1.2 $mL/(cmH_2O{\cdot}kg)$ for premature infants and 1.4 $mL/(cmH_2O{\cdot}kg)$ for full-term neonates [50]. Severe bronchopulmonary dysplasia (BPD) decreases lung compliance and may result in a compliance of 1.04 (SD 0.36) $mL/(cmH_2O{\cdot}kg)$ [51, 52]. Therefore, the physiological range of lung compliance was set at 0.68 - 1.4 $mL/(cmH_2O{\cdot}kg)$. Chest wall compliance is high in preterm infants due to weakness of intercostal muscles and flexibility of the ribs [53]. Chest wall compliance is five times greater than lung compliance in preterm infants, and three times greater than lung compliance in term neonates [50].

Literature was inconclusive about respiratory resistance parameters in preterm infants. The model by Morozoff et al. used a total resistance of 25 $(cmH_2O{\cdot}s)/L$ [25]. This value was deemed less appropriate for the current MOTP because the literature on which this number was based concentrated on newborns with a mean weight of 3000g [54, 55]. A different MOTP implemented resistances of 86.7, 180.5, 274, and 355 $(cmH_2O{\cdot}s)/L$ for full-term neonates, preterm infants, extremely preterm infants, and extremely preterm infants with BPD, respectively [51, 52, 56, 57]. Garcia-Fernandez et al. state that neonates have an airway resistance of more than 75 $(cmH_2O{\cdot}s)/L$ and that preterm infants can even have an airway resistance exceeding 150 $(cmH_2O{\cdot}s)/L$ [58]. Based on the provided information, the resistance range was set at 75 - 350 $(cmH_2O{\cdot}s)/L$.

The diffusion coefficient was derived from the measured total lung diffusion coefficient of $2.263{\cdot}10^{-5}$ (SD $6.7016{\cdot}10^{-6}$) $L/(s{\cdot}kPa{\cdot}kg)$ [59]. The lung diffusion coefficient for O_2 was obtained by multiplying this total lung diffusion coefficient with factor 1.23 [60]. The lung diffusion coefficient for CO_2 is 20 times higher than the lung diffusion coefficient for O_2 [61].

No unambiguous literature-based range of shunting fractions could be derived. According to Smith et al., normal total shunt rates are under 8% [62]. However, higher shunt rates can occur in preterm infants due to various causes. $s1$ is caused by intrapulmonary shunting and may result from collapsed alveoli [63]. Right-to-left shunts $s2$ and $s3$ are known to occur when there is high pulmonary pressure and unrestricted communication between the right and left sides of the circulation through an OFO and PDA, respectively.

Table 2.1: The fixed neonatal parameters used in the MOTP.

Parameter	Definition	Value or formula	Unit	Reference
$V_{lung,0}$	Unstressed lung volume	$0.932 \cdot Vt$	mL	[25]
$V_{br,0}$	Unstressed bronchial volume	$0.142 \cdot V_{lung,0}$	mL	[25]
$V_{alv,0}$	Unstressed alveolar volume	$0.858 \cdot V_{lung,0}$	mL	[25]
$V_{CW,0}$	Unstressed chest wall volume	$4.6 \cdot V_{lung,0}$	mL	[32]
R_{br}	Resistance bronchi	$0.8 \cdot R$	$(cmH_2O \cdot s)/L$	[51]
R_{alv}	Resistance alveoli	$0.2 \cdot R$	$(cmH_2O \cdot s)/L$	[51]
C_{br}	Compliance bronchi	$0.085 \cdot C$	$mL/(cmH_2O \cdot kg)$	[25]
C_{alv}	Compliance alveoli	$0.915 \cdot C$	$mL/(cmH_2O \cdot kg)$	[25]
C_{CW}	Compliance chest wall	$5 \cdot C$	$mL/(cmH_2O \cdot kg)$	[50, 51]
Q_{tot}	Total blood volume	80	mL/kg	[44]
Q_{PC}	Blood volume pulmonary capillaries	$0.022 \cdot Q_{tot}$	mL/kg	[36]
Q_{SC}	Blood volume systemic capillaries	$0.06 \cdot Q_{tot}$	mL/kg	[36]
Q_{Ao1}	Blood volume compartment Ao1	0.1	mL	–
Q_{Ao2}	Blood volume compartment Ao2	0.1	mL	–
dQ_{CO}	Cardiac output	$SV \cdot HR$ (181 - 317)	$mL/(min \cdot kg)$	[36, 44, 45]
s	Solubility $[O_2\ CO_2]$	$[2.4 \cdot 10^{-4}\ 5 \cdot 10^{-3}]$	$L_{gas}/(L_{blood} \cdot kPa)$	[64, 65]
$k_{O_2\text{-binding}}$	O_2 binding speed	5	$L_{O_2}/(L_{blood} \cdot kPa \cdot s)$	–
$Hb_{O_2\text{-capacity}}$	Binding capacity of O_2 to haemoglobin	1.34	mL_{O_2}/g_{Hb}	[66]

Table 2.2: The measured variable parameters used in the MOTP.

Parameter	Definition	Range or formula	Unit	Reference
FiO_2	Fraction of inspired oxygen	21 - 100	%	[67]
$P_{support}$	Support pressure	< (25 - PEEP)	cmH_2O	[46]
PEEP	Positive end-expiratory pressure	4 - 8	cmH_2O	[46]
RR	Respiratory rate	30 - 60	1/min	[68]
I:E	Inspiratory to expiratory ratio	–	dimensionless	[46]
Vt	Tidal volume	4 - 7	mL/kg	[46]
HR	Heart rate	100 - 165	bpm	[69]
Hb	Haemoglobin	> 12/10/9 at 1/2/3 weeks of age	g_{Hb}/dL_{blood}	[47]
xHbF	Fraction of fetal haemoglobin	0.6 - 0.9 at birth, declines to 0.02	dimensionless	[48, 49]

Table 2.3: The non-measured variable parameters used in the MOTP.

Parameter	Definition	Range or formula	Unit	Reference
R	Resistance	75 - 350	$(cmH_2O \cdot s)/L$	[51, 58]
C	Compliance	0.68 - 1.4	$mL/(cmH_2O \cdot kg)$	[25, 50–52]
D_{O_2}	Diffusion coefficient of oxygen	$1.13 \cdot 10^{-5}$ - $4.43e \cdot 10^{-5}$	$L/(kPa \cdot s \cdot kg)$	[59, 60]
D_{CO_2}	Diffusion coefficient of carbon dioxide	$2.26 \cdot 10^{-4}$ - $8.86 \cdot 10^{-4}$	$L/(kPa \cdot s \cdot kg)$	[59, 60]
SV	Stroke volume	1.2 - 2.3	mL/kg	[45]
s1	Fraction of intrapulmonary shunt	–	dimensionless	–
s2	Fraction of open foramen ovale shunt	–	dimensionless	–
s3	Fraction of ductus arteriosus	–	dimensionless	–
MR_{O_2}	Metabolic rate of oxygen	5 - 10	$ml/(min \cdot kg)$	[70–73]
MR_{CO_2}	Metabolic rate of carbon dioxide	$0.8 \cdot MR_{O_2}$	$ml/(min \cdot kg)$	[73]

2.4 Study population

Patient data was acquired to select FiO_2-SpO_2 responses for model calibration and to provide insight into the FiO_2-SpO_2 response. The study population consisted of patients admitted to the NICU from the Sophia Children's Hospital, Erasmus MC. This NICU population consists mainly of premature infants and very sick term infants. The patient is often transferred to a peripheral hospital as soon as the patient is stable enough. Because of this NICU population, this study focuses on preterm infants. Patients of various weights were included.

2.5 Data acquisition

Continuous data and data extracted from the electronic health record (EHR) were acquired retrospectively. The measured variable parameters, discussed in Section 2.3.2, were determined using this data. The acquired continuous data contained data recorded by the patient monitor (Dräger M540, Drägerwerk AG Co. KGaA, Lübeck, Germany) and mechanical ventilator (Fabian, Acutronic Medical AG, Hirzel, Switzerland). The Dräger and Fabian files had a sampling frequency of approximately 1 and 2 seconds, respectively. The data were saved in separate files for every day a patient was admitted and the patient monitor or mechanical ventilator was connected. General information was extracted from the EHR for included patients. Extracted data contained: BW, GA and indications for respiratory distress syndrome (RDS), OFO, PDA, and pulmonary hypertension (PH). For model calibration, laboratory values from the arterial blood gas analysis that was the most proximate in time to the corresponding FiO_2 steps were extracted from the EHR (see Section 2.7.1). Extracted data contained: postmenstrual age (PMA) at blood gas, time of blood gas, pH, pCO_2, pO_2, SaO_2, Hb, and xHbF.

2.6 Valid FiO_2 step selection

The acquired data were anonymised and preprocessing steps were executed to select valid FiO_2 steps. Valid FiO_2 steps were desired to be stable and suitable for model calibration. For every detected FiO_2 step, a fragment from 120 seconds before to 120 seconds after the moment of the FiO_2 change was saved. The initial FiO_2, initial SpO_2, FiO_2 step size and percentage FiO_2 step size were documented. The latter is computed by taking the FiO_2 step size as a percentage of the initial FiO_2 value prior to the step. A common time vector was created based on the data file with the highest sampling frequency. Linear interpolation of the data from the other file was performed.

The continuously monitored measured variable parameters were transformed into a mean value before and after the FiO_2 step. The average parameter value before the step was based on data points from the 20 seconds prior to the FiO_2 step. The average parameter value after the step was based on data points from 60 to 80 seconds after the FiO_2 step. The pause of 60 seconds results from the expected time delay of the FiO_2-SpO_2 response. Several AOCs compensate for this delay by delaying the application of a new FiO_2 adjustment by 30 to 180 seconds [18].

The acquired data included inspiratory and expiratory Vt (Vt_{insp} and Vt_{exp}), but no Vt. Therefore, Vt had to be estimated. An endotracheal tube without a cuff is the standard of care in neonatal mechanical ventilation [74]. Leak rates result in a difference between the measured Vt_{insp} and Vt_{exp} and are generally higher with a cuffless tube compared to a cuffed tube [75]. It is not measured whether the leak originates from the inspiratory or expiratory part of the breathing cycle. However, it is acknowledged that leakage is generally more substantial during inspiration, as the inspiratory pressure is higher than the expiratory pressure [76]. Hence, it was assumed that Vt_{exp} makes up a larger portion of the actual Vt than Vt_{insp}. Vt was defined as:

$$Vt = 0.75 \cdot Vt_{exp} + 0.25 \cdot Vt_{insp}. \tag{2.1}$$

As mentioned before, valid FiO_2 steps were desired to be stable and suitable for model calibration. The system had to be as stable as possible to ensure that the change in SpO_2 was solely due to a change in FiO_2, and was not influenced by other confounding factors. In addition, an FiO_2 step had to contain all required data for model calibration. Exclusion criteria were formulated to exclude unstable and unsuitable FiO_2 steps. The number of exclusions due to each criterion was tracked. The exclusion criteria were:

1. The ventilation mode was non-invasive.
2. The step exceeds the maximum step duration of 6 seconds. This criterion was formulated to exclude two consecutive distinct FiO_2 values due to a standby event of the mechanical ventilator.
3. The FiO_2 change is smaller than 3% and is therefore too small. The step needs to be substantial enough to prevent the FiO_2-SpO_2 response from being smaller than the data noise.
4. The FiO_2 changes within 2 minutes before or after the current FiO_2 step. The goal was to make sure that the system was as stable as possible, except for the FiO_2 step. An additional FiO_2 step could influence the FiO_2-SpO_2 response of the target FiO_2 step.
5. The fragment of 4 minutes contains less than 20 data points.
6. The SpO_2, HR or Vt signal was considered unstable. The goal was to eliminate confounding factors to keep only those FiO_2 steps where the SpO_2 response results from a change in FiO_2 and not from other influencing factors. The SpO_2 signal before or after the FiO_2 step was considered unstable if the standard deviation (SD) was bigger than 2%. This corresponded with less than 95% of the data points laying within a range of -4% and +4%. The HR and Vt both affect the SpO_2 by affecting the cardiac output and level of fresh alveolar air, respectively. HR was considered unstable if the difference between the mean HR before and mean HR after the FiO_2 step differed more than 10 beats per minute (bpm). Vt was considered unstable if the difference between mean Vt before and mean Vt after the FiO_2 step differed more than 3 mL.
7. One or more of the mechanical ventilation parameters (FiO_2, SpO_2, P_{insp}, $PEEP$, RR, $I{:}E$, Vt, R, C) is not recorded for more than 20 data points.
8. More than 20% of the data points measured a leak of more than 50%.

The resulting valid FiO_2 steps were visualised into sets according to the initial SpO_2 and FiO_2 values. Initial SpO_2 value categories were: $\leq$ 85%, 86% - 90%, 91% - 95%, and 96% - 100%. Initial FiO_2 value categories were: 21% - 50%, 51% - 75%, and 76% - 100%. This was done because, when given a high FiO_2 compared to a low FiO_2, lungs and oxygenation status are probably in a worse condition. The SpO_2 recordings of the resulting valid FiO_2 steps were normalised by the percentage FiO_2 step size because a larger percentage FiO_2 step size leads to a more significant SpO_2 response.

2.7 Model calibration

Model calibration was performed to answer two questions. First of all, can the model be calibrated to reproduce the measured Vt and SpO_2 of a valid FiO_2 step? Secondly, can a model calibrated to a valid FiO_2 step be used to reproduce the measured Vt and SpO_2 of another valid FiO_2 step? In summary, can the model be calibrated and can a calibrated model be generalised to different FiO_2 steps? Ideally, the model would be calibrated to all valid FiO_2 steps. However, this was not feasible in the time span of this project. Hence, the choice was made to calibrate the model to separate FiO_2 steps.

2.7.1 FiO_2 step selection for model calibration

Two increasing and two decreasing calibration steps were selected for each patient. Selecting two comparable steps was essential to test whether the calibrated model was able to be generalised to another FiO_2 step. Two steps were selected from the subfigure with the maximum number of valid FiO_2 steps in the histogram bin with the highest frequency. If more than two steps remained, the steps were selected of which the moments of an arterial blood gas were closest to the recorded FiO_2 step. If still no decision could be made, the steps with the biggest FiO_2 step size and the biggest difference in SpO_2 before and after the FiO_2 step were selected. Going forward, the two selected increasing or decreasing steps are called measurements 1 and 2.

2.7.2 Calibration procedure

Measurements 1 and 2 were used for calibration of the FiO_2-SpO_2 response of the model. The measured variable parameters of measurement 1 were used in the model. Non-measured variable parameters were calibrated to Vt and SpO_2 of measurement 1. Subsequently, the generalisability of the model was investigated. The measured variable parameters of measurement 2 were used in the model. Model outputs were acquired with the calibrated non-measure variable parameters from measurement 1. This was done to investigate the generalisability of the model. Finally, non-measured variable parameters were calibrated to Vt and SpO_2 of measurement 2. Manual calibration was done separately for the time before and after the FiO_2 change. The model was calibrated for a measurement based on the calibration protocol:

1. R and C were calibrated to reach the measured mean Vt value. Pressure-controlled mechanical ventilation aims to reach the target Vt with as little pressure as possible to prevent ventilator-induced lung injury. Optimal ventilation was assumed, meaning that Vt was reached at the end of the inspiratory phase with an end-inspiratory flow rate of zero [77, 78].

2. D, SV, $s1$, $s2$, $s3$ and MR were calibrated within physiological literature ranges to reach the mean SpO_2 extracted from the patient data. It was intended to have minimal changes in MR before and after the FiO_2 change because MR was assumed not to change within short time ranges. $s2$ was assumed to exist only in the presence of PH and OFO, and $s3$ was assumed to exist only in the presence of PH and PDA.

According to the protocol, all patient SpO_2 measurements were acquired pre-ductally, and the averaging time of the Masimo RD SET Neo sensor was set at 12 seconds. It was presumed that no deviation from the protocol occurred.

2.8 Simulation scenarios

Generally, the underlying cause of a decrease in SpO_2 is uncertain, and adjusting the FiO_2 is merely a way of symptom control. Simulating different scenarios can offer further insight into the potential cause of the SpO_2 decrease. In addition, the MOTP is intended for the development and evaluation of AOCs, in which simulating physiologically common phenomena can be extra beneficial. A shunting and an apnea scenario were simulated to see the ability of the model to reproduce these physiological scenarios. Both scenarios were performed on the calibrated increase measurement 2 model (after the FiO_2 change) of every included patient.

2.8.1 Shunting scenario

Preterm infants often have one or more simultaneous shunts. Shunting events can produce dangerously low SpO_2 levels and are therefore essential in the evaluation and development of AOCs. The shunting scenario was designed to be comparable to that in Morozoff et al., enabling a direct comparison of the results [25]. The shunting scenario was simulated as an increase of the intrapulmonary shunt fraction ($s1$) from 0.10 to 0.55 at a simulation time of 200 seconds and subsequently a decrease back to 0.10 at a simulation time of 400 seconds.

2.8.2 Apnea scenario

Apnea of prematurity (AOP) affects more than 85% of premature newborns [79]. AOP is characterized by breathing pauses of 15 to 20 seconds that are accompanied by desaturations and can lead to hypoxia or even death [79]. Invasive ventilation has a built-in safety net for apneas by taking over the respiratory rate in case of AOP. Hence, this apnea scenario is introduced for potential future AOC testing on a non-invasively ventilated MOTP. Even though it is more logical to apply the apnea scenario on an MOTP including spontaneous breathing, a mechanically ventilated MOTP has minimal impact on most of the model behaviour. The apnea scenario was simulated as a decrease in RR from the original rate to zero at a simulation time of 200 seconds. As a result, $P_{support}$ was no longer applied, but simply a constant $PEEP$ was applied. Subsequently, RR is set back to the original value at a simulation time of 220 seconds. The original RR was set according to the measured RR. The shunt rates were altered to create comparable initial situations for the different patients.

3 Results

3.1 Study population

Two patients of different birth weights have been included. Their characteristics can be found in Table 3.1.

Table 3.1: Patient characteristics.

	Patient 1	Patient 2
Birth weight	750 g	1300 g
Gestational age (weeks+days)	24+0	30+2
Respiratory distress syndrome	yes	yes
Pulmonary hypertension	no	no
Open foramen ovale	yes	yes
Patent ductus arteriosus	yes	no
Days of measurement data	99	17

Table 3.2: Valid FiO_2 step selection for patients 1 and 2. The amount percentage of excluded steps is noted for every exclusion criterion. The valid FiO_2 steps for patients 1 and 2 are divided into increasing and decreasing steps.

	Patient 1		Patient 2	
	Amount (-)	Percentage (%)	Amount (-)	Percentage (%)
Total number of FiO_2 steps	68733	100.00	297	100.00
Unwanted ventilation settings	6481	9.43	0	0.00
Step too long	15	0.02	5	1.68
Step too small	47917	69.71	59	19.87
FiO_2 changes within 2 min before step	12776	18.59	138	46.46
FiO_2 changes within 2 min after step	1202	1.75	56	18.86
Not enough data entries	0	0.00	0	0.00
Unstable SpO_2 before step	46	0.07	1	0.34
Unstable SpO_2 after step	31	0.05	1	0.34
Unstable HR	27	0.04	1	0.34
Unstable Vt	14	0.02	0	0.00
Not enough respiratory mechanics data	149	0.22	18	6.06
Too much leak	2	0.00	0	0.00
Valid FiO_2 steps	73	0.11	18	6.06
Valid increasing FiO_2 steps	13	0.02	8	2.69
Valid decreasing FiO_2 steps	60	0.09	10	3.37

Table 3.3: Step characteristics for all valid increasing and decreasing FiO_2 steps for patients 1 and 2. The mean and standard deviation (SD) values for the initial FiO_2, FiO_2 step size and initial SpO_2 are provided.

	Patient 1		Patient 2	
	Increasing	Decreasing	Increasing	Decreasing
Initial FiO_2 (mean ± SD %)	28.1 ± 6.0	36.6 ± 3.1	23.0 ± 2.4	29.6 ± 1.5
FiO_2 step size (mean ± SD %)	5.3 ± 3.1	5.3 ± 3.1	4.6 ± 1.9	4.3 ± 1.5
Initial SpO_2 (mean ± SD %)	81 ± 4.9	98.1 ± 2.2	86.1 ± 2.0	97.2 ± 1.7

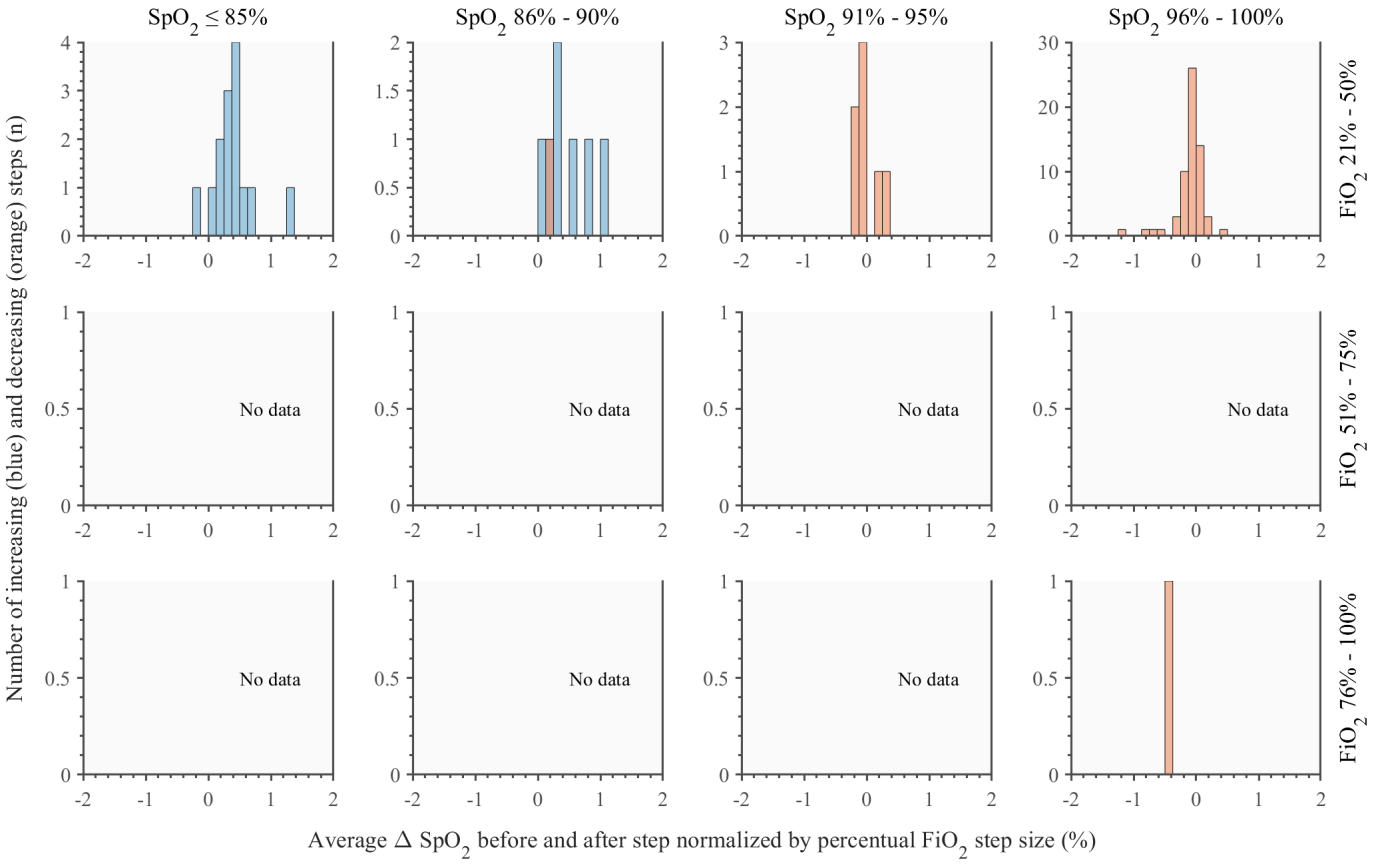

Figure 3.1: Distribution of Δ SpO_2 for all valid increasing and decreasing FiO_2 steps of patient 1. Δ SpO_2 is the difference between the average SpO_2 before and after the FiO_2 change, normalised by the percentage FiO_2 step size (the FiO_2 step size expressed as percentage of the initial FiO_2 value before the FiO_2 change). The steps have been categorised based on initial SpO_2 and FiO_2 values at the moment of the FiO_2 change.

3.2 Valid FiO_2 step selection

The selection of valid FiO_2 steps according to Section 2.6 and their characteristics are summarised in Table 3.2 and Table 3.3, respectively. Patients 1 and 2 experienced 68733 and 297 FiO_2 changes during 99 and 17 days of data acquisition, respectively. After selection, patient 1 had a total of 13 increasing and 60 decreasing valid FiO_2 steps. Patient 2 had a total of 8 increasing and 10 decreasing valid FiO_2 steps.

Figure 3.1 shows twelve subfigures with histograms of the SpO_2 change during the step, normalised by the percentual FiO_2 step size, of patient 1. The steps were categorised based on their initial SpO_2 and FiO_2 values. Each of the subfigures displays a histogram with a single peak that resembles a normal distribution. The histograms of the increasing steps are shifted to the right, indicating a positive SpO_2 change resulting from the increasing FiO_2 step. The decreasing histograms are shifted to the left, indicating a negative SpO_2 change due to the decreasing FiO_2 step. However, not all increasing and decreasing FiO_2 steps resulted in a respectively increasing and decreasing SpO_2 change. Figures of the SpO_2 responses of both patients and the histograms of the normalised SpO_2 change during the step of patient 2 can be found in Appendix B.

Table 3.4: The characteristics of the used measurements for model calibration, including blood gas and ventilation characteristics.

		Patient 1				Patient 2			
		Increase		Decrease		Increase		Decrease	
	Unit	M1	M2	M1	M2	M1	M2	M1	M2
PMA	W+D	24+5	25+0	24+4	24+4	31+5	31+6	31+5	31+5
Time FiO_2 change	hh:mm:ss	00:59:49	19:32:17	17:12:40	20:05:50	11:48:26	10:47:51	04:44:24	07:04:53
Time bloodgas	hh:mm:ss	08:24:00	09:45:00	20:00:00	20:00:00	12:47:00	10:24:00	06:01:00	06:01:00
pH	–	7.05	7.15	7.07	7.07	7.32	7.39	7.26	7.26
SaO_2	%	92	85	88	88	90	95	93	93
pO_2	kPa	7.3	5.6	6.1	6.1	6	5.1	5.1	5.1
pCO_2	kPa	6.7	6.2	6.1	6.1	6	7.7	7.6	7.6
Ventilation mode	–	SIPPV	SIPPV	SIPPV	SIPPV	SIPPV	SIPPV	SIPPV	SIPPV

M1: measurement 1, M2: measurement 2, PMA: postmenstrual age, W+D: weeks + days.

Table 3.5: The measured variable parameters of the used measurements for model calibration of patient 1. Parameters above the grey line are input parameters for the MOTP. Hb and xHbF are parameters measured in the blood gas of the patient and do not differ before and after the FiO_2 change. Parameters under the grey line are measured patient variables and used to check the model output. The total Vt is used as an input parameter for the MOTP and the relative Vt per kg is used to check the model output.

		Increase				Decrease			
		M1		M2		M1		M2	
Parameter	Unit	Before	After	Before	After	Before	After	Before	After
FiO_2	%	21	24	32	37	30	21	28	21
$P_{support}$	cmH_2O	12	12	12	12	12	12	12	12
PEEP	cmH_2O	6	6	6	6	6	6	6	6
RR	1/min	62	61	71	73	67	72	64	63
I:E	–	1:2.3	1:2.3	1:2.3	1:2.3	1:2.3	1:2.3	1:2.3	1:2.3
Vt	mL	6.4	4.2	5.7	5.1	4.6	4.9	4.8	6.5
HR	bpm	164	156	157	158	156	156	146	151
Hb	g/dL	12.1	12.1	11.6	11.6	12.4	12.4	12.4	12.4
xHbF	–	0.53	0.53	0.42	0.42	0.55	0.55	0.55	0.55
SpO_2	%	81.3	87.8	74.3	80.8	100	96.5	100	98.3
Vt	mL/kg	8.5	5.6	7.6	6.8	6.1	6.5	6.4	8.7
C_{Fabian}	$mL/(cmH_2O \cdot kg)$	0.61	0.49	0.53	0.45	0.40	0.44	0.40	0.61
R_{Fabian}	$cmH_2O \cdot s/L$	382	452	391	422	355	355	390	384
Leak	%	0	0	0	0	0	0	0	0

M1: measurement 1, M2: measurement 2.

3.3 Model calibration

3.3.1 FiO_2 step selection for model calibration

Per patient, two increasing and two decreasing FiO_2 steps were used for model calibration according to Section 2.7.1. The two selected increasing or decreasing steps are called measurements 1 and 2. Increasing measurements for patient 1 were selected from the subfigure $SpO_2 \leq 85\%$ with FiO_2 21% - 50%. Decreasing measurements for patient 1 were selected from the subfigure SpO_2 96% - 100% with FiO_2 21% - 50%. Increasing measurements for patient 2 were selected from the subfigure SpO_2 86% - 90% with FiO_2 21% - 50%. Decreasing measurements for patient 2 were selected from the subfigure SpO_2 96% - 100% with FiO_2 21% - 50%. Characteristics of the measurements selected for model evaluation are summarised in Table 3.4.

3.3.2 Calibration

Table 3.5 shows the measured variable parameters of patient 1. The inspiratory and expiratory flows were not measured, so the FiO_2 delay block was set as a filled humidifier with a flow of 8 L/min. Table 3.6 contains the non-measured variable parameters which were manually calibrated for measurements 1 and 2. Note that uncalibrated measurement 2 used non-measured variable parameters from measurement 1. Model outputs of patients 1 and 2 are summarised in Tables 3.7 and 3.8. The calibrated measurements were employed successfully to achieve low errors in Vt and SpO_2 (Figures 3.3 and 3.4). The maximum absolute error of the calibrated models for Vt was 0.6 mL/kg for patient 1 and 0.1 mL/kg for patient 2. The maximum absolute error of the calibrated models for SpO_2 was 2% for patient 1 and 0.2% for patient 2. For both patients, the calibrated measurement 2 resulted in lower errors for Vt and SpO_2 when compared to the uncalibrated measurement 2. Figures 3.2 and 3.3 also illustrate this observation.

The model outputs for SaO_2, pO_2, and pCO_2 (see Table 3.7 exhibit substantial differences when compared to the corresponding blood gas values in Table 3.4. Additionally, it is worth noting that the SaO_2 values obtained from blood gas measurements did not consistently match with the measured SpO_2 values (Table 3.5). Moreover, significant discrepancies were occasionally observed between the time of FiO_2 change and the time of blood gas measurements.

The resistance and compliance of the respiratory system, including the endotracheal tube, were measured by the Fabian ventilator (Table 3.5). The measured R and C were in all cases respectively larger and smaller than the non-measured variable parameters R and C in the calibrated MOTP (Table 3.6).

In the process of calibrating increasing measurement 1 of patient 1, an alternative calibration order was employed. Specifically, the changes in cardiac output were initially made by adjusting SV. This approach was undertaken to investigate whether the model could be calibrated to the desired SpO_2 value using different parameter changes. Manipulating SV alone from 1.2 to 2.0 mL/kg resulted in an increase in SpO_2 levels from 81.3% to 86.8%. A minor alteration of $s1$ of 0.35 to 0.31 was then required to achieve the desired saturation level of 87.8% (Table 3.6).

The upper figures in Figures 3.2 to 3.4 reveal the difference between the inconstant measured SpO_2 signal of the patient and the average SpO_2 values before and after the FiO_2 change. Depending on the specific time span and moment of averaging, the average SpO_2 will differ. The lower figures show the need for the model to slowly stabilise. Stabilisation of the model appears in an oscillatory manner at the beginning of the simulation, and results from the incorporated time delays in the model's circulation submodule. In addition, the SaO_2 output of the MOTP showed oscillatory behaviour, consistent with the breathing frequency Figure C.11. The model's SaO_2 signal was downsampled with a factor of 100 to minimise the oscillatory motion and facilitate better visualisation in the results section. Figures 3.2 to 3.4 also show a time delay between the moment of the FiO_2 change and the reaction of the modelled SaO_2 and SpO_2. This section shows the most essential results. Additional results can be found in Appendix C.

Table 3.6: The non-measured variable parameters of the used measurements for model calibration of patient 1. These parameters were used to calibrate the MOTP to a specific FiO_2 change.

		Increase				Decrease			
		M1		M2		M1		M2	
Parameter	Unit	Before	After	Before	After	Before	After	Before	After
R	$cmH_2O{\cdot}s/L$	150	190	150	150	150	150	150	150
C	$mL/(cmH_2O{\cdot}kg)$	0.90	0.60	0.75	0.70	0.63	0.66	0.63	0.87
D_{O_2}	$L/(kPa{\cdot}s{\cdot}kg)$	$1.67{\cdot}10^{-5}$	$1.67{\cdot}10^{-5}$	$1.67{\cdot}10^{-5}$	$1.67{\cdot}10^{-5}$	$2.78{\cdot}10^{-5}$	$2.78{\cdot}10^{-5}$	$3.00{\cdot}10^{-5}$	$3.50{\cdot}10^{-5}$
D_{CO_2}	$L/(kPa{\cdot}s{\cdot}kg)$	$3.34{\cdot}10^{-4}$	$3.34{\cdot}10^{-4}$	$3.34{\cdot}10^{-4}$	$3.34{\cdot}10^{-4}$	$5.56{\cdot}10^{-4}$	$5.56{\cdot}10^{-4}$	$6.00{\cdot}10^{-4}$	$7.00{\cdot}10^{-4}$
SV	mL/kg	1.2	2.0	1.5	1.7	1.9	1.9	1.9	1.9
s1	–	0.35	0.31	0.55	0.51	0	0	0	0
s2	–	0	0	0	0	0	0	0	0
s3	–	0	0	0	0	0	0	0	0
MR_{O_2}	$mL/(min{\cdot}kg)$	9.0	9.0	9.5	9.5	8.0	8.0	8.0	7.5
MR_{CO_2}	$mL/(min{\cdot}kg)$	7.2	7.2	7.6	7.6	6.4	6.4	6.4	6.0

M1: measurement 1, M2: measurement 2.

Table 3.7: The model outputs of increasing and decreasing measurements 1 and 2 of patient 1.

		Increase						Decrease					
		M1		M2*		M2		M1		M2*		M2	
Output	Unit	Before	After	Before	After	Before	After	Before	After	Before	After	Before	After
Vt	mL/kg	9.1	5.9	8.8	6.0	7.5	6.9	6.1	6.7	6.3	6.7	6.3	8.5
ϵ Vt	mL/kg	0.6	0.3	1.2	0.8	0.1	0.1	0	0.2	-0.1	-2.0	-0.1	-0.2
SpO_2	%	81.3	87.8	84.9	91.3	74.3	80.6	98.0	96.4	98.0	96.8	98.0	97.6
ϵ SpO_2	%	0	0	10.6	10.8	0	-0.2	-2.0	-0.1	-2.0	-1.5	-2.0	-0.7
SaO_2	%	78.9	87.8	84.8	93.4	69.6	78.4	99.4	96.8	99.3	97.9	99.4	98.7
pO_2	kPa	5.0	6.3	5.9	8.2	4.3	5.1	18.2	10.3	17.8	11.9	17.6	14.0
pCO_2	kPa	6.7	6.5	7.3	7.0	11.8	10.3	3.6	3.8	3.5	3.3	3.5	2.4
dO_2	$mL/(min{\cdot}kg)$	25.6	45.3	25.2	46.8	25.9	33.3	50.8	96.0	47.3	47.7	47.3	48.4

M1: measurement 1, M2: measurement 2, ϵ: $parameter_{model} - parameter_{patient}$.
* uncalibrated model.

Table 3.8: The model outputs of increasing and decreasing measurements 1 and 2 of patient 2.

		Increase						Decrease					
		M1		M2*		M2		M1		M2*		M2	
Output	Unit	Before	After	Before	After	Before	After	Before	After	Before	After	Before	After
Vt	mL/kg	5.8	5.7	5.2	7.0	7.7	8.3	6.4	6.9	6.4	6.8	5.9	5.7
ϵ Vt	mL/kg	0	0.1	-2.6	-1.3	-0.1	0	0.1	0	0.5	1.0	0	-0.1
SpO_2	%	88.5	93.1	79.7	92.6	85.9	91.1	97.8	96.1	97.8	96.1	97.2	95.1
ϵ SpO_2	%	-0.1	0	-6.3	-1.6	-0.1	0.1	-0.2	0.1	0.5	1.0	-0.1	0
SaO_2	%	88.1	93.8	75.7	93.4	84.6	91.9	99.1	96.6	99.2	97.0	98.4	95.6
pO_2	kPa	6.3	8.2	4.7	8.0	5.8	7.4	16	10.1	16.5	10.7	13.2	9.3
pCO_2	kPa	6.2	5.4	7.8	5.7	5.9	5.7	3.5	3.4	3.4	3.1	4.0	3.9
dO_2	$mL/(min{\cdot}kg)$	44.2	46.6	42.8	52.9	47.9	52.1	47.8	46.4	48.0	46.5	47.4	45.8

M1: measurement 1, M2: measurement 2, ϵ: $parameter_{model} - parameter_{patient}$.
* uncalibrated model.

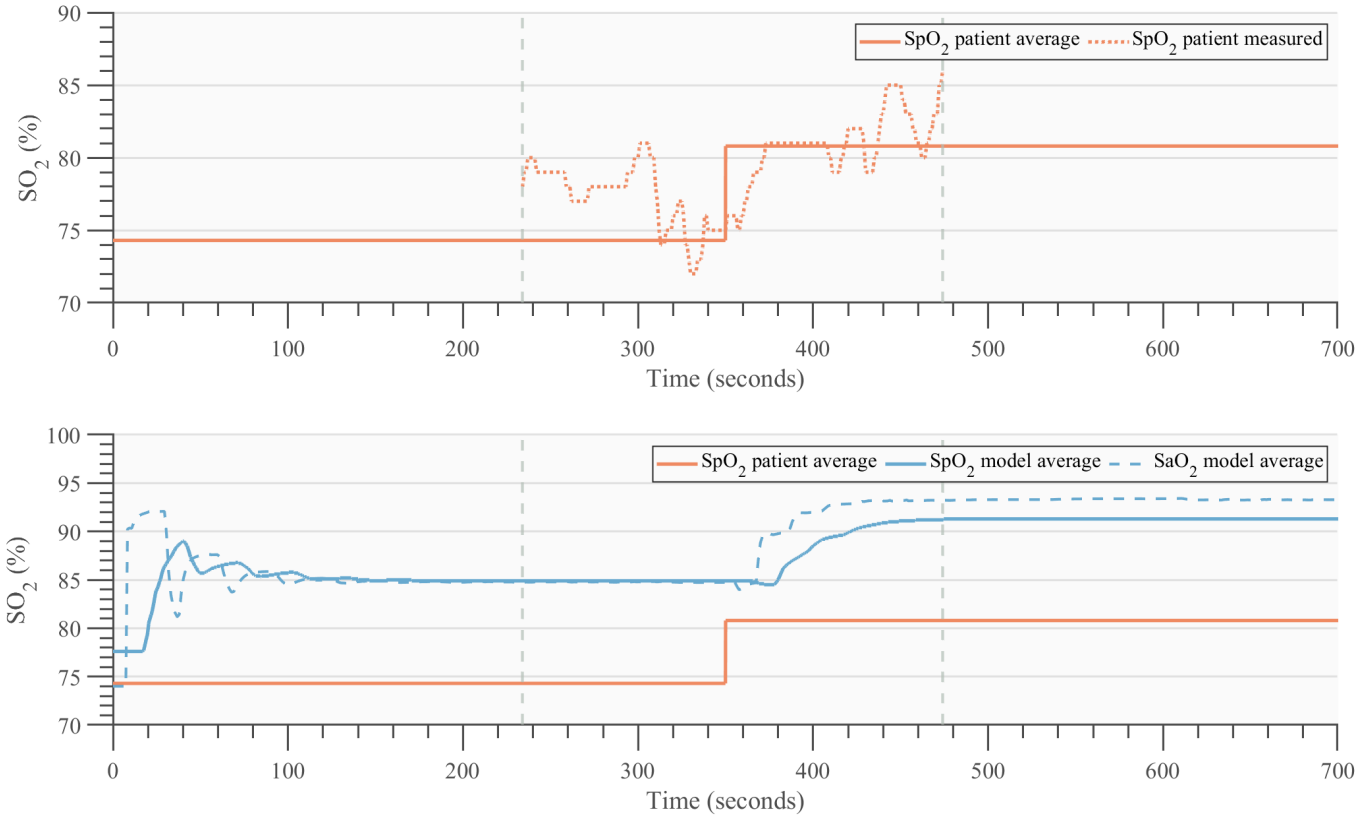

Figure 3.2: True and modelled FiO_2-SpO_2 response of uncalibrated increase measurement 2 of patient 1. Measured variable parameters are set for increasing measurement 2 of patient 1. Non-measured variable parameters are set for increasing measurement 1 of patient 1. The FiO_2 changed at time = 350 seconds from 32% to 37%. The upper figure shows the continuous SpO_2 signal extracted from the measured patient data from patient 1. The measured SpO_2 signal was available from 120 seconds before to 120 seconds after the FiO_2 (grey dashed lines). Based on the signal 20 seconds before and 60 to 80 seconds after the FiO_2, the average SpO_2 signal before and after the FiO_2 change was calculated. This average SpO_2 signal was modelled with the complete model. The lower figure shows the SaO_2 output of the MOTP, the SpO_2 output of the SpO_2 sensor system and the average SpO_2 signal of the patient. The sample rate of SaO_2 signal is decreased by a factor of 100 for reduction of the oscillations and clear visualisation.

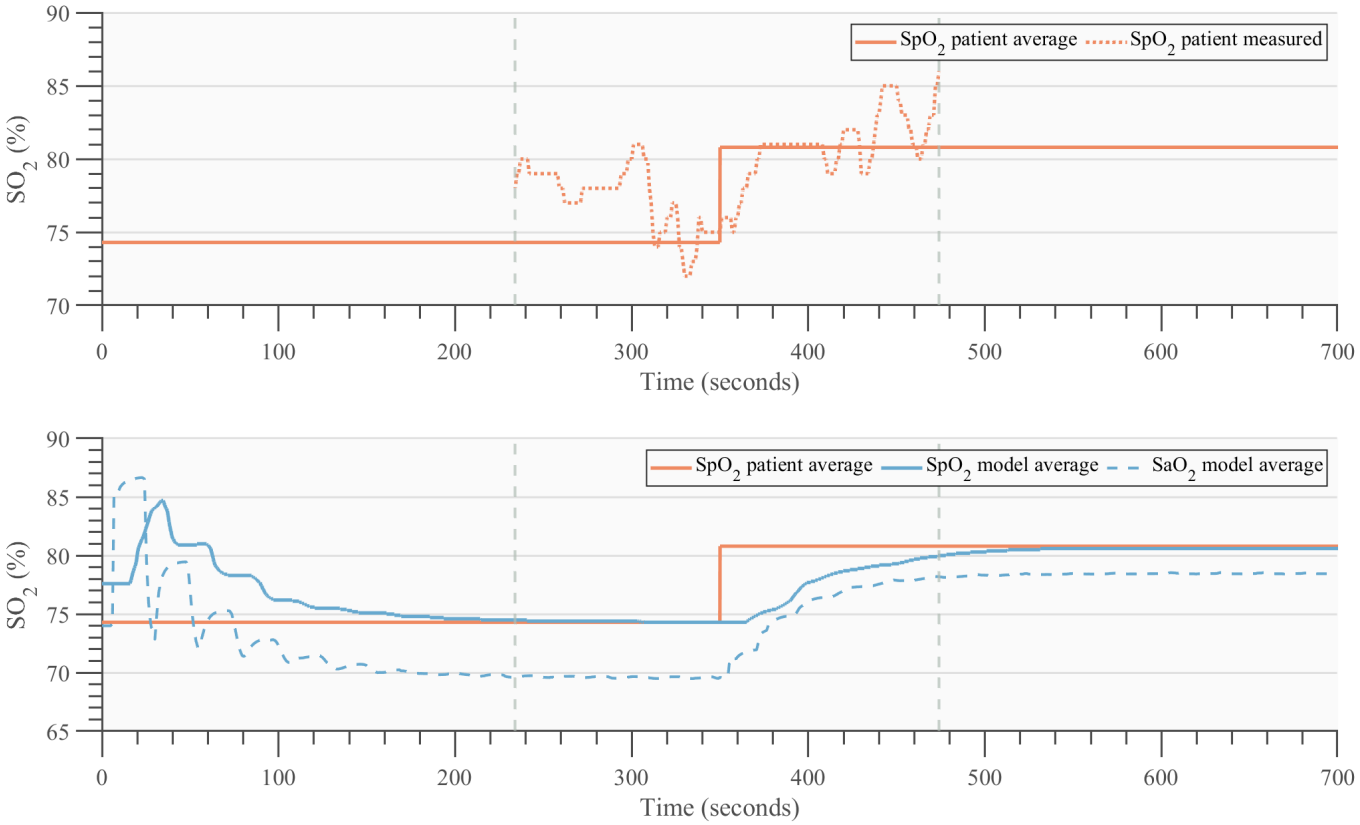

Figure 3.3: True and modelled FiO_2-SpO_2 response of calibrated increasing measurement 2 of patient 1. Measured and non-measured variable parameters are set for increasing measurement 2 of patient 1. The FiO_2 changed at time = 350 seconds from 32% to 37%. The upper figure shows the continuous SpO_2 signal extracted from the measured patient data from patient 1. The measured SpO_2 signal was available from 120 seconds before to 120 seconds after the FiO_2 change (grey dashed lines). Based on the signal 20 seconds before and 60 to 80 seconds after the FiO_2 change, the average SpO_2 signal before and after the FiO_2 change was calculated. This average SpO_2 signal was modelled with the complete model. The lower figure shows the SaO_2 output of the MOTP, the SpO_2 output of the SpO_2 sensor system and the average SpO_2 signal of the patient. The sample rate of SaO_2 signal is decreased by a factor of 100 for reduction of the oscillations and clear visualisation.

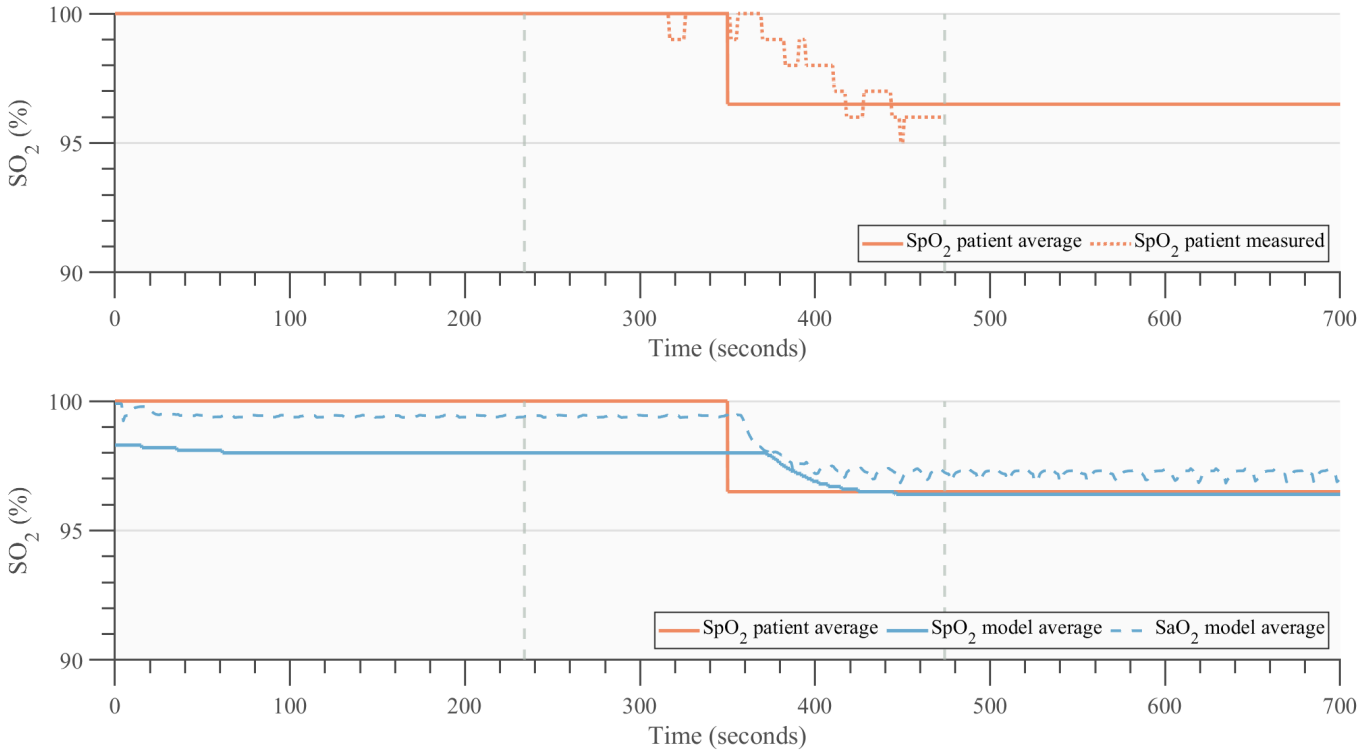

Figure 3.4: True and modelled FiO_2-SpO_2 response of calibrated decreasing measurement 1 of patient 1. Measured and non-measured variable parameters are set for decreasing measurement 1 of patient 1. The FiO_2 changed at time = 350 seconds from 30% to 21%. The upper figure shows the continuous SpO_2 signal extracted from the measured patient data from patient 1. The measured SpO_2 signal was available from 120 seconds before to 120 seconds after the FiO_2 change (grey dashed lines). Based on the signal 20 seconds before and 60 to 80 seconds after the FiO_2 change, the average SpO_2 signal before and after the FiO_2 change was calculated. This average SpO_2 signal was modelled with the complete model. The lower figure shows the SaO_2 output of the MOTP, the SpO_2 output of the SpO_2 sensor system and the average SpO_2 signal of the patient. The sample rate of SaO_2 signal is decreased by a factor of 100 for reduction of the oscillations and clear visualisation.

3.4 Simulation scenarios

Figures 3.5 to 3.8 demonstrate the effect of the shunting and apnea simulation scenarios on the SaO_2 modelled by the MOTP. The first 200 seconds in each graph represent the stabilisation of the model and were removed.

3.4.1 Shunting scenario

The model's reaction of both patients to the shunting scenario was nonlinear and can be found in Figures 3.5 and 3.7. Patient 1 had an SaO_2 desaturation size of 24.0%, with a desaturation and saturation time constant of 30.8 and 13.3 seconds, respectively. Patient 2 had an SaO_2 desaturation size of 18.3%, with a desaturation and saturation time constant of 32.7 and 33.2 seconds, respectively. The ratio of saturation to desaturation for patients 1 and 2 was 0.43 and 1.02, respectively. The time constant is the time it takes for the system's response to reach 63% of its final response value. In addition, the transients were not smooth due to the effect of the time delays in the circulation subsystem. A moving average was applied to the signal to smooth out the signal. In addition, no time delay can be seen after the changes in the shunting fraction. Therefore, the desaturation and saturation time constants were derived from the SaO_2 signal subjected to a moving mean procedure. Finally, the lower weight of patient 1 resulted in lower Q_{tot}, Vt and CO compared to patient 2.

3.4.2 Apnea scenario

The model's reaction of both patients to the apnea scenario can be found in Figures 3.6 and 3.8. The SaO_2 desaturation due to the apnea simulation scenario was 4.3% in patient 1, and 9.5% in patient 2. Patients 1 and 2 had an FiO_2 input value of 37% and 25%, respectively. The FiO_2 influenced the alveolar pO_2. During the apnea simulation, the alveolar pO_2 decreased from 32.0 to 17.1 kPa in patient 1 and from 21.3 to 10.8 kPa in patient 2. Similar to the shunting scenario, the results of the apnea scenario showed non-smooth transients due to the impact of time delays in the circulation subsystem. As discussed in Section 2.8.2, shunt rates were altered to create comparable initial situations for both patients. This resulted in values for s1, s2 and s3 of 0.2, 0, and 0, respectively, in both patients.

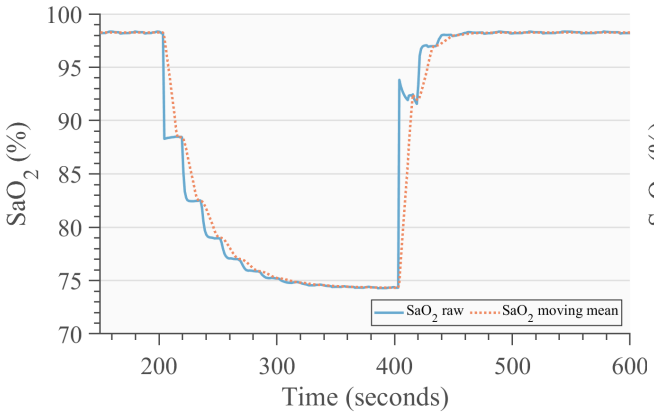

Figure 3.5: Shunting scenario of patient 1. The shunt fraction instantly increased from 0.10 to 0.55 at a simulation time of 200 seconds and instantly decreased back to 0.10 at a simulation time of 400 seconds. A moving mean was utilized on the SaO_2 signal.

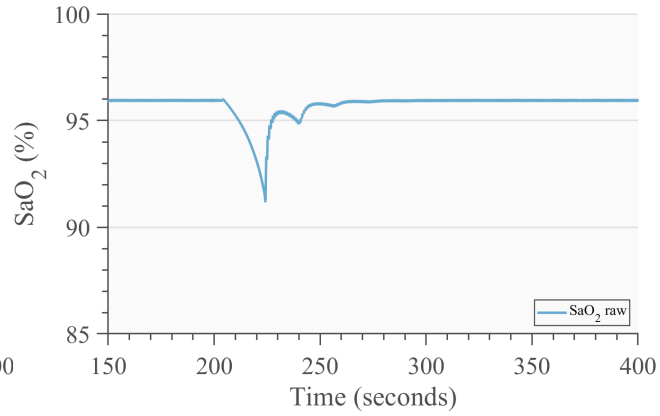

Figure 3.6: Apnea scenario of patient 1. The respiratory rate instantly decreased from the original rate to zero at a simulation time of 200 seconds and instantly increased back to the original rate at a simulation time of 220 seconds.

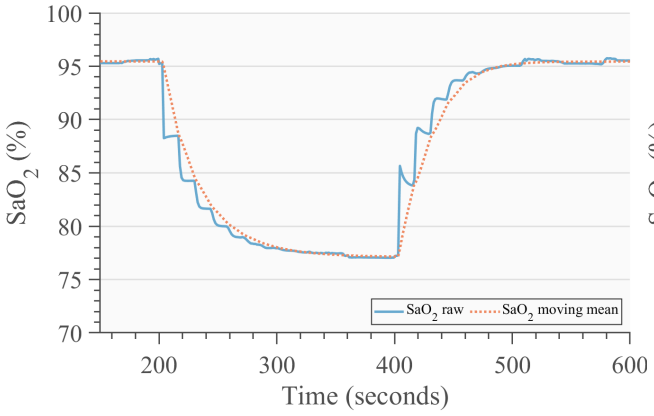

Figure 3.7: Shunting scenario of patient 2. The shunt fraction instantly increased from 0.10 to 0.55 at a simulation time of 200 seconds and instantly decreased back to 0.10 at a simulation time of 400 seconds. A moving mean was utilized on the SaO_2 signal.

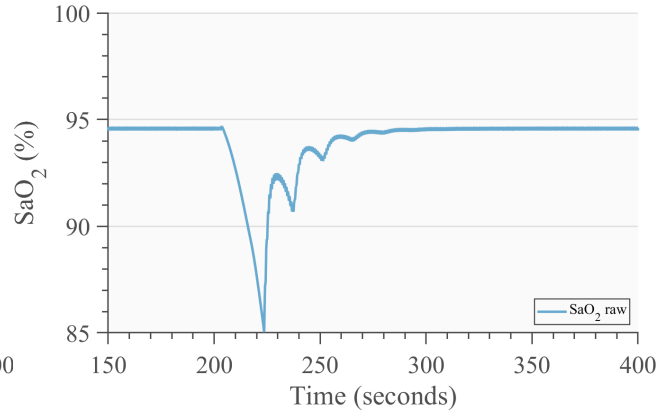

Figure 3.8: Apnea scenario of patient 2. The respiratory rate instantly decreased from the original rate to zero at a simulation time of 200 seconds and instantly increased back to the original rate at a simulation time of 220 seconds.

4 Discussion

The aim of the study was to create a modular and well-documented computational model of oxygen transport in preterm infants for the development and evaluation of automated oxygen controllers. To reach this objective, FiO_2-SpO_2 responses in preterm infants were studied. Many detected FiO_2 steps did not fulfil our criteria (Section 2.6) and were therefore excluded from further analysis. The remaining FiO_2 steps still included a high level of variability. The model could be calibrated to a specific FiO_2-SpO_2 response using model parameter values within literature-based ranges. However, the specific parameter set resulting from the calibration could not reproduce another similar FiO_2-SpO_2 response. The model reproduced physiologically expected shunting and apnea scenarios.

4.1 Valid FiO_2 steps

Despite the exclusion of unstable and unsuitable FiO_2 steps for model calibration, there remained high variability in the FiO_2-SpO_2 response (Figure 3.1). Some increasing FiO_2 steps even resulted in a decreasing SpO_2 response and the other way around. It seems like we lack details on the oxygenation status and patient instability. There may be other confounding factors, like unmeasured physiological parameters and grouping based on the FiO_2 step size, that have not been taken into account. In addition, 99.89% and 93.93% of the detected FiO_2 steps of patients 1 and 2, respectively, were deemed invalid and were therefore excluded. Hence, our conclusions are based on merely a small part of all detected FiO_2-SpO_2 responses. The variability within all detected FiO_2-SpO_2 steps might therefore be even greater. Fathabadi et al. also found this high variability and were not able to model all detected FiO_2-SpO_2 responses using a single model [17, 80].

On the other hand, Figure 3.1 seems to show normal distributions. The central tendency of the normal distribution is positive for increasing FiO_2 steps and decreasing for FiO_2 steps, as expected. With more data, it could be possible to gain even more insight into and predict the FiO_2-SpO_2 response.

The subset with an initial SpO_2 of 96% - 100% showed very small normalised Δ SpO_2, where the most common normalised Δ SpO_2 was very close to zero. This is in line with what we expected due to the oxygen dissociation curve. At high SpO_2 values, an equal change in pO_2 resulted in a smaller change in SpO_2 compared to lower values of SpO_2.

4.2 Model calibration

4.2.1 Reproducibility of the FiO_2-SpO_2 response

The model could be calibrated to a particular FiO_2-SpO_2 response using non-measured variable parameter values that fall within literature-based ranges and measured variable parameter values extracted from data. R and C were calibrated to reach the desired Vt. D, SV, $s1$, $s2$, $s3$, and MR were calibrated to match the mean SpO_2 extracted from the patient data. The maximum differences in the outcome measures between the calibrated model and patient data were 0.6 mL/kg for Vt and 2% for SpO_2.

Measured variable parameters were determined by averaging over a 20-second interval before and after the FiO_2 step, respectively. A 60-second delay was included to determine the average value after the FiO_2 step. Figures 3.2 to 3.4 show substantial variability of the SpO_2 signal. Therefore, the decision in the interval and delay sizes influence the average SpO_2 values used as endpoints for model calibration. The great variability of the SpO_2 signal also implies that the patient was not entirely stable during the measurements, even after the exclusion of invalid FiO_2 steps.

The residual instability of the patient is also shown by the difference in non-measured variable parameters before and after the FiO_2 change. The decreasing measurement 1 of patient 2 was the only step in which non-measured parameters, except C, did not differ before and after the step. In the other measurements, the measured variable parameters were unable to explain differences in Vt and SpO_2 before and after the

FiO_2 change. Therefore, non-measured variable parameters had to be altered to reach these desired outcome measures. In order to gain a better understanding of the underlying physiological changes in patients, future research should focus on measuring the current study's non-measured variable parameters. The current study revealed that various combinations of the non-measured parameters can result in the same desired model outcome, making it impossible to determine which specific physiological changes were responsible for the observed differences before and after the FiO_2 change.

However, it is crucial to bear in mind that a change in FiO_2 may also cause changes in certain non-measured parameters. For example, an increase in FiO_2 causes dilatation in the pulmonary capillaries, which decreases pulmonary hypertension and result in lower values for $s2$ and $s3$ [81].

4.2.2 Generisability to other FiO_2-SpO_2 responses

The specific set of non-measured parameters resulting from the model calibration could not be generalised to another similar FiO_2-SpO_2 response. The SpO_2 error was up to 10.6% in the uncalibrated model and consistently equal or higher compared to the calibrated model (Tables 3.7 and 3.8). Despite this, the Δ SpO_2 of before and after the step was 6.4% in the model versus 6.5% in the patient data. These relative SpO_2 responses were very similar for the model and patient data.

The difficulty of creating a generalisable model for FiO_2-SpO_2 responses has previously been demonstrated by Fathabadi et al, who found a large variation in the observed FiO_2-SpO_2 responses. This prevented them from generalising the FiO_2-SpO_2 responses to a single first-order plus deadtime response [17, 80]. Rafl et al. developed an MOTP, of which the model parameters could be estimated for single episodes of oxygen saturation but could not be generalised for multiple episodes [28].

However, it should be noted that the model was manually calibrated with one specific set of parameters, while numerous sets of parameters could have been selected to achieve the desired result. Hence, it is impossible to state that the model is unable to be generalised to other FiO_2-SpO_2 responses. Merely the calibrated model with the specific set of non-measured parameter values could not be generalised to another FiO_2-SpO_2 response. Utilizing computational parameter estimation instead of manual parameter selection would be a more systemic approach and could yield valuable insights into the optimal parameter set [82]. In parameter estimation, the best-fit set of parameters is produced by minimising the performance measures in relation to the parameter values. Often the mean square error is minimised. By performing computational instead of manual calibration of the model, all valid FiO_2 steps can be included in the optimisation process. In this way, a more reliable statement can be made whether or not the model is generalisable to other FiO_2-SpO_2 responses. An important consideration in the optimisation phase is to incorporate physiological knowledge as much as possible. For instance, it is not sufficient to solely calibrate the R and C parameters to achieve the desired Vt, but the end-expiratory flow rate also has to be zero. This highlights the significance of including relevant physiological factors in the optimisation process. It is also possible to include parameter bounds based on Table 2.3.

4.2.3 Calibration to Vt

C was found to be higher per kg for patients with higher body weights in this study, which is in line with literature [50–52]. Compliance and resistance were also measured by the Fabian ventilator. However, these data may not be entirely reliable because they reflect the values of the entire system, including the patient and the endotracheal tube. The C and R values measured by the ventilator are therefore respectively lower and higher than the actual values. This difference was also consistently present in the results of the present study.

Interestingly, Table 3.6 shows a significant difference in C values before and after the FiO_2 change of the decreasing calibrated measurement 2 of 0.24/kg (almost 1.4 times higher). Although the measured R and C values may not be entirely reliable, we can reliably compare the relative difference before and after the FiO_2 change. In this case, the measured compliance after the FiO_2 change was 1.5 times higher than before the FiO_2

change (Table 3.5), which corresponds to the value of the non-measured parameter C. Also, the Vt increased by approximately a factor of 1.4.

Diseases affecting the respiratory mechanics often present heterogeneously. Representing lung compliance and resistance as single values for all alveoli and assuming homogeneous behaviour is therefore a simplification. Another simplification was the assumption that the lung and chest wall compliances were linear instead of non-linear. As a result, compliance is underestimated at low inspiratory pressures and overestimated at high inspiratory pressures. This did not lead to a major problem in this study, because C was altered to achieve the aimed Vt based on the measured pressures in the respiratory system. However, this may become a bigger problem when you assume the compliance to be constant while changing the $PEEP$ and/or $P_{support}$ in the model. The continuous measurements of C by the Fabian ventilator could play a role in detecting changes in compliance during alterations of the inspiratory pressure and give more insight into the nonlinearity of the compliance of the respiratory system.

A calculation error in the conversion of RR to the appropriate input of the mechanical ventilator during the final stage of this master thesis resulted in a lower simulated RR than the measured RR. Since the error was discovered in the final stage, not all results were re-obtained, except for the apnea simulation, which was performed using the correct model. Additionally, Figure C.11 represents the correct RR. Calibration was conducted on Vt and SpO_2, therefore, these values would remain unchanged in the absence of this error. The error had two main effects. Firstly, a higher RR results in a shorter breathing period. In this case, achieving the desired Vt at the end of the inspiratory phase with an end-inspiratory flow rate of zero requires higher compliance and/or lower resistance. Secondly, the minute ventilation, which is calculated by multiplying Vt and RR, is reduced when the RR is lower and Vt is constant. A reduced minute ventilation results in less CO_2 removal and higher pCO_2 in the blood. Additionally, a higher minute volume leads to more inhalation of O_2. Because the metabolic rate remained constant, the pulmonary diffusing rate of O_2 did not change. Increased O_2 inhalation and constant O_2 diffusion rate result in a higher pO_2 in the alveoli and pulmonary capillaries. The latter subsequently results in a higher SO_2.

4.2.4 Calibration to SpO_2

In increasing measurement 1 of patient 1, changing the SV from 1.2 mL/kg before the FiO_2 change to 2.0 mL/kg after the FiO_2 change led to a 5.5% increase in SpO_2, while the target was a 6.5% increase. This suggests that SV and cardiac output play a major role in the oxygenation status. An increased cardiac output increases dO_2. If the metabolic O_2 delivery remains constant, this will lead to an increase in SpO_2.

Compared to other studies, this MOTP required high shunt rates (up to 55%). Morozoff et al. and Sands et al. implemented a shunt rate of 8.7% for a healthy infant [25, 73]. Another study showed shunt rates ranging from 5.9% to 31.0% in neonates with pulmonary failure [62]. A possible explanation is that the implemented ODC is assumed to be independent of pH, whereas it is affected by pH in reality. Based on the mathematical approximation of the ODC it was assumed that a difference in pH within the typical values of 7.35-7.45 would not shift the ODC significantly [83, 84]. However, the blood gases of the included patients contained pH values as low as 7.05 (see Table 3.4). A low pH shifts the ODC to the right, resulting in a lower SaO_2 at an equal pO_2 value. The high shunt rates were used to reduce the SpO_2. Therefore, making the ODC dependent on pH might in the cases of the two included patients result in lower shunt rates.

The MOTP's SaO_2 output displayed respiratory-induced oscillations due to breathing movement (Figure C.11). Due to the breathing pattern in combination with O_2 diffusion, p_{alv,O_2} was high during inspiration and low during expiration. This change in p_{alv,O_2} is reflected in oscillations in p_{PC,O_2}, which is translated to the SaO_2. In a real patient, these oscillations quickly disappear due to the infinite mixing chambers in the circulatory system. However, in the MOTP, the circulation is mostly simulated as a time delay, without adapting the signal and therefore not eliminating the oscillation. These oscillations are more observable with low shunt rates, because the oscillations are reduced in the SC, a mixing chamber with a relatively large volume. With

a larger shunt, more blood comes from the PA, which contains fewer oscillations, while with a smaller shunt, more blood comes from the PC, where the oscillations are created. A possible solution could be to apply a moving average to the signal that comes from the time delay block. Another solution would be to simulate the circulatory system with multiple mixing chambers, like Morozoff et al. [25].

The accuracy of SpO_2 obtained by pulse oximetry is limited [18, 41, 42, 85]. Unfortunately, there are currently no adequate alternatives for pulse oximetry. Masimo SET (Masimo, Irwine, CA, USA) pulse oximetry for neonates has an accuracy of 1.5% and 3.83% in SpO_2 ranges of 70-100% and 60-80%, respectively [86, 87]. Signal quality and accuracy may be compromised due to sensor misplacement and external disturbances such as body movement and changes in ambient light [88]. Moreover, pulse oximetry in critically ill patients is less accurate [89]. Therefore, it is uncertain whether it is possible to maintain the SaO_2 within a narrow target range using AOC with SpO_2 as its proxy. Nevertheless, currently, there are no alternatives to pulse oximetry for continuous saturation monitoring, and manual FiO_2 adjustments are also based on SpO_2 measurements obtained by pulse oximetry. Consequently, switching to AOCs would not alter this practice. In addition, arterial blood gases can be taken to verify the measured SpO_2 values. The limitations and inaccuracies of SpO_2 measurements are a problem on a higher level than the mere evaluation of this MOTP.

The model calibration was performed based on continuously measured SpO_2 values. Ideally, the bias between SaO_2 and SpO_2 would be eliminated in the development phase and the model calibration would be performed based on SaO_2 data. Unfortunately, this data is not continuously available, and the time stamps of the arterial blood gases did not match the time stamps of the FiO_2 steps. Even in cases where the time stamps were not that far apart, the SaO_2 and SpO_2 could differ greatly (e.g. decreasing measurement 2 of patient 1 in Tables 3.4 and 3.5. A solution would be to find FiO_2 steps with simultaneous blood gases. This could be achieved by extracting blood gases more often and by obtaining more patient data.

The SpO_2 sensor was modelled based on measurements from a single sensor. These measurements included a structural bias between the simulated SaO_2 values and measured SpO_2 by pulse oximetry (Figure A.5). The results of the measured bias resulted in a restriction of the maximum SpO2 value to 98.2%. Future improvements to the model can be made by incorporating measurements of multiple SpO_2 sensors into the model.

4.3 Simulation scenarios

4.3.1 Shunting scenario

The response of the model to a right-to-left shunting scenario resulted in a non-linear decrease and subsequent increase of SaO_2. This was physiologically expected because an increase in right-to-left shunt rate results in a reduction in blood flow across the lungs. This leads to less oxygenated blood and a reduction in SaO_2. Patient 1 exhibited a greater desaturation response to the same shunting scenario compared to patient 2. This may be explained by their lower weight, resulting in a lower Vt, cardiac output, and blood volume, potentially leading to a decreased buffer capacity to tolerate the shunting scenario.

After the shunt rate returns to the original value, a small desaturation occurred (Figures 3.5 and 3.7). At this moment, the deoxygenated blood which flowed through the shunt suddenly flows through the pulmonary capillaries again and could not be fully oxygenated in the pulmonary capillaries.

The observed desaturation and saturation transients exhibited non-smooth characteristics, which were attributed to the arterial and venous time delays incorporated in the circulation submodule. These time delays did not consider the mixing of partial pressures or saturations and were also evident in the model's stabilisation before the FiO_2 step (Figure 3.3. In contrast, the shunting scenario simulated by Morozoff et al. was smoother, possibly because they employed a more extensive circulatory model with 13 compartments, including 9 mixing chambers [25].

The saturation to desaturation time constant ratio was 0.43 and 1.02 in patients 1 and 2, respectively, and

was not comparable to the ratio of 0.25 derived from the model of Morozoff et al. [25]. The saturation and desaturation time constants were determined by applying a moving mean procedure to the SaO_2 signal to reduce the non-smooth characteristics. However, this procedure may have influenced the saturation and desaturation time constants.

4.3.2 Apnea scenario

The response of the model to an apnea scenario resulted in a desaturation of 4.3% and 9.5% in patients 1 and 2, respectively. The desaturation was followed by an increase in SaO_2 after the apnea incident stopped. The subsequent decrease and increase in SaO_2 was the expected response of the MOTP to an apnea scenario. The difference in desaturation response between the patients resulted from the difference in administered FiO_2, which was 37% in patient 1, and 25% in patient 2. A higher FiO_2 led to a higher alveolar pO_2. This increase in oxygen availability provided a greater buffer for the patient to endure the apnea scenario. Similar to the shunting scenario, the results of the apnea scenario showed non-smooth transients due to the impact of time delays in the circulation subsystem.

Apnea scenarios are relevant in AOC evaluation for two reasons. First of all, to evaluate how an AOC reacts to apnea during non-invasive mechanical ventilation. Secondly, to assess how quickly the patient or ventilator resumes breathing to avoid unnecessary FiO_2 administration during invasive mechanical ventilation.

4.4 Applications

Despite the variety in FiO_2-SpO_2 responses and the fact that the MOTP is currently not shown to be generalisable to different FiO_2-SpO_2 responses, The MOTP can be used to reproduce an FiO_2-SpO_2 response. The MOTP is therefore useful for the evaluation and development of AOCs. However, improvements that have been outlined in this discussion should be implemented first. One proposal would be to establish test scenarios and specify the model accordingly. The goal is to incorporate as many variations encountered in clinical practice as possible with as few scenarios as possible. This includes, for example, GA, PMA, comorbidities, shunts, etc. Subsequently, data can be collected specifically for each scenario. The model and its parameters can be calibrated to that data, and the average value per parameter can be set as the definitive parameter value for that scenario. After this is done for each scenario, the AOC can be tested on all scenarios to evaluate how the AOC responds to the specific previously defined scenarios.

4.5 Further research

The collection of more data can be used to provide more insight into the FiO_2-SpO_2 responses and their intra-patient and inter-patient variability. To provide a more complete image of the patient population, it is advisable to incorporate patients with diverse birth weights and gestational ages.

The model could be improved by a number of improvements. Implementation ODC dependency of the ODC on pH would make the relation between pO_2 and SO_2 more accurate in the case of deviating pH measurements. Additionally, the modelled SpO_2 sensor could be improved by performing more measurements using more different SpO_2 sensors.

This study has shown that the MTOP can be calibrated to specific FiO_2-SpO_2 responses. However, manual calibration was performed, while many different parameter sets could lead to the same result. The next step could be to perform computational parameter estimation. This can also be used to investigate whether the MOTP can be generalisable to other FiO_2-SpO_2 responses. Moreover, focusing on measuring the current study's non-measured variable parameters could lead to a deeper understanding of the underlying physiological changes in patients during FiO_2-SpO_2 responses. This, in turn, could enhance the accuracy of parameter estimations.

The FiO_2-SpO_2 delay consists of multiple parts, caused by the mechanical ventilator, transportation within the patient, and the pulse oximeter. The time delays in the first and last part of this model were isolated and based on measurements. The time delay within the patient was not validated and remains a subject for future investigation. It is advisable to explore whether the time delay inside the patient can primarily be explained by cardiac output, or if other factors also contribute. Further investigation of the FiO_2-SpO_2 delay can provide useful information for tailoring pause times after an FiO_2 adjustment in AOCs.

The modular structure of the MOTP allows for adaptation to evaluate new AOC features. An example of a potential feature is customizing PEEP to improve oxygenation along with adjustments to FiO_2. Moreover, the MOTP could also facilitate the development and evaluation of future tools, such as patient-specific ventilation adaptations, which currently exist for adult patients but not for other patient populations [90].

5 Conclusion

In conclusion, a computer simulation model of oxygen transport in preterm infants, including complementary literature-based parameter ranges, was developed. The study found that the FiO_2-SpO_2 responses in preterm infants exhibited a high level of variability. Despite this variability, the model could successfully be calibrated to specific FiO_2-SpO_2 responses using literature-based ranges of model parameters. The model demonstrated the ability to replicate physiologically expected shunting and apnea scenarios. However, the calibrated model with a specific set of parameters was not generalisable to different FiO_2-SpO_2 responses. Nevertheless, the model can be used in the evaluation and development of automated oxygen controllers. Even though many assumptions have been made in the development process, the result is a useful, modular, and well-documented framework that can reproduce specific FiO_2-SpO_2 responses. Consequently, there exist sufficient opportunities and potential avenues to enhance and extend the model, enabling a deeper comprehension of the FiO_2-SpO_2 response in preterm infants, and a better platform for the evaluation and development of automated oxygen controllers.

References

[1] M. Abdo et al. "Automated versus manual oxygen control in preterm infants receiving respiratory support: a systematic review and meta-analysis". In: *J Matern Fetal Neonatal Med* (2021), pp. 1–8.

[2] E. G. Abu Jawdeh. "Intermittent hypoxemia in preterm infants: etiology and clinical relevance". In: *NeoReviews* 18.11 (2017), pp. 637–646.

[3] M. P. Collins et al. "Hypocapnia and other ventilation-related risk factors for cerebral palsy in low birth weight infants". In: *Pediatric Research* 50.6 (2001), pp. 712–719.

[4] C. Dani. "Automated control of inspired oxygen (FiO2) in preterm infants: Literature review". In: *Pediatric Pulmonology* 54.3 (2019), pp. 358–363.

[5] J. M. Di Fiore, P. M. MacFarlane, and R. J. Martin. "Intermittent hypoxemia in preterm infants". In: *Clin Perinatol* 46.3 (2019), pp. 553–565.

[6] R. J. Martin et al. "Intermittent hypoxic episodes in preterm infants: do they matter?" In: *Neonatology* 100.3 (2011), pp. 303–310.

[7] Jr. Northway W. H., R. C. Rosan, and D. Y. Porter. "Pulmonary disease following respirator therapy of hyaline-membrane disease. Bronchopulmonary dysplasia". In: *N Engl J Med* 276.7 (1967), pp. 357–368.

[8] A. E. Richter et al. "Postnatal cerebral hyperoxia is associated with an increased risk of severe retinopathy of prematurity". In: *Neonatology* 116.4 (2019), pp. 356–362.

[9] B. Stenson, P. Brocklehurst, and W. Tarnow-Mordi. "Increased 36-week survival with high oxygen saturation target in extremely preterm infants". In: *N Engl J Med* 364.17 (2011), pp. 1680–1682.

[10] S. K. M. Ali et al. "Oxygen therapy in preterm infants: recommendations for practice". In: *Paediatrics and Child Health* 31.1 (2021), pp. 1–6.

[11] J. I. Hagadorn et al. "Achieved versus intended pulse oximeter saturation in infants born less than 28 weeks' gestation: the AVIOx study". In: *Pediatrics* 118.4 (2006), pp. 1574–1582.

[12] A. R. Laptook et al. "Pulse oximetry in very low birth weight infants: can oxygen saturation be maintained in the desired range?" In: *J Perinatol* 26.6 (2006), pp. 337–341.

[13] K. Lim et al. "Oxygen saturation targeting in preterm infants receiving continuous positive airway pressure". In: *J Pediatr* 164.4 (2014), pp. 730–736.

[14] A. Van der Eijk et al. "An observational study to quantify manual adjustments of the inspired oxygen fraction in extremely low birth weight infants". In: *Acta paediatrica* 101 (2012), pp. 97–104.

[15] N. Claure and E. Bancalari. "Automated closed loop control of inspired oxygen concentration". In: *Respiratory Care* 58.1 (2013), pp. 151–161.

[16] N. Claure and E. Bancalari. "New modes of respiratory support for the premature infant: automated control of inspired oxygen concentration". In: *Clin Perinatol* 48.4 (2021), pp. 843–853.

[17] O. S. Fathabadi et al. "Assessment of validity and predictability of the FiO2-SpO2 transfer-function in preterm infants". In: *Physiol Meas* 35.7 (2014), pp. 1425–1437.

[18] H. H. Salverda et al. "Automated oxygen control in preterm infants, how does it work and what to expect: a narrative review". In: *Arch Dis Child Fetal Neonatal Ed* 106.2 (2021), pp. 215–221.

[19] O. S. Fathabadi et al. "Automated control of inspired oxygen for preterm infants: What we have and what we need". In: *Biomedical Signal Processing and Control* 28 (2016), pp. 9–18.

[20] J. G. Chase et al. "Next-generation, personalised, model-based critical care medicine: A state-of-the art review of in silico virtual patient models, methods, and cohorts, and how to validation them". In: *Biomed Eng Online* 17.1 (2018).

[21] Food and Drug Administration (FDA). *Technical considerations for medical devices with physiologic closed-Loop control technology. Draft guidance for industry and Food and Drug Administration staff.* Report. 2021. URL: `https://www.fda.gov/regulatory-information/search-fda-guidance-documents/technical-considerations-medical-devices-physiologic-closed-loop-control-technology`.

[22] E. Morozoff, J. A. Smyth, and M. Saif. "Applying computer models to realize closed-loop neonatal oxygen therapy". In: *Anesthesia Analgesia* 124 (2017), pp. 95–103.

[23] J. S. Gray. "The multiple factor theory of respiratory regulation." In: *AAF School of Aviation Med* Project Report Nr. 386 (1945).

[24] C. Corno, G. B. Fiore, and M. L. Costantino. "A mathematical model of neonatal tidal liquid ventilation integrating airway mechanics and gas transfer phenomena". In: *IEEE Trans Biomed Eng* 51.4 (2004), pp. 604–611.

[25] E. Morozoff and M. Saif. "Oxygen therapy control of neonates - Part I: a model of neonatal oxygen transport". In: *Control. Intell. Syst.* 36 (2008).

[26] The MathWorks Inc. *MATLAB version: 9.13.0 (R2022b)*. Natick, Massachusetts, United States, 2022. URL: `https://www.mathworks.com`.

[27] The MathWorks Inc. *Simulink: Simulation and Model-Based Design version: 10.6 (R2022b)*. Natick, Massachusetts, United States, 2022. URL: `https://www.mathworks.com`.

[28] J. Rafl et al. "Computer model of oxygenation in neonates: A demonstration of utility". In: *Current Directions in Biomedical Engineering* 5.1 (2019), pp. 73–76.

[29] L. Tejkl, J. Ráfl, and P. Kudrna. "The time delay of air/oxygen mixture delivery after the change of set FiO2: An improvement of a neonatal mathematical model". In: *Lek Tech* 49.3 (2019), pp. 77–82.

[30] A. Albanese et al. "An integrated mathematical model of the human cardiopulmonary system: model development". In: *Am J Physiol Heart Circ Physiol* 310.7 (2016), pp. 899–921.

[31] C. A. Sarmiento et al. "An integrated mathematical model of the cardiovascular and respiratory response to exercise: Model-building and comparison with reported models". In: *Am J Physiol Heart Circ Physiol* 320.4 (2021), pp. 1235–1260.

[32] P. Somhorst and T. G. Goos. "KT3401. Computersimulatie: Ademhaling en mechanische beademing. Versie 22-2". Unpublished Work. 2023.

[33] L. E. Fix et al. "Theoretical open-loop model of respiratory mechanics in the extremely preterm infant". In: *PLoS One* 13.6 (2018).

[34] J. T. Ottesen, M. S. Olufsen, and J. K. Larsen. *Applied Mathematical Models in Human Physiology*. Society for Industrial and Applied Mathematics, 2004.

[35] B. Maury. *The Respiratory System in Equations*. Springer Publishing Company, Incorporated, 2013. ISBN: 8847052130.

[36] W.F. Boron and E.L. Boulpaep. *Medical Physiology: A Cellular and Molecular Approach*. W.B. Saunders, 2003. ISBN: 9780721632568.

[37] C. Rüegger, H. U. Bucher, and R. A. Mieth. "Pulse oximetry in the newborn: is the left hand pre- or post-ductal?" In: *BMC Pediatr* 10 (2010), p. 35.

[38] J. W. Severinghaus. "Simple, accurate equations for human blood O2 dissociation computations". In: *J Appl Physiol Respir Environ Exerc Physiol* 46.3 (1979), pp. 599–602.

[39] R. W. D. Nickalls. "Inverse solutions of the Severinghaus and Thomas equations which allow Po2 to be derived directly from So2". In: 2011.

[40] S. A. McLellan and T. S. Walsh. "Oxygen delivery and haemoglobin". In: *Continuing Education in Anaesthesia Critical Care Pain* 4.4 (2004), pp. 123–126.

[41] S. Sturrock et al. "Closed loop automated oxygen control in neonates-A review". In: *Acta Paediatr* 109.5 (2020), pp. 914–922.

[42] V. Nair et al. "Automated oxygen delivery in neonatal intensive care". In: *Frontiers in Pediatrics* 10 (2022).

[43] P. J. Brown. *Parameters and variables*. URL: `https://www.ill.eu/sites/ccsl/mk4man/c5node2.html`.

[44] S. A. Sands et al. "A dynamic model for assessing the impact of diffusing capacity on arterial oxygenation during apnea". In: *Respiratory Physiology Neurobiology* 171.3 (2010), pp. 193–200.

[45] F. J. Walther et al. “Pulsed doppler determinations of cardiac output in neonates: normal standards for clinical use”. In: *Pediatrics* 76.5 (1985), pp. 829–833.

[46] P. A. Dargaville and M. Keszler. “Setting the Ventilator in the NICU”. In: *Pediatric and Neonatal Mechanical Ventilation* (2013), pp. 1101–1125.

[47] H. Boix et al. “Recommendations for transfusion of blood products in neonatology”. In: *Anales de Pediatría (English Edition)* 97.1 (2022), pp. 601–608.

[48] M. Delivoria-Papadopoulos and J. E. McGowan. “Oxygen transport and delivery”. In: *Fetal and neonatal physiology*. Ed. by R. A. Polin and W. W. Fox. Second Edition. W.B. Saunders Company, 1998, pp. 1105–1117.

[49] J. A. Olaniyi, O. G. Arinola, and A. B. Odetunde. “Foetal haemoglobin (HbF) status in adult sickle cell anaemia patients in Ibadan, Nigeria”. In: *Ann Ib Postgrad Med* 8.1 (2010), pp. 30–33.

[50] T. Gerhardt and E. Bancalari. “Chestwall compliance in full-term and premature infants”. In: *Acta Paediatr Scand* 69.3 (1980), pp. 359–364.

[51] B. Stankiewicz et al. “A new infant hybrid respiratory simulator: preliminary evaluation based on clinical data”. In: *Medical Biological Engineering Computing* 55.11 (2017), pp. 1937–1948.

[52] K. Lui et al. “Early changes in respiratory compliance and resistance during the development of bronchopulmonary dysplasia in the era of surfactant therapy”. In: *Pediatr Pulmonol* 30.4 (2000), pp. 282–90.

[53] G. P. Heldt and M. B. McIlroy. “Dynamics of chest wall in preterm infants”. In: *J Appl Physiol* 62.1 (1987).

[54] G. Polgar. “Airway resistance in the newborn infant: Preliminary communication”. In: *The Journal of Pediatrics* 59.6 (1961).

[55] C. D. Cook et al. “Studies of respiratory physiology in the newborn infant. III. Measurements of mechanics of respiration”. In: *J Clin Invest* 36.3 (1957).

[56] M. Szymankiewicz, D. Vidyasagar, and J. Gadzinowski. “Predictors of successful extubation of preterm low-birth-weight infants with respiratory distress syndrome”. In: *Pediatric Critical Care Medicine* 6.1 (2005), pp. 44–49.

[57] B. Stankiewicz et al. “A new endotracheal tube for infants – laboratory and clinical assessment: a preliminary study”. In: *Pediatric Anesthesia* 23.5 (2013), pp. 440–445.

[58] J. Garcia-Fernandez, L. Castro, and F. J. Belda. “Ventilating the newborn and child”. In: *Current Anaesthesia Critical Care* 21.5 (2010), pp. 262–268.

[59] A. N. Krauss, D. B. Klain, and P. A. M. Auld. “Carbon monoxide diffusing capacity in newborn infants”. In: *Pediatric Research* 10.9 (1976), pp. 771–776.

[60] M. Meyer et al. “Pulmonary diffusion capacities for O2 and CO measured by a rebreathing technique”. In: *J Appl Physiol Respir Environ Exerc Physiol* 51.6 (1981), pp. 1643–1650.

[61] H. T. Milhorn and P. E. Pulley. “A theoretical study of pulmonary capillary gas exchange and venous admixture”. In: *Biophys J* 8.3 (1968), pp. 337–357.

[62] H L Smith and J G Jones. “Non-invasive assessment of shunt and ventilation/perfusion ratio in neonates with pulmonary failure”. In: *Archives of Disease in Childhood - Fetal and Neonatal Edition* 85.2 (2001), pp. 127–132.

[63] R. W. Wilmott and B. A. Becker. “Chapter 17 - Pulmonology”. In: *Pediatric Secrets (Fifth Edition)*. Mosby, 2011, pp. 648–678. ISBN: 978-0-323-06561-0.

[64] Frank L. Powell, Peter D. Wagner, and John B. West. “4 - Ventilation, Blood Flow, and Gas Exchange”. In: *Murray and Nadel’s Textbook of Respiratory Medicine (Sixth Edition)*. Ed. by V. C. Broaddus et al. Philadelphia: W.B. Saunders, 2016.

[65] G. J. Arthurs and M. Sudhakar. “Carbon dioxide transport”. In: *Continuing Education in Anaesthesia Critical Care Pain* 5.6 (2005), pp. 207–210.

[66] R. Pittman. “Regulation of Tissue Oxygenation”. In: *Colloquium Series on Integrated Systems Physiology: From Molecule to Function* 3 (2011).

[67] Acutronic Medical Systems AG. *Communication protocol acuLink*. 2011.

[68] S. Reuter, C. Moser, and M. Baack. "Respiratory distress in the newborn". In: *Pediatr Rev* 35.10 (2014), pp. 417–428.

[69] H. L Ord and M. J. Griksaitis. "Cardiac output diversity: Are children just small adults?" In: *Physiology News* (2019).

[70] J. R. Hill and D. C. Robinson. "Oxygen consumption in normally grown, small-for-dates and large-for-dates new-born infants". In: *J Physiol* 199.3 (1968), pp. 685–703.

[71] J. W. Scopes and I. Ahmed. "Minimal rates of oxygen consumption in sick and premature newborn infants". In: *Arch Dis Child* 41.218 (1966), pp. 407–416.

[72] O. N. Bhakoo and J. W. Scopes. "Minimal rates of oxygen consumption in small-for-dates babies during the first week of life". In: *Arch Dis Child* 49.7 (1974), pp. 583–585.

[73] S. Sands et al. "A model analysis of arterial oxygen desaturation during apnea in preterm infants". In: *PLoS computational biology* 5 (Dec. 2009).

[74] V. Dariya et al. "Cuffed versus uncuffed endotracheal tubes for neonates". In: *Cochrane Database of Systematic Reviews* 1 (2022).

[75] R. A. Mahmoud et al. "Effect of endotracheal tube leakage on respiratory function monitoring: Comparison of three neonatal ventilators". In: *J Pediatr Intensive Care* 1.2 (2012), pp. 61–69.

[76] A. A. Chakkarapani et al. "Current concepts in assisted mechanical ventilation in the neonate" - Part 2: Understanding various modes of mechanical ventilation and recommendations for individualized disease-based approach in neonates". In: *International Journal of Pediatrics and Adolescent Medicine* 7.4 (2020), pp. 201–208.

[77] S. Sosio and G. Bellani. "Plateau Pressure during Pressure Control Ventilation". In: *AboutOpen* 6.1 (2019), pp. 76–77.

[78] A. Yartsev. *Interpreting the shape of the ventilator flow waveform*. July 2022. URL: https://derangedphysiology.com/main/cicm-primary-exam/required-reading/respiratory-system/Chapter%5C%20553/interpreting-shape-ventilator-flow-waveform.

[79] A. Goryniak et al. "Apnea of prematurity - characteristic and treatment". In: *Postepy Biochem* 63.2 (2017), pp. 151–154.

[80] O.S. Fathabadi et al. "Characterisation of the oxygenation response to inspired oxygen adjustments in preterm infants". In: *Neonatology* 109.1 (2016), pp. 37–43.

[81] S. Green and D. Stuart. "Oxygen and pulmonary arterial hypertension: effects, mechanisms, and therapeutic benefits". In: *Eur J Prev Cardiol* 28.1 (2021), pp. 127–136.

[82] G. Marion and D. S. Lawson. *An Introduction to Mathematical Modelling*. Bioinformatics and Statistics Scotland, 2008.

[83] Centre of Clinical Excellence - Women and Children Safer Care Victoria. *Blood gas interpretation for neonates*. 2018. URL: https://www.safercare.vic.gov.au/clinical-guidance/neonatal/blood-gas-interpretation-for-neonates.

[84] O. Siggaard-Andersen et al. "Measured and derived quantities with modern pH and blood gas equipment: Calculation algorithms with 54 equations". In: *Scandinavian Journal of Clinical and Laboratory Investigation* 48.189 (1988), pp. 7–15.

[85] M. A. Blanchet et al. "Accuracy of multiple pulse oximeter brands in stable critically ill patients - Oxygap study". In: *Respiratory Care* (2023), respcare.10582.

[86] Masimo. *Assessing the accuracy of pulse oximetry in true clinical settings*. Report. 2007. URL: https://www.masimo.co.uk/siteassets/uk/documents/pdf/clinical-evidence/whitepapers/lab4709a_whitepapers_pulse_oximetry_accuracy.pdf.

[87] Masimo. *Improved SpO2 Accuracy with RD SET*. 2021. URL: https://www.masimo.com/improved-accuracy/.

[88] A. Sola, L. Chow, and M. Rogido. "Pulse oximetry in neonatal care in 2005. A comprehensive state of the art review". In: *An Pediatr (Barc)* 62.3 (2005), pp. 266–281.

[89] A. Van de Louw et al. "Accuracy of pulse oximetry in the intensive care unit". In: *Intensive Care Med* 27.10 (2001), pp. 1606–1613.

[90] Hamilton Medical. *Adaptive support ventilation (ASV): Hamilton Medical*. URL: `https://www.hamilton-medical.com/en_NL/Products/Technologies/ASV.html`.

[91] J. B. West and A. M. Luks. *Respiratory physiology : the essentials*. Wolters Kluwer, 2016. ISBN: 978-1-4963-1011-8.

[92] Andrew B. Lumb and Deborah Horner. "Chapter 25 - Pulmonary Physiology". In: *Pharmacology and Physiology for Anesthesia*. W.B. Saunders, 2013, pp. 445–457. ISBN: 978-1-4377-1679-5.

[93] Pediatric cardiology. *Left-to-Right Shunts*. Mar. 2023. URL: `https://www.utmb.edu/pedi_ed/CoreV2/Cardiology/Cardiology8.html`.

[94] P. M. Olley and F. Coceani. "Prostaglandins and the ductus arteriosus". In: *Annu Rev Med* 32 (1981), pp. 375–385.

[95] R. I. Clyman. "Chapter 57 - Mechanisms Regulating Closure of the Ductus Arteriosus". In: *Fetal and Neonatal Physiology (Fifth Edition)*. Elsevier, 2017, pp. 592–599. ISBN: 978-0-323-35214-7.

[96] F. T. Tehrani. "Mathematical analysis and computer simulation of the respiratory system in the newborn infant". In: *IEEE Transactions on Biomedical Engineering* 40.5 (1993), pp. 475–481.

[97] P. M. Sá Couto et al. "Mathematical model for educational simulation of the oxygen delivery to the fetus". In: *Control Engineering Practice* 10.1 (2002). Modelling and Control in Biomedical Systems, pp. 59–66.

[98] PT Medical. *Ox-1 OxSim optische SpO2 pulse oximeter simulator*. URL: `https://www.pt-medical.nl/ox-1-oxsim-optische-spo2-pulse-oximeter-simulator.html`.

A Full model description

The computer simulation model for oxygen transport in preterm infants was developed to reproduce the FiO_2-SpO_2 response. The physiological respiratory and circulatory systems are complex and include many details. A mathematical computer model is a simplified version of certain features of a real system. This appendix includes the choice of features and associated assumptions of the model. AOCs use the measured SpO_2 to alter the administrated FiO_2. Therefore, FiO_2 and SpO_2 were chosen as the input and output data of the full model.

The full model consists of three main parts, the mechanical ventilator, the model of oxygen transport in preterm infants (MOTP), and the SpO_2 sensor (Figure 2.1). The mechanical ventilator and SpO_2 sensor were designed to detach the involved devices from the MOTP. The mechanical ventilator system includes the administered ventilatory pressure and the FiO_2 time delay block. The MOTP is the true patient model and contains all relations and reactions happening inside the patient's body. The MOTP consists of respiration, pulmonary gas exchange, and circulation submodules (Figure 2.2). The SpO_2 sensor models the SpO_2 measured by the pulse oximeter and based on the arterial oxygen saturation (SaO_2) from the MOTP. The full model will be discussed in the order of the FiO_2-SpO_2 response, from the mechanical ventilator, through the MOTP, to the SpO_2 sensor.

A.1 Mechanical ventilator

A.1.1 Ventilatory pressure

Neonates are often ventilated in a support pressure ventilation mode. In this mode the neonate's own breaths are supported and mandatory breaths are performed in the absence of the neonate's breaths. The ventilation submodule simulates mandatory pressure ventilation without breathing activity from the patient to simplify the ventilation submodule. The ventilatory pressure (P_{vent}) is an addition of the positive end-expiratory pressure ($PEEP$) and the support pressure ($P_{support}$):

$$P_{vent} = PEEP + P_{support}, \tag{A.1}$$

where $PEEP$ is a constant pressure (cmH_2O) and $P_{support}$ is simulated as a square wave using the pulse generator block (cmH_2O). The period and pulse width of $P_{support}$ were based on the respiratory rate (RR) and the inspiratory to expiratory ratio ($I{:}E$).

A.1.2 FiO_2 delay block

The FiO_2 delay block was added to account for the time delay between the moment of FiO_2 adjustment on the mechanical ventilator and the moment of arrival of the gas mixture with the adjusted FiO_2 at the Y-piece. The time delay is based on measurements with the same mechanical ventilator hardware as was used for data acquisition for the study. The delay time was measured for flow rates of 2 to 12 L/min in steps of 1 L/min. Measurements were done with a typically filled humidifier and with an empty humidifier. A power function was fitted on the measured data points:

$$y = a \cdot x^b + c, \tag{A.2}$$

where y is the time delay (s), x is the flow (L/min), and a, b and c are fitting constants. A function was fitted on the data for each humidifier status (Figure A.1).

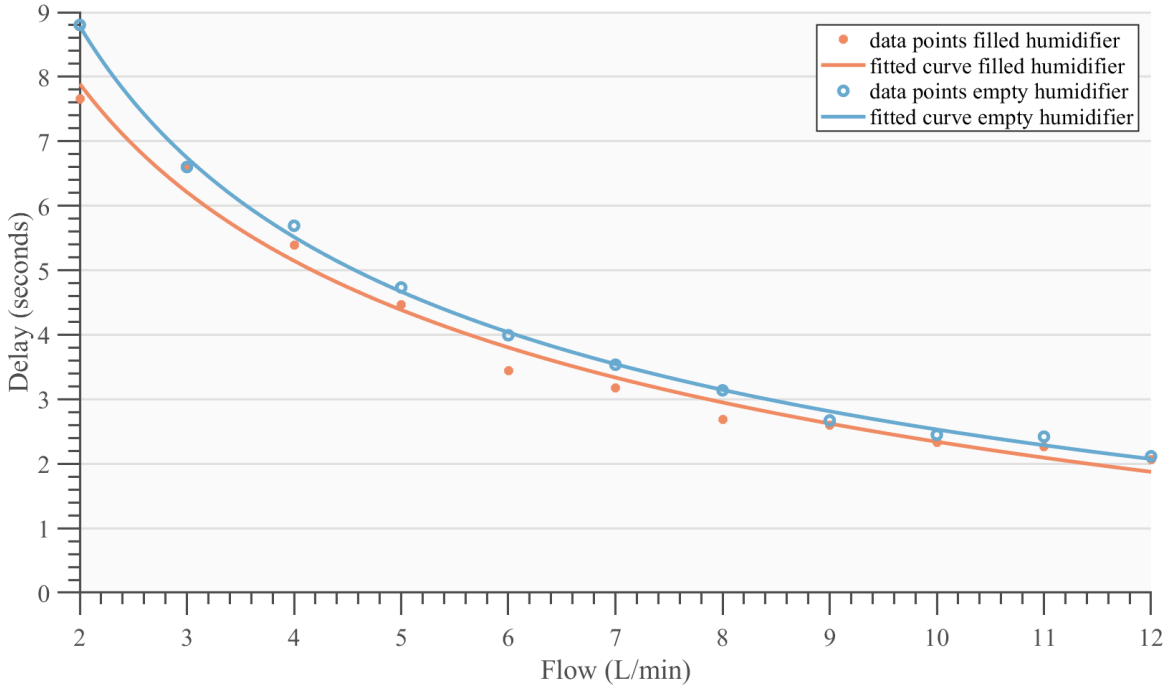

Figure A.1: FiO_2 delay times for both a filled and empty humidifier. The FiO_2 delay curves were fitted to measurements for ventilator (inspiratory and expiratory) flow rates from 2 L/min to 12 L/min. Measurements were obtained using the Fabian ventilator (Acutronic Medical AG, Hirzel, Switzerland).

A.2 Respiration submodule

In reality, air flows from the mechanical ventilator's endotracheal tube into the last part of the trachea, and subsequently into the bronchi, bronchioles, and alveoli. This airflow was simplified by modelling the lung in two different components, the bronchi and alveoli. The bronchi represent the anatomical dead space, and also include the bronchioles. The alveoli represent the compartment where gas exchange of O_2 and CO_2 to and from the pulmonary capillaries occurs [91].

The respiration submodule consists of respiratory mechanics and gas transfer within the lungs. The respiratory mechanics part calculates the change of pressures, volumes and flows of air in the lung compartments resulting from P_{vent}. The gas transfer part calculates the fractions and partial pressures of O_2 and CO_2 in the lung compartments.

A.2.1 Respiratory mechanics

The respiratory mechanics have been modelled as an electric circuit analogy. The model includes pressure, flow, resistance and compliance as analogies of voltage, current, resistance and capacitance, respectively. Inertial effects have been omitted in the model because they are assumed to have negligible effects on the physiological breathing frequencies [30, 33, 34]. The air starts to flow as a result of a difference in pressure, proportional to Ohm's law:

$$U = I \cdot R, \tag{A.3}$$

where U is the voltage (V), I is the current (A), and R is the resistance (Ω). For the respiratory mechanics model, this results in:

$$P_R = V' \cdot R, \tag{A.4}$$

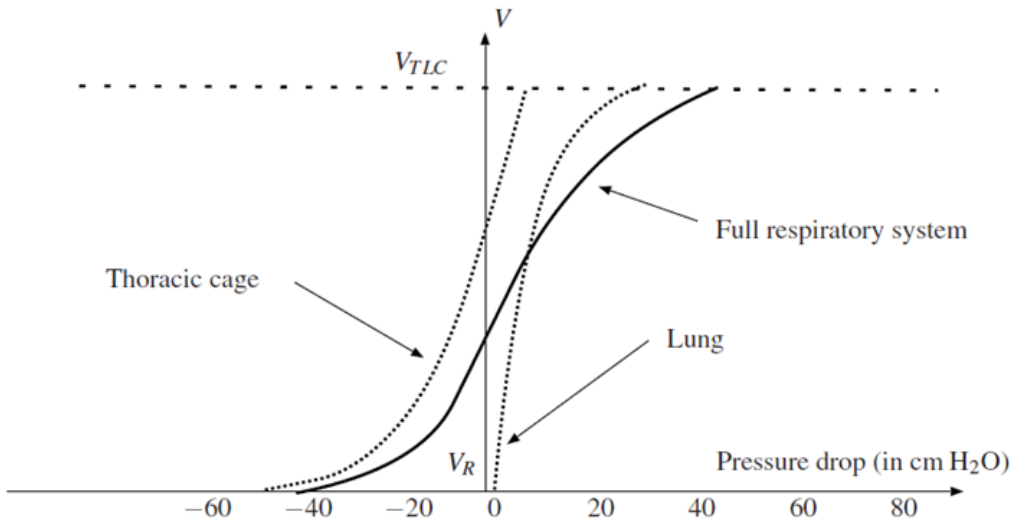

Figure A.2: The non-linear relation between pressure and volume of the lung, thoracic cage and full respiratory system. V_R and V_{TLC} indicate the resting lung volume and total lung capacity, respectively. Adapted from [35].

where P_R is the pressure caused by the resistance (cmH_2O), V' is the air flow (L/s), and R is the resistance ($cmH_2O{\cdot}s/L$). Compliance defines the relationship between the pressure and volume within a compartment. Elastance is defined as the inverse of compliance:

$$E = \frac{1}{C}, \tag{A.5}$$

where E is the elastance (cmH_2O/L), and C is the compliance (L/cmH_2O). The pressure caused by the elastance can be calculated by:

$$P_E = E \cdot (V - V_0), \tag{A.6}$$

where P_E is the pressure caused by the elastance (cmH_2O), E is the elastance (cmH_2O/L), V is the volume in the compartment (L), and V_0 is the resting volume when the pressure in the compartment is zero (L). The total pressure in a compartment results from summation of Equation (A.4) and Equation (A.6):

$$P = P_E + P_R = E \cdot (V - V_0) + V' \cdot R. \tag{A.7}$$

The lung's and chest wall's elastances have non-linear properties [35] (Figure A.2). Unfortunately, no literature on the parameters of the non-linear elastances of neonates is available. Therefore, it was decided to implement linear elastance in the patient model as simplification.

The respiratory mechanics have been modelled as a double-balloon model [32, 35] (Figure 2.3). The inner balloon represents the lung and the outer balloon represents the chest wall. The theory and assumptions above have led to:

$$V'_{br} = V'_{vent \to br} - V'_{br \to alv}, \tag{A.8}$$

$$V'_{alv} = V'_{br \to alv} - V'_{alv \to PC}, \tag{A.9}$$

$$V'_{vent \to br} = \frac{P_{vent} - P_{br}}{R_{br}} = \frac{P_{vent} - (P_{E,br} + P_{E,CW})}{R_{br}}, \tag{A.10}$$

$$V'_{br \to alv} = \frac{P_{br} - P_{alv}}{R_{alv}} = \frac{(P_{E,br} + P_{E,CW}) - (P_{E,alv} + P_{E,CW})}{R_{alv}} = \frac{P_{E,br} - P_{E,alv}}{R_{alv}}, \tag{A.11}$$

$$P_{E,br} = E_{br} \cdot (V_{br} - V_{br,0}), \tag{A.12}$$

$$P_{E,alv} = E_{alv} \cdot (V_{alv} - V_{alv,0}), \tag{A.13}$$

$$P_{E,CW} = E_{CW} \cdot (V_{lung} - V_{CW,0}) = E_{CW} \cdot (V_{br} + V_{alv} - V_{CW,0}), \tag{A.14}$$

where the arrow indicates the direction of airflow and alv, br and CW indicate the alveoli, bronchi and chest wall, respectively.

A.2.2 Gas transfer

The air flowing back and forth through the lung during inspiration and expiration consists of a mixture of different gases. The most important gases in the respiratory system are O_2 and CO_2. O_2 and CO_2 are exchanged through diffusion between the alveoli and pulmonary capillaries. The fractions of O_2 and CO_2 in the atmosphere are 20.95% and 0.03%, respectively. The fraction of inspired CO_2 ($FiCO_2$) leaving the mechanical ventilator is equal to the fraction of CO_2 in the atmosphere. The FiO_2 from the ventilator can be set between 21% and 100%.

Air leaving the mechanical ventilator is dry. A humidifier moisturises the air before the air enters the patient. Air humidification influences the FiO_2 and $FiCO_2$ and is implemented by multiplying the FiO_2 and $FiCO_2$ with the humidity factor:

$$\frac{P_{atm} - p_{H2O}}{P} = \frac{760 - 47}{760}, \tag{A.15}$$

where P_{atm} is the atmospheric pressure (mmHg) and p_{H_2O} is the partial pressure of water at sea level (mmHg) [36]. The functions for the change in fractions in the two compartments have been derived from:

$$c = f \cdot V, \tag{A.16}$$

where c is the content (L) of a specific gas in a compartment, f is the fraction of a specific gas (fraction) in a compartment and V is the total volume in a compartment (L) [32]. Because f and V are both functions, the derivative of c was acquired by applying the product rule to Equation (A.16):

$$c' = f' \cdot V + f \cdot V'. \tag{A.17}$$

The content change c' can be approached in different ways. The content flowing from the bronchi to the alveoli is the same as the content leaving the bronchi and as the content enters the alveoli.

$$c'_{br \to alv} = f'_{br \to alv} \cdot V_{alv} + f_{alv} \cdot V'_{br \to alv} \tag{A.18}$$

shows the perspective of content entering the alveoli. Because all the air originates from the bronchi, Equation (A.18) can be rewritten as

$$c'_{br \to alv} = f'_{br} \cdot V_{br} + f_{br} \cdot V'_{br \to alv}. \tag{A.19}$$

If air flows out of the bronchi, the fraction does not change in the bronchi [34]. Therefore, $f_{LW} = 0$ and Equation (A.19) can be rewritten as:

$$c'_{br \to alv} = f_{br} \cdot V'_{br \to alv}. \tag{A.20}$$

Equation (A.18) and Equation (A.20) could be equated to each other and led to:

$$f_{br} \cdot V'_{br \to alv} = f'_{br \to alv} \cdot V_{alv} + f_{alv} \cdot V'_{br \to alv}, \tag{A.21}$$

which could be rewritten as:

$$f'_{br\to alv} = (f_{br} - f_{alv}) \cdot \frac{V'_{br\to alv}}{V_{alv}}, \tag{A.22}$$

and generalised as:

$$f'_{a\to b} = (f_a - f_b) \cdot \frac{V'_{a\to b}}{V_b}. \tag{A.23}$$

The fractions, and later also the partial pressures, of O_2 and CO_2 have been implemented in the model as a vector. Therefore, f_{alv} contains the fractions of both O_2 and CO_2 in the alveoli, like:

$$f_{alv} = \begin{bmatrix} f_{alv,O_2} \\ f_{alv,CO_2} \end{bmatrix}. \tag{A.24}$$

Equation (A.25) to Equation (A.29) have been implemented in the model:

$$f'_{br} = f'_{vent\to br} + f'_{alv\to br}, \tag{A.25}$$
$$f'_{alv} = f'_{br\to alv} - f'_{alv\to PC}, \tag{A.26}$$

$$f'_{vent\to br} = (f_{vent} - f_{br}) \cdot \frac{V'_{vent\to br}}{V_{br}}, \tag{A.27}$$
$$f'_{alv\to br} = (f_{alv} - f_{br}) \cdot \frac{V'_{alv\to br}}{V_{br}}, \tag{A.28}$$
$$f'_{br\to alv} = (f_{br} - f_{alv}) \cdot \frac{V'_{br\to alv}}{V_{alv}}, \tag{A.29}$$

where PC is the pulmonary capillaries compartment. Only $f'_{alv\to PC}$ and $V'_{alv\to PC}$ still had to be defined. Equation (A.16) could be rewritten as:

$$f = \frac{c}{V}. \tag{A.30}$$

Applying the quotient rule to Equation (A.30) resulted in:

$$f' = \frac{c' \cdot V - c \cdot V'}{V^2}. \tag{A.31}$$

Application of Equation (A.31) to the fractional change from the alveoli to the pulmonary capillaries under the assumption that $V' = 0$ resulted in:

$$f'_{alv\to PC} = \frac{c'_{alv\to PC}}{V_{alv}}. \tag{A.32}$$

The assumption that the total volume change over the alveolar wall consists of the content changes of O_2 and CO_2 resulted in:

$$V'_{alv\to PC} = \sum (c'_{alv\to PC,O2} + c'_{alv\to PC,CO2}) \tag{A.33}$$

Before being used as input for the pulmonary gas exchange submodule, the results from the respiratory mechanics and gas transfer are combined. First, the pressures were converted from relative to absolute and pressure units were converted from cmH_2O to kilopascal (kPa):

$$1\ cmH_2O = 0.0980638\ kPa. \tag{A.34}$$

Pressures in the respiratory system are often expressed in cmH_2O, while pressures in the circulatory system are often expressed in mmHg or kPa. kPa has a more direct relationship to barometric pressure, whereas mmHg has a more direct relationship to blood pressure. Therefore, the unit kPa is used in this model. In addition, the absolute pressure and gas fractions were multiplied to calculate the partial pressures of O_2 and CO_2:

$$p_{alv} = f_{alv} \cdot P_{alv}, \tag{A.35}$$

where p_{alv} is the partial alveolar pressure of O_2 and CO_2 (kPa), P_{alv} is the absolute pressure in the alveoli (kPa), and f_{alv} contains the fractions of O_2 and CO_2.

A.3 Pulmonary gas exchange submodule

The diffusion of gases over the alveolar membrane is driven by a difference in partial pressures between both sides of the membrane. The diffusion rate between the two compartments is determined by a simplified version of Fick's law [36]. The gas exchange submodule contains diffusion of O_2 and CO_2 between the alveoli to the pulmonary capillaries according to:

$$c'_{alv \to PC} = D \cdot (p_{alv} - p_{PC}), \tag{A.36}$$

where $c'_{alv \to PC}$ is the content change from the alveoli to the pulmonary capillaries (L/s), p_{alv} and p_{PC} are the partial pressures of O_2 and CO_2 in respectively the alveoli and pulmonary capillaries (kPa), and D is the diffusing coefficient (L/kPa·s). The diffusing coefficient is influenced by multiple factors:

$$D = k \cdot \frac{A \cdot s}{a\sqrt{MW}}, \tag{A.37}$$

where A is the area of the membrane, a is the thickness of the membrane, s is the solubility, MW is the molecular weight of the diffusing molecule, and k is a constant that describes the interaction of the gas with the membrane.

A.4 Circulation submodule

The circulation submodule consists of multiple parts: partial pressures, oxygen buffering and oxygen delivery. The partial pressures part contains the circulation of partial pressures of O_2 and CO_2, pO_2 and pCO_2, respectively. This includes the effects of alveolar diffusion in the pulmonary capillaries and metabolism in the systemic capillaries. Oxygen buffering describes the relation between pO_2, SaO_2 and the concentration of bound oxygen. Oxygen buffering also contains calculation of the change in pO_2 in each compartment as a result of binding and unbinding of oxygen to haemoglobin (Hb) molecules. Oxygen delivery is calculated in the compartment before the gas exchange with the body tissue occurs.

The circulation consists of multiple compartments (Figure 2.2). Diffusion occurs between the alveoli and the pulmonary capillaries (PC). Blood flows from PC, through the aorta (Ao) and systemic arteries (SA) to the systemic capillaries (SC). The metabolic rate (MR) affects the gas exchange between the SC and the tissue. Next, blood flows to the pulmonary arteries (PA) and back to the PC. The circulation submodule is complicated by implementing right-to-left shunting. Blood flowing through right-to-left shunts bypass the lungs and therefore contribute to the admixture of deoxygenated blood in the arterial system. Three types of shunting are included. Intrapulmonary shunting ($s1$) develops when blood passes through the lungs but fails to take part in gas exchange. Causes can be alveoli filled with fluid or collapsed alveoli [63]. This is also referred to as a ventilation-perfusion ratio (V/Q) of zero [92].

Right-to-left shunting through the open foramen ovale ($s2$) bypasses pulmonary circulation as blood flows directly from the right to the left atrium. This only occurs when the pressure in the right atrium is bigger than the pressure in the left atrium. For example, in the case of pulmonary hypertension. Right-to-left shunting in

neonates may also occur over the ductus arteriosus ($s3$). In fetal circulation, the ductus arteriosus, and not the pulmonary circulation, transports the majority of the blood in that area of the circulation. After birth air enters the lungs and the alveoli open up, resulting in a pressure drop in the pulmonary circulation. As blood flow chooses the road of least resistance, most of the blood flows now through the pulmonary circulation and not through the ductus arteriosus anymore. The decrease in prostaglandins secretion caused by pO_2 increase helps close the ductus arteriosus [94]. After a few days, the duct is closed. However, an often occurring complication is a patent ductus arteriosus (PDA), where the ductus arteriosus remains open and blood can still flow from right to left while skipping the pulmonary circulation [95]. Blood flowing from $s1$ and $s2$ congregates with the non-shunted blood before entering the aorta. Blood from $s3$ enters the main circulation in the aortic arch (Figure A.3). Compartment Ao1 is pre-ductal, while compartment Ao2 is post-ductal. SpO_2 measurements by pulse-oximetry of the right hand are pre-ductal and of the feet are post-ductal. The SpO_2 saturation in the left hand can be influenced by both the pre-ductal and post-ductal SaO_2 [37]. The MOTP allows for selecting pre- or post-ductal SpO_2 sensor placement. Pre-ductal SpO_2 is derived from compartment Ao1, while post-ductal SpO_2 is derived from compartment Ao2.

A.4.1 Partial pressures

The circulation submodule includes four compartments in which mixing and equilibrating of partial pressures and saturations occurs (PC, Ao1, Ao2, SC). Two compartments are reached without mixing, but with a delay time (SA, PA). The compartments will be discussed one by one.

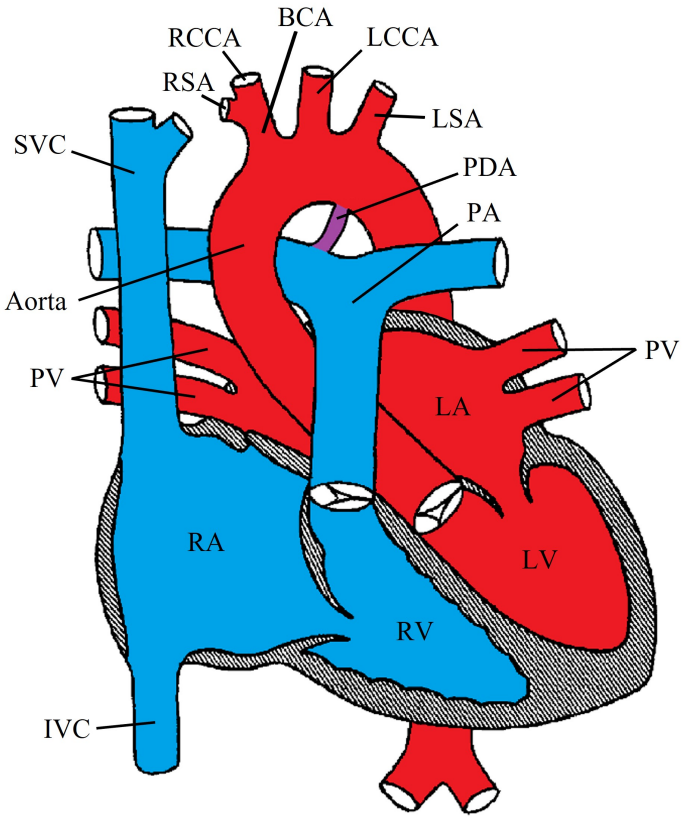

Figure A.3: Schematic overview of the heart, aortic arch and arteries branching from the aortic arch, in the presence of a patent ductus arteriosus. RA: right atrium, RV: right ventricle, LA: left atrium, LV: left ventricle, SVC: superior vena cava, IVC: inferior vena cava, PV: pulmonary vein, PA: pulmonary artery, PDA: patent ductus arteriosus, RSA: right subclavian artery, RCCA: right common carotid artery, BCA: branchiocephalic artery, LCCA: left common carotid artery, LSA: left subclavian artery. The RSA provides the right hand with blood. The LSA provides the left hand and both feet with blood [23, 93].

Pulmonary capillaries The partial pressures in the pulmonary capillaries are influenced by three factors:

$$p'_{PC} = p'_{alv\to PC} + p'_{PA\to PC} - p'_{Hb,PC}, \tag{A.38}$$

where p'_{PC} is the diffusion over the alveolar membrane, $p'_{alv\to PC}$ is the change in partial pressure due to blood flow that renews the capillary blood, and $p'_{Hb,PC}$ is the association of O_2 to Hb. The first two factors are discussed in this section and the third factor is explained in Appendix A.4.2.

We defined the amount of dissolved gas in the blood using a rewritten form of Henry's law:

$$c = p \cdot s \cdot Q, \tag{A.39}$$

where c is the gas content in the blood (L), p is the partial pressure in the blood (kPa), s is the solubility of the gas (L/L·kPa), and Q is the blood volume (L) [36]. Relating the change in partial pressure to the change in gas content in the case of a constant volume resulted in:

$$p' = \frac{c'}{s \cdot Q}. \tag{A.40}$$

For the pulmonary capillaries compartment, this resulted in:

$$p'_{alv\to PC} = \frac{c'_{alv\to PC}}{s \cdot Q_{PC}}. \tag{A.41}$$

The rate at which the partial pressure changes as a result of blood entering the capillaries is defined by:

$$p'_{PA\to PC} = (p_{PA} - p_{PC}) \cdot \frac{(1 - s1 - s2 - s3) \cdot Q'_{CO}}{Q_{PC}}, \tag{A.42}$$

where p_{PA} and p_{PC} are partial pressures in respectively PA and PC (kPa), Q'_{CO} is the blood flow (L/s), and Q_{PC} is the blood volume in the PC compartment (L). The blood flow is corrected by the present shunts, derived from Figure 2.2. Equation (A.42) is comparable to Equation (A.23), except for the differences V' and Q', V and Q, and f and p. Circulatory control is absent and the cardiac output is assumed to be constant and pre-set in the model [25, 29, 96]. The cardiac output is based on the measured heart rate from the patient and the assumed stroke volume (SV).

Aortic arch part 1 The partial pressures in the first part of the aortic arch are influenced by three factors: 1) blood flow from PC to Ao1, 2) blood flow from PA to Ao1 and 3) association of O_2 to Hb:

$$p'_{Ao1} = p'_{PC\to Ao1} + p'_{PA\to Ao1} - p'_{Hb,Ao1}. \tag{A.43}$$

The same argumentation as with the pulmonary capillaries led to:

$$p'_{PC\to Ao1} = (p_{PC} - p_{Ao1}) \cdot \frac{(1 - s1 - s2 - s3) \cdot Q'_{CO}}{Q_{Ao1}}, \tag{A.44}$$

and

$$p'_{PA\to Ao1} = (p_{PA} - p_{Ao1}) \cdot \frac{(s1 + s2) \cdot Q'_{CO}}{Q_{Ao1}}. \tag{A.45}$$

Aortic arch part 2 The partial pressures in the second part of the aortic arch are influenced by three factors: 1) blood flow from Ao1 to Ao2, 2) blood flow from PA to Ao2 and 3) association of O_2 to Hb:

$$p'_{Ao2} = p'_{Ao1\to Ao2} + p'_{PA\to Ao2} - p'_{Hb,Ao2}. \tag{A.46}$$

The same argumentation as with the pulmonary capillaries led to:

$$p'_{Ao1\rightarrow Ao2} = (p_{Ao1} - p_{Ao2}) \cdot \frac{(1 - s3) \cdot Q'_{CO}}{Q_{Ao2}}, \tag{A.47}$$

and

$$p'_{PA\rightarrow Ao1} = (p_{PA} - p_{Ao2}) \cdot \frac{s3 \cdot Q'_{CO}}{Q_{Ao2}}. \tag{A.48}$$

Systemic arteries The blood which passed Ao2 flows through the main arteries to the systemic arteries. This was implemented in the model as a time delay:

$$dt_{art} = \frac{0.216 \cdot Q_{tot}}{Q'_{CO}}, \tag{A.49}$$

where 0.216 is the fraction of blood volume in the arterial system [36], Q_{tot} is the total blood volume (L) and Q'_{CO} is the cardiac output (L/s).

Systemic capillaries The partial pressures in the systemic capillaries are influenced by three factors: 1) metabolism, 2) blood flow that renews the capillary blood and 3) association of O_2 to Hb:

$$p'_{SC} = p'_{SC,met} + p'_{SA\rightarrow SC} - p'_{Hb,SC}. \tag{A.50}$$

The same argumentation as with the pulmonary capillaries led to:

$$p'_{SC,met} = \frac{c'_{met}}{s \cdot Q_{SC}}, \tag{A.51}$$

and

$$p'_{SA\rightarrow SC} = (p_{SA} - p_{SC}) \cdot \frac{Q'_{CO}}{Q_{SC}}. \tag{A.52}$$

Pulmonary arteries The blood which passed the systemic capillaries flows through the venous system to the pulmonary arteries. This was implemented in the model as a time delay:

$$dt_{ven} = \frac{0.666 \cdot Q_{tot}}{Q'_{CO}}, \tag{A.53}$$

where 0.666 is the fraction of blood volume in the venous system [36], Q_{tot} is the total blood volume (L) and Q'_{CO} is the cardiac output (L/s).

A.4.2 Oxygen buffering

The oxygen buffering part models the change in the level of free O_2 and O_2 bound to Hb ($p'_{O2,Hb}$). O_2 binds to Hb as an effective way to transport a greater amount of O_2. The SaO_2 describes the percentage of Hb which is bound to O_2 and depends on the pO_2. This relation is called the oxygen dissociation curve (ODC) and has an S-shape (Figure A.4). The concentration bound O_2 ($C_{O_2,Hb}$) can also be related to the ODC if the level of Hb is known. The ODC is influenced by multiple factors, e.g. temperature, pH, pCO_2, fraction of fetal Hb (xHbF) and 2,3-diphosphoglycerate. The influence of xHbF on the ODC has been modelled in the model. The other factors are assumed to be stable. Oxygen buffering is based on an integrating controller and has the same form as Equations (A.23), (A.36) and (A.42):

$$change = (wanted\ value - measured\ value) \cdot amplifier, \tag{A.54}$$

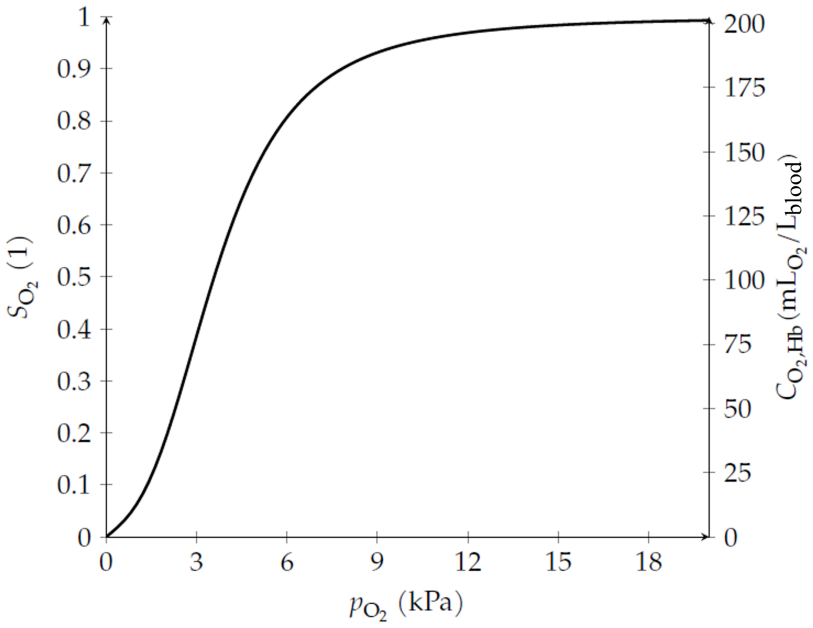

Figure A.4: A normal haemoglobin-saturation curve for adult Hb. The oxygen saturation (SO_2) is given in this model as a fraction, where usually the percentage is used. The right y-axis shows the concentration of oxygen bound to haemoglobin in a haemoglobin concentration of 15 g/dL. Oxygen binding is slow at very low pO_2 and accelerates between 1 kPa and 2 kPa. The saturation hardly increases above SO_2 = 9 kPa [32].

and can be written as:

$$C'_{O_2,Hb} = (p_{O_2} - p_{O_2,Hb}) \cdot k_{O_2-binding}, \tag{A.55}$$

where $C'_{O_2,Hb}$ is the change in concentration of O_2 bound to Hb. p_{O_2} is the updated oxygen partial pressure, which is therefore the wanted value. $p_{O_2,Hb}$ is the oxygen partial pressure corresponding to the SO_2, as defined by the ODC. $k_{O_2-binding}$ is the binding speed. The value for $k_{O_2-binding}$ was chosen so the oxygen buffering was faster than the diffusion speed so the O_2-binding does not lack behind the diffusion rate.

The result of this integrating controller is:

- If the new p_{O_2} is higher than the $p_{O_2,Hb}$ which corresponds to the current SaO_2, this results in more O_2 binding ($C'_{O_2,Hb}$ is positive).
- If the new p_{O_2} is lower than the $p_{O_2,Hb}$ which corresponds to the current SaO_2, this results in less O_2 binding ($C'_{O_2,Hb}$ is negative).
- If the new p_{O_2} is the same as the $p_{O_2,Hb}$ which corresponds to the current SaO_2, this results in constant O_2 binding ($C'_{O_2,Hb}$ is 0).

$p_{O_2,Hb}$ is calculated from S_{O_2} and the ODC. Originally, the ODC was defined as [38]:

$$\begin{cases} S_{O_2} = \dfrac{1}{1 + \dfrac{\frac{8}{3375}\cdot m}{(p_{O_2,Hb})^3 + \frac{8}{3}\cdot p_{O_2,Hb}}} \\ m = \begin{cases} 23400 & \text{for adult Hb} \\ 10400 & \text{for fetal Hb.} \end{cases} \end{cases} \tag{A.56}$$

The equation was adjusted to fetal Hb [48, 97]. Because $p_{O_2,Hb}$ is calculated from S_{O_2}, Equation (A.56) had to be rewritten as its inverse. Nickalls et al. developed a simplified inverse function [39]:

$$\begin{cases} p_{O_2,Hb} = \sqrt[3]{\frac{1}{2}(y_N + \sqrt{y_N^2 + h^2})} + \sqrt[3]{\frac{1}{2}(y_N - \sqrt{y_N^2 + h^2})} \\ y_N = \frac{8}{3375} \cdot m \cdot \frac{S_{O_2}}{1 - S_{O_2}} \\ h^2 = 4 \cdot \frac{8^3}{9} \\ m = \begin{cases} 23400 & \text{for adult Hb} \\ 10400 & \text{for fetal Hb.} \end{cases} \end{cases} \tag{A.57}$$

Pulmonary capillaries The total change in concentration of O_2 bound to Hb is influenced by two factors: 1) blood flow that renews the capillary blood and 2) oxygen buffering:

$$C'_{O_2,Hb,PC,tot} = C'_{O_2,Hb,PC} + C'_{O_2,Hb,PA \to PC}. \tag{A.58}$$

The influence of blood flow is calculated similarly as in Appendix A.4.1:

$$C'_{O2,Hb,PA \to PC} = (C'_{O2,Hb,PA} - C'_{O2,Hb,PC}) \cdot \frac{(1 - s1 - s2 - s3) \cdot Q'_{CO}}{Q_{PC}}. \tag{A.59}$$

Rewriting Equation (A.55) to the pulmonary capillaries gave:

$$C'_{O_2,Hb,PC} = (p_{O_2} - p_{O_2,Hb}) \cdot k_{O_2-binding}, \tag{A.60}$$

where p_{O_2} was derived from the partial pressure part, and $p_{O_2,Hb}$ was calculated based on Equation (A.57). S_{O_2} from Equation (A.57) can be calculated from:

$$S_{O_2,PC} = \frac{C_{O_2,Hb,PC}}{C_{O_2,Hb,max}}, \tag{A.61}$$

where

$$C_{O_2,Hb,PC} = \int C'_{O_2,Hb,tot}, \tag{A.62}$$

and

$$C_{O_2,Hb,max} = Hb_{O_2,capacity} \cdot Hb, \tag{A.63}$$

with $Hb_{O_2,capacity}$ in $\mathrm{ml_{O_2}/g_{Hb}}$, and Hb in $\mathrm{g_{Hb}/dL_{blood}}$. The change in p_{O_2} due to oxygen association and dissociation ($p'_{O2,Hb}$) is calculated by:

$$p'_{O_2,Hb,PC} = \frac{C'_{O_2,Hb,PC}}{s_{O_2}}, \tag{A.64}$$

where s_{O_2} is the solubility of O_2 (L/L·kPa). Equation (A.64) is used as input in the partial pressure part (Appendix A.4.1) as:

$$p'_{Hb,PC} = \begin{bmatrix} p'_{O_2,Hb,PC} \\ p'_{CO_2,Hb,PC} \end{bmatrix} = \begin{bmatrix} p'_{O_2,Hb,PC} \\ 0 \end{bmatrix}. \tag{A.65}$$

xHbF is a model parameter which influenced the size of the ODC shift by influencing the percentage of the ODC based on adult and fetal values for m in Equation (A.57). An increased xHbF resulted in a shift to the left.

Other compartments Calculations for the other compartments were performed similarly. The influence of blood flow is calculated similarly as in Appendix A.4.1 and the influence of oxygen buffering is calculated as described for the pulmonary capillaries.

A.4.3 Oxygen delivery

The SaO_2 reflects how much of the haemoglobin is bound to O_2, but is not a good measure of the amount of O_2 arriving at the tissues. The oxygen delivery d_{O2} (L_{O_2}/min) is a measure of the amount of oxygen which arrives at your organs. The d_{O2} is a sum of the amount of oxygen dissolved in a litre of blood and the amount of oxygen bound to haemoglobin in a litre of blood, multiplied together by cardiac output [40]:

$$d_{O_2} = (C_{O_2,Hb,SA} + p_{O_2,SA} \cdot s_{O_2}) \cdot Q'_{CO} \cdot 60, \tag{A.66}$$

A.5 SpO_2 sensor

The SpO_2 sensor block simulates the dynamic system of an SpO_2 sensor. The model is based on data acquired by step tests on the real hardware of the Masimo RD SET Neo SpO_2 sensor. The data was acquired using the OxSim optical SpO_2 pulse oximeter simulator [98]. SaO_2 values were set on the OxSim and the response of the SpO_2 sensor was measured and modelled as first-order plus dead time model:

$$y'(t) = \frac{-y(t)}{\tau} + \frac{\mathrm{K}}{\tau} \cdot u(t - \Theta), \tag{A.67}$$

where $y(t)$ is the output signal SpO_2, $u(t)$ is the input signal SaO_2, K is the gain, τ is the time constant, and Θ is the dead time. In addition, a specific bias per SpO_2 output value was added based on the measurements (Figure A.5). The measurements were performed on one Masimo RD SET Neo SpO_2 sensor.

The SaO_2 on which the SpO_2 is based can differ depending on the location of the pulse oximeter. The MOTP includes an option to select whether the pulse oximeter is placed pre- or post-ductally. Pre-ductal SpO_2 is derived from compartment Ao1 and post-ductal SpO_2 is derived from compartment Ao2.

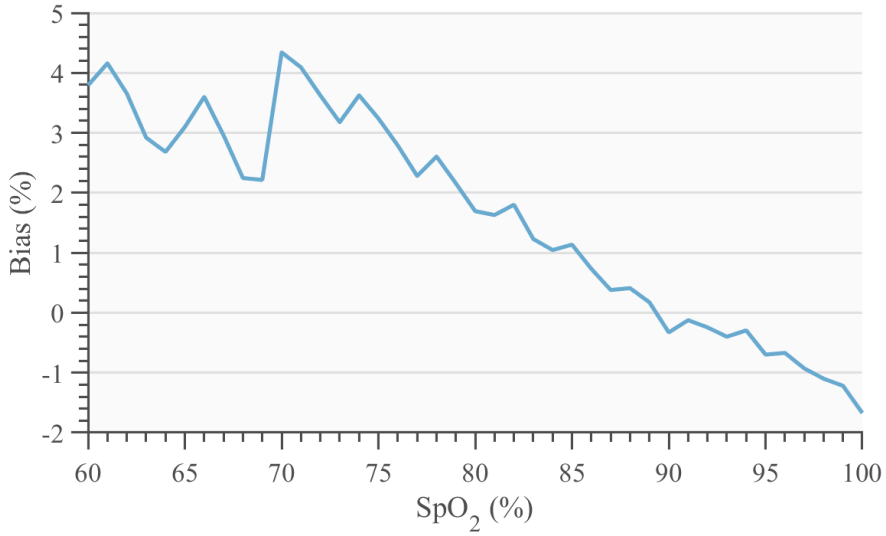

Figure A.5: Additional bias of the Masimo RD SET Neo SpO_2 sensor, apart from the first-order plus deadtime model. Bias values were measured for SpO_2 output values between 60 and 100%.

B Valid FiO_2 steps

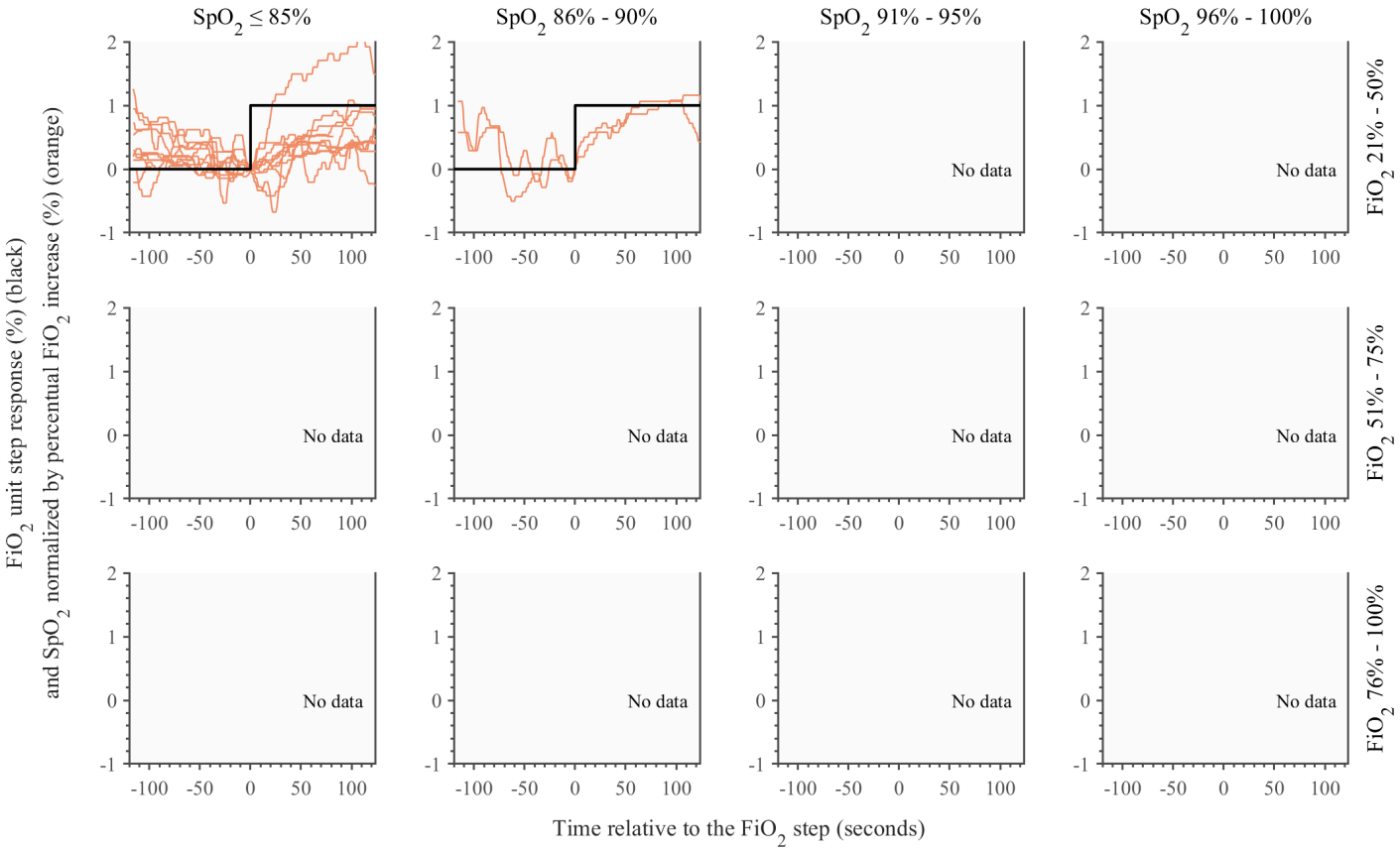

Figure B.1: The corrected and normalised SpO_2 responses for all valid FiO_2 increasing steps of patient 1. The SpO_2 signal is corrected by the initial SpO_2 signal at the moment of the FiO_2 step and normalised by the percentage FiO_2 step (the FiO_2 step size expressed as percentage of the initial FiO_2 value before the FiO_2 change). The steps have been categorised based on initial SpO_2 and FiO_2 values at the moment of the step.

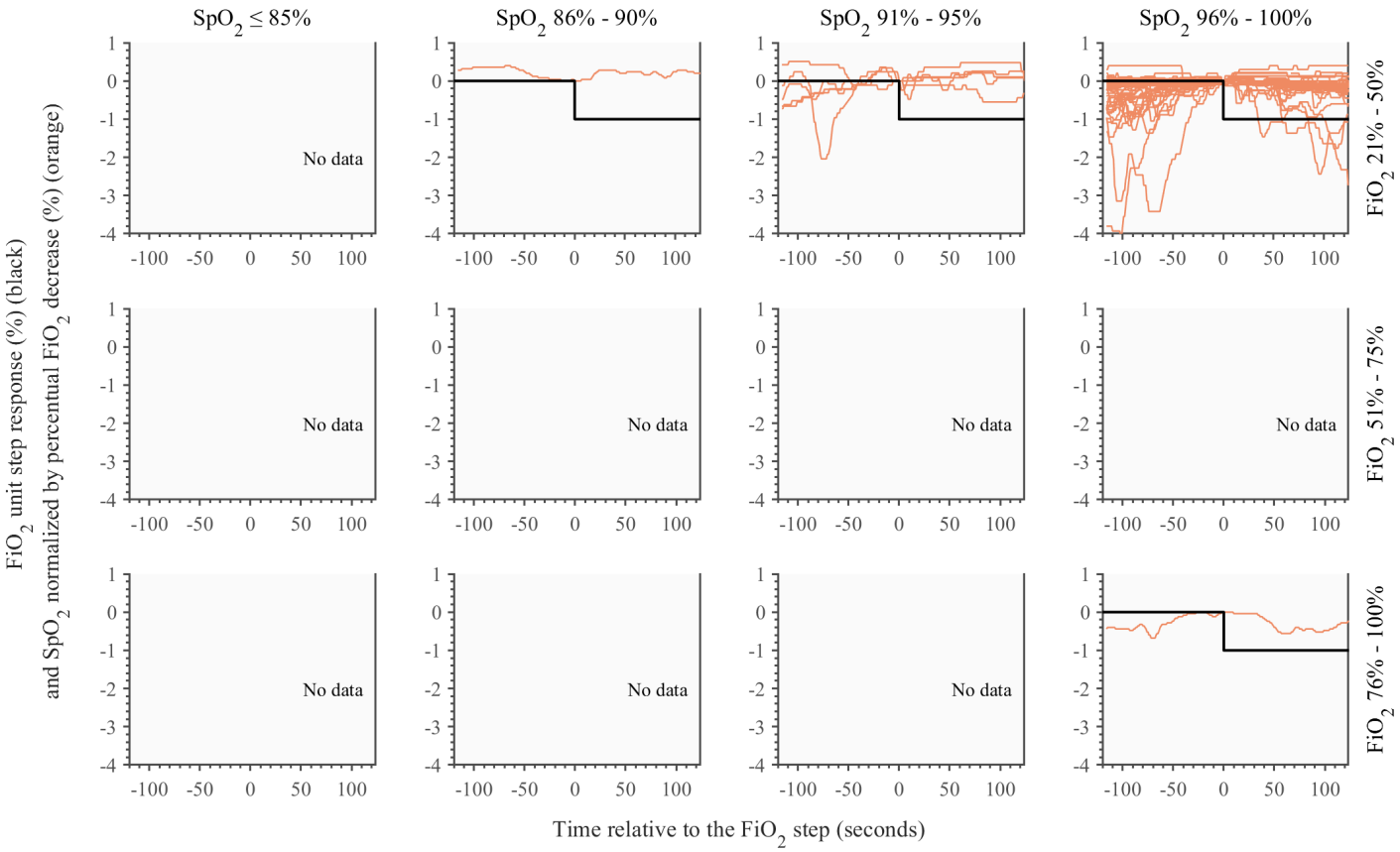

Figure B.2: The corrected and normalised SpO_2 responses for all valid FiO_2 decreasing steps of patient 1. The SpO_2 signal is corrected by the initial SpO_2 signal at the moment of the FiO_2 step and normalised by the percentage FiO_2 step (the FiO_2 step size expressed as percentage of the initial FiO_2 value before the FiO_2 change). The steps have been categorised based on initial SpO_2 and FiO_2 values at the moment of the step.

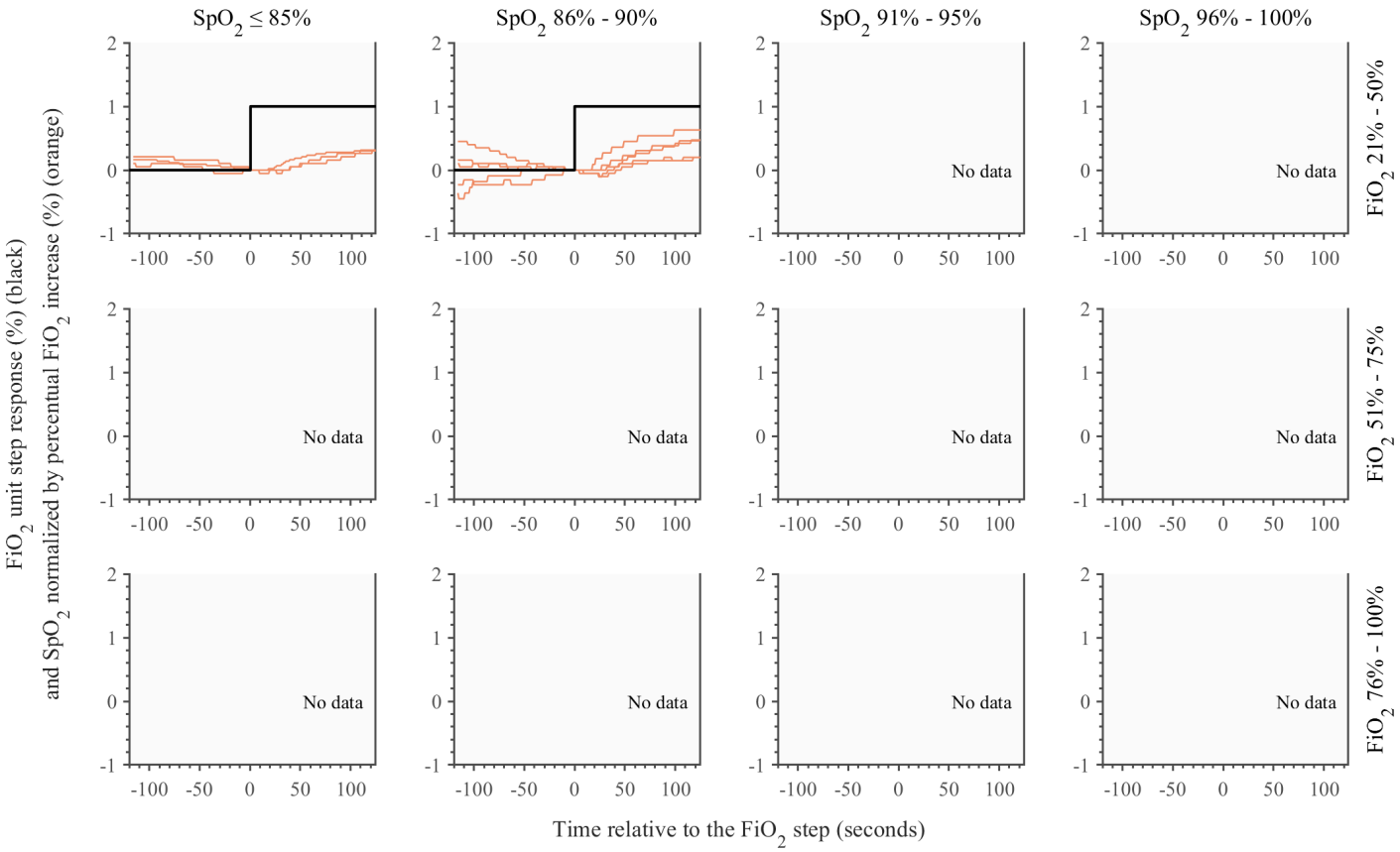

Figure B.3: The corrected and normalised SpO_2 responses for all valid FiO_2 increasing steps of patient 2. The SpO_2 signal is corrected by the initial SpO_2 signal at the moment of the FiO_2 step and normalised by the percentage FiO_2 step (the FiO_2 step size expressed as percentage of the initial FiO_2 value before the FiO_2 change). The steps have been categorised based on initial SpO_2 and FiO_2 values at the moment of the step.

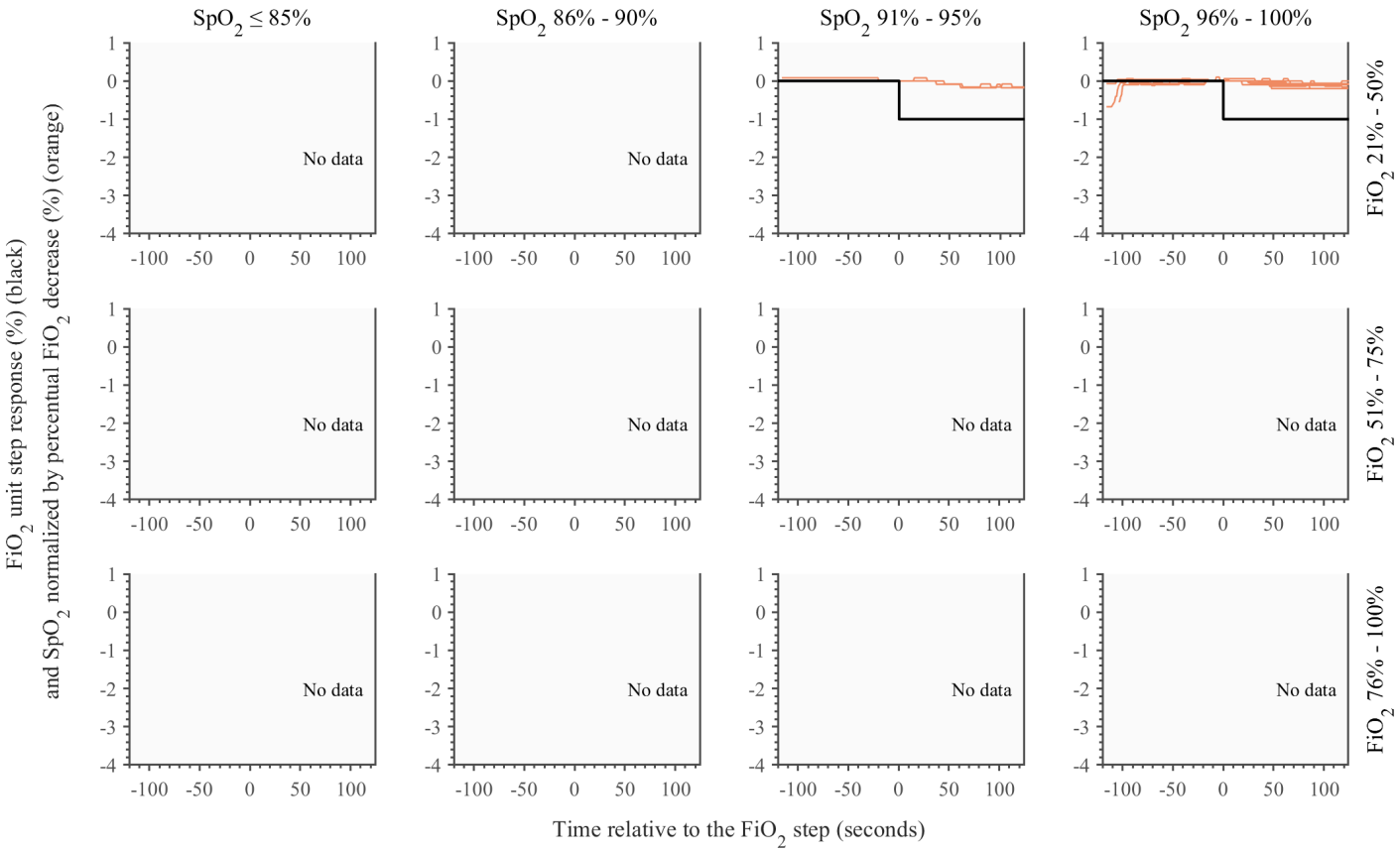

Figure B.4: The corrected and normalised SpO_2 responses for all valid FiO_2 decreasing steps of patient 2. The SpO_2 signal is corrected by the initial SpO_2 signal at the moment of the FiO_2 step and normalised by the percentage FiO_2 step (the FiO_2 step size expressed as percentage of the initial FiO_2 value before the FiO_2 change). The steps have been categorised based on initial SpO_2 and FiO_2 values at the moment of the step.

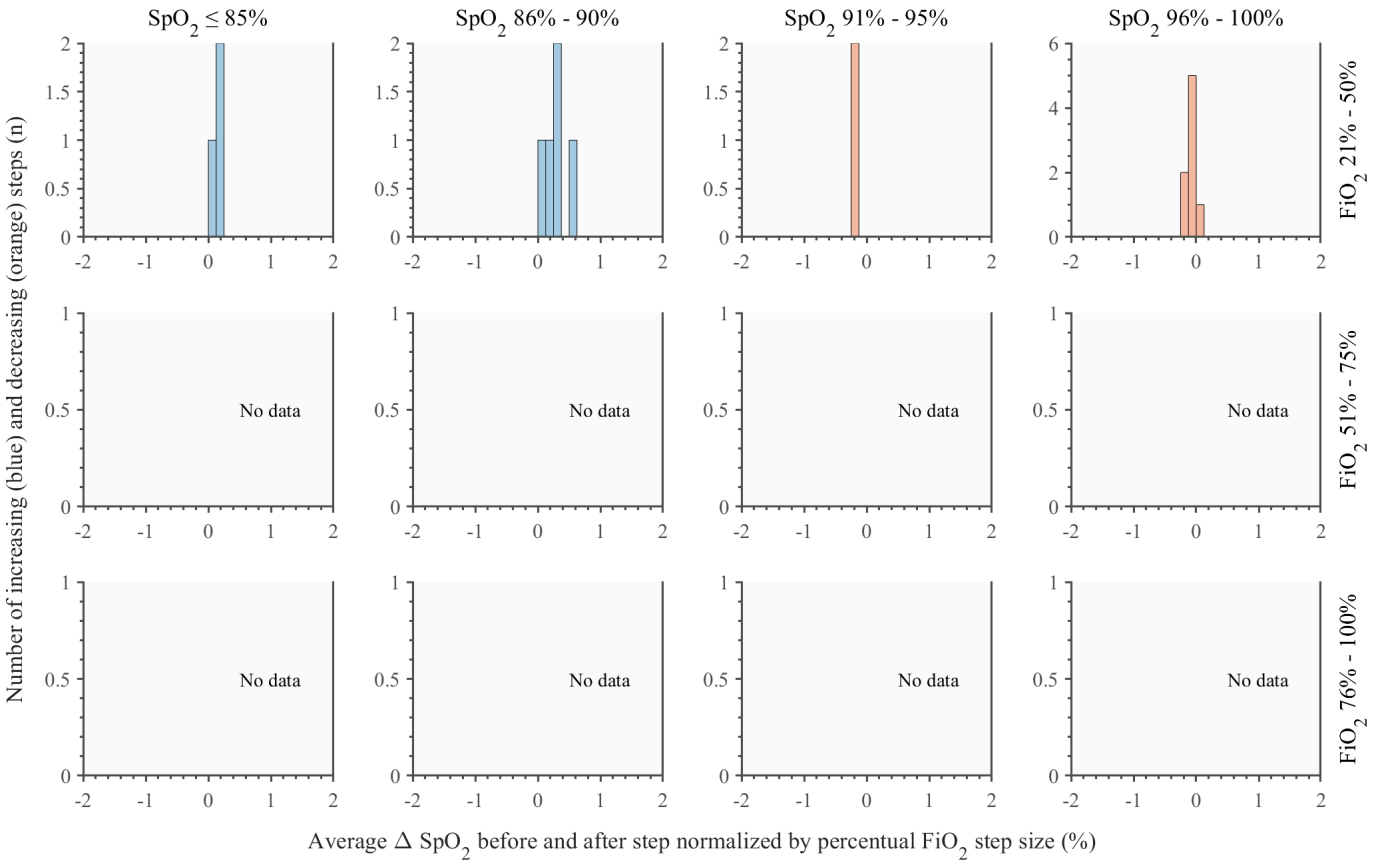

Figure B.5: Distribution of Δ SpO_2 for all valid increasing and decreasing FiO_2 steps of patient 2. Δ SpO_2 is the difference between the average SpO_2 before and after the FiO_2 change, normalised by the percentage FiO_2 step size (the FiO_2 step size expressed as percentage of the initial FiO_2 value before the FiO_2 change). The steps have been categorised based on initial SpO_2 and FiO_2 values at the moment of the FiO_2 change.

C Model calibration

Table C.1: The measured variable parameters of the used measurements for model calibration of patient 2. Parameters above the grey line are input parameters for the MOTP. Hb and xHbF are parameters measured in the blood gas of the patient and do not differ before and after the FiO_2 change. Parameters under the grey line are measured patient variables and used to check the model output. The total Vt is used as an input parameter for the MOTP and the relative Vt per kg is used to check the model output. M1: measurement 1, M2: measurement 2.

		Increase				Decrease			
		M1		M2		M1		M2	
Parameter	Unit	Before	After	Before	After	Before	After	Before	After
FiO_2	%	23	26	21	25	27	21	28	21
$P_{support}$	cmH_2O	9	9	8	11	9	9	9	9
PEEP	cmH_2O	6	6	6	6	6	6	6	6
RR	1/min	60	60	72	82	65	64	63	61
I:E	–	1:1.9	1:1.9	1:2.4	1:2.4	1:1.9	1:1.9	1:1.9	1:1.9
Vt	mL	7.6	7.3	10.2	10.8	8.2	9.0	7.7	7.5
HR	bpm	177	175	194	192	190	192	194	192
Hb	g/dL	12.2	12.2	13.1	13.1	11.0	11.0	11.0	11.0
xHbF	–	0.51	0.51	0.51	0.51	0.51	0.51	0.51	0.51
SpO_2	%	88.6	93.1	86.0	91.0	98.0	96.0	97.3	95.1
Vt	mL/kg	5.8	5.6	7.8	8.3	6.3	6.9	5.9	5.8
C_{Fabian}	$mL(cmH_2O{\cdot}kg)$	0.54	0.54	0.88	0.69	0.61	0.69	0.57	0.59
R_{Fabian}	$cmH_2O{\cdot}s/L$	188	185	155	168	209	203	202	222
Leak	%	7	18	0	0	0	0	0	0

Table C.2: The non-measured variable parameters of the used measurements for model calibration of patient 2. These parameters were used to calibrate the MOTP to a specific FiO_2 change. M1: measurement 1, M2: measurement 2.

		Increase				Decrease			
		M1		M2		M1		M2	
Parameter	Unit	Before	After	Before	After	Before	After	Before	After
R	$cmH_2O{\cdot}s/L$	110	110	90	90	110	110	110	110
C	$mL/(cmH_2O{\cdot}kg)$	0.80	0.78	1.20	0.91	0.88	0.96	0.80	0.78
D_{O_2}	$L/(kPa{\cdot}s{\cdot}kg)$	$1.89{\cdot}10^{-5}$	$1.89{\cdot}10^{-5}$	$1.89{\cdot}10^{-5}$	$1.89{\cdot}10^{-5}$	$2.22{\cdot}10^{-5}$	$2.22{\cdot}10^{-5}$	$2.22{\cdot}10^{-5}$	$2.22{\cdot}10^{-5}$
D_{CO_2}	$L/(kPa{\cdot}s{\cdot}kg)$	$3.78{\cdot}10^{-4}$	$3.78{\cdot}10^{-4}$	$3.78{\cdot}10^{-4}$	$3.78{\cdot}10^{-4}$	$4.45{\cdot}10^{-4}$	$4.45{\cdot}10^{-4}$	$4.45{\cdot}10^{-4}$	$4.45{\cdot}10^{-4}$
SV	mL/kg	1.7	1.7	1.7	1.7	1.7	1.7	1.7	1.7
s1	–	0.31	0.20	0.28	0.26	0	0	0.07	0.04
s2	–	0	0	0	0	0	0	0	0
s3	–	0	0	0	0	0	0	0	0
MR_{O_2}	$mL/(min{\cdot}kg)$	9.0	9.0	9.5	9.5	8.0	8.0	8.0	8.0
MR_{CO_2}	$mL/(min{\cdot}kg)$	7.2	7.2	7.6	7.6	6.4	6.4	6.4	6.4

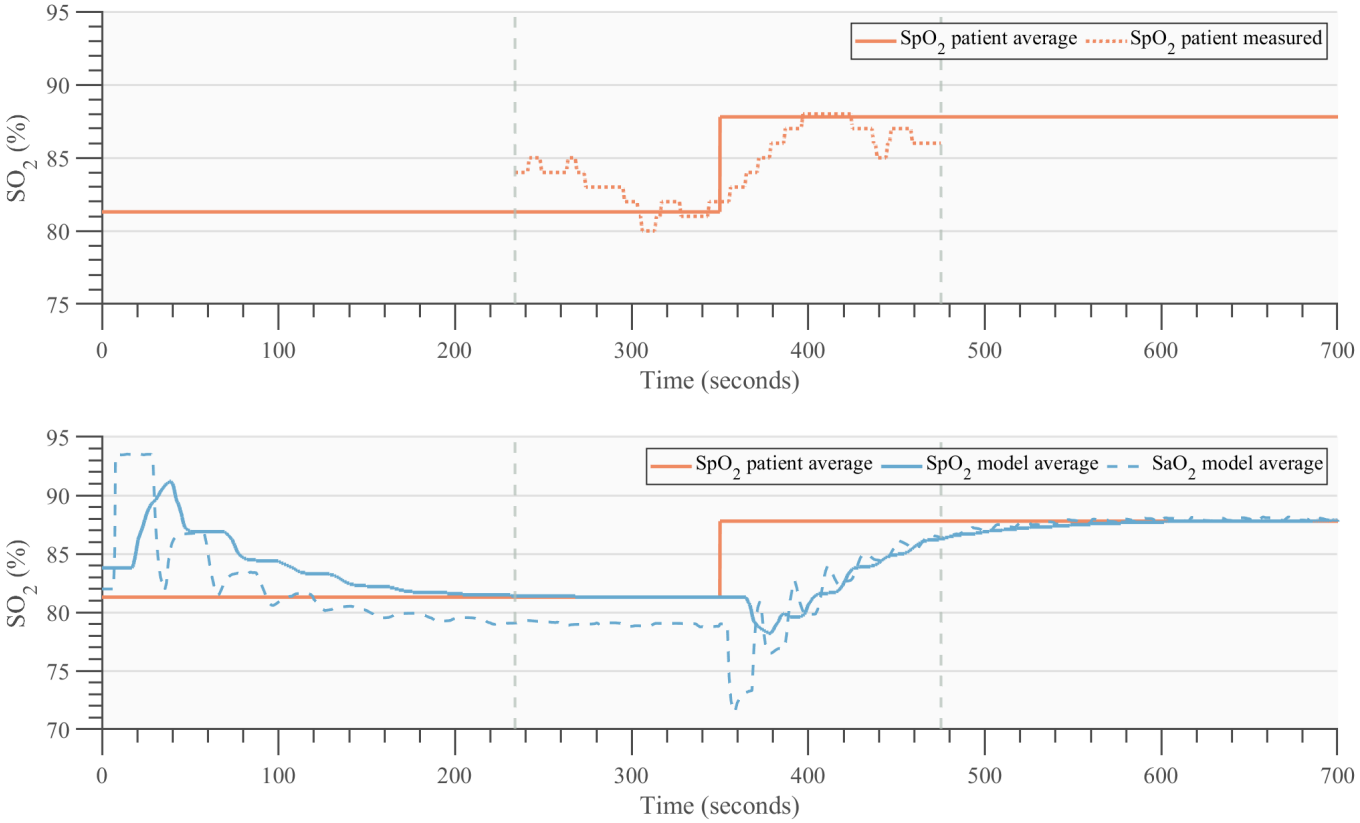

Figure C.1: True and modelled FiO_2-SpO_2 response of calibrated increasing measurement 1 of patient 1. Measured and non-measured variable parameters are set for increasing measurement 1 of patient 1. The FiO_2 changed at time = 350 seconds from 21% to 24%. The upper figure shows the continuous SpO_2 signal extracted from the measured patient data from patient 1. The measured SpO_2 signal was available from 120 seconds before to 120 seconds after the FiO_2 change (grey dashed lines). Based on the signal 20 seconds before and 60 to 80 seconds after the FiO_2 change, the average SpO_2 signal before and after the FiO_2 change was calculated. This average SpO_2 signal was modelled with the complete model. The lower figure shows the SaO_2 output of the MOTP, the SpO_2 output of the SpO_2 sensor system and the average SpO_2 signal of the patient. The sample rate of SaO_2 signal is decreased by a factor of 100 for reduction of the oscillations and clear visualisation.

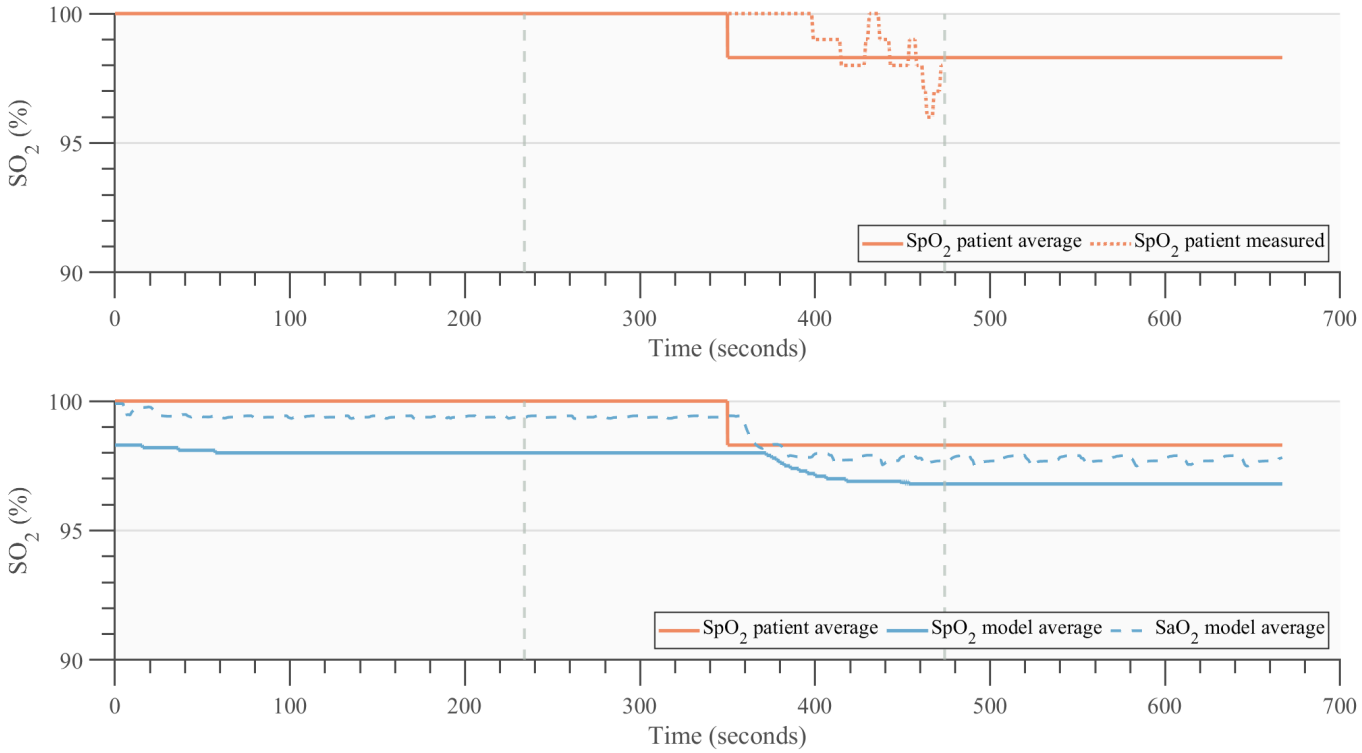

Figure C.2: True and modelled FiO_2-SpO_2 response of uncalibrated decreasing measurement 2 of patient 1. Measured variable parameters are set for decreasing measurement 2 of patient 1. Non-measured variable parameters are set for decreasing measurement 1 of patient 1. The FiO_2 changed at time = 350 seconds from 28% to 21%. The upper figure shows the continuous SpO_2 signal extracted from the measured patient data from patient 1. The measured SpO_2 signal was available from 120 seconds before to 120 seconds after the FiO_2 (grey dashed lines). Based on the signal 20 seconds before and 60 to 80 seconds after the FiO_2, the average SpO_2 signal before and after the FiO_2 change was calculated. This average SpO_2 signal was modelled with the complete model. The lower figure shows the SaO_2 output of the MOTP, the SpO_2 output of the SpO_2 sensor system and the average SpO_2 signal of the patient. The sample rate of SaO_2 signal is decreased by a factor of 100 for reduction of the oscillations and clear visualisation.

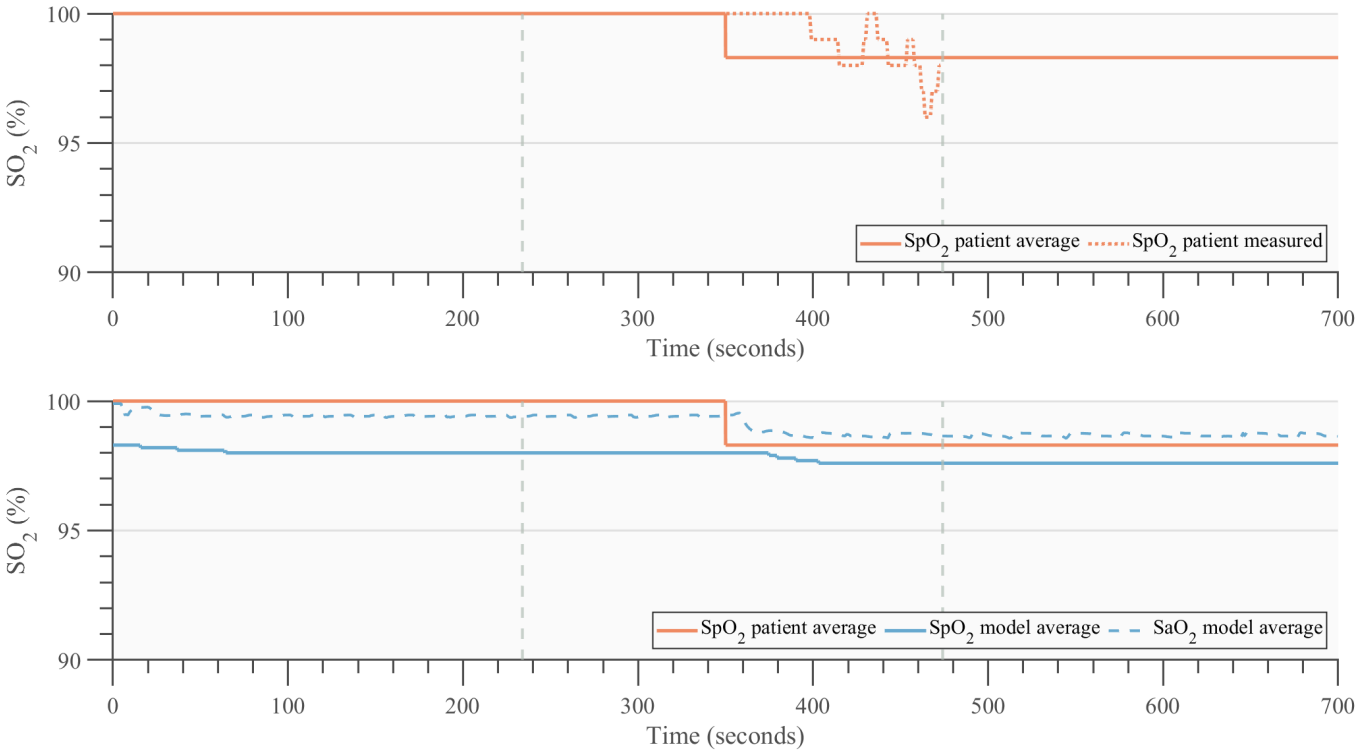

Figure C.3: True and modelled FiO_2-SpO_2 response of calibrated decreasing measurement 2 of patient 1. Measured and non-measured variable parameters are set for decreasing measurement 2 of patient 1. The FiO_2 changed at time = 350 seconds from 28% to 21%. The upper figure shows the continuous SpO_2 signal extracted from the measured patient data from patient 1. The measured SpO_2 signal was available from 120 seconds before to 120 seconds after the FiO_2 change (grey dashed lines). Based on the signal 20 seconds before and 60 to 80 seconds after the FiO_2 change, the average SpO_2 signal before and after the FiO_2 change was calculated. This average SpO_2 signal was modelled with the complete model. The lower figure shows the SaO_2 output of the MOTP, the SpO_2 output of the SpO_2 sensor system and the average SpO_2 signal of the patient. The sample rate of SaO_2 signal is decreased by a factor of 100 for reduction of the oscillations and clear visualisation.

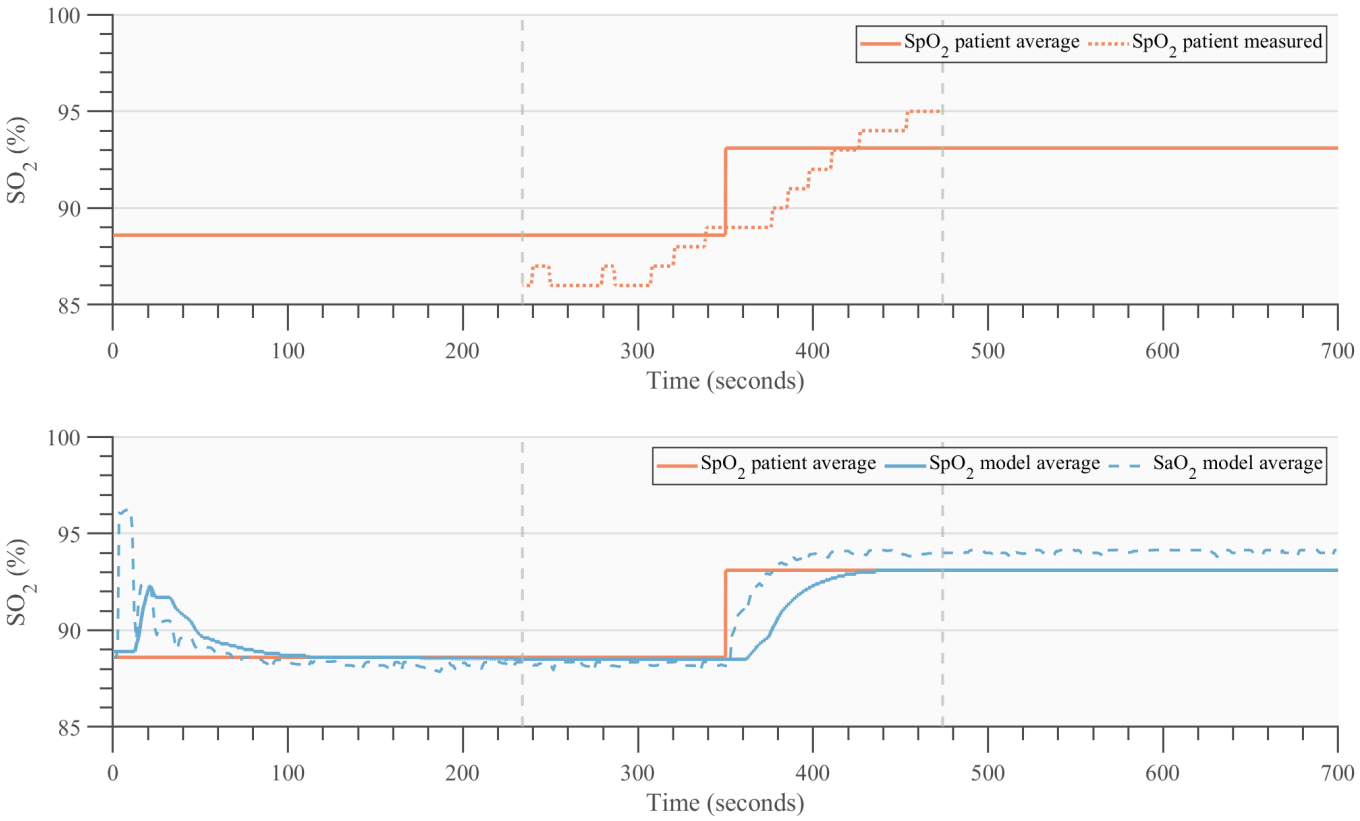

Figure C.4: True and modelled FiO_2-SpO_2 response of calibrated increasing measurement 1 of patient 2. Measured and non-measured variable parameters are set for increasing measurement 1 of patient 2. The FiO_2 changed at time = 350 seconds from 23% to 26%. The upper figure shows the continuous SpO_2 signal extracted from the measured patient data from patient 1. The measured SpO_2 signal was available from 120 seconds before to 120 seconds after the FiO_2 change (grey dashed lines). Based on the signal 20 seconds before and 60 to 80 seconds after the FiO_2 change, the average SpO_2 signal before and after the FiO_2 change was calculated. This average SpO_2 signal was modelled with the complete model. The lower figure shows the SaO_2 output of the MOTP, the SpO_2 output of the SpO_2 sensor system and the average SpO_2 signal of the patient. The sample rate of SaO_2 signal is decreased by a factor of 100 for reduction of the oscillations and clear visualisation.

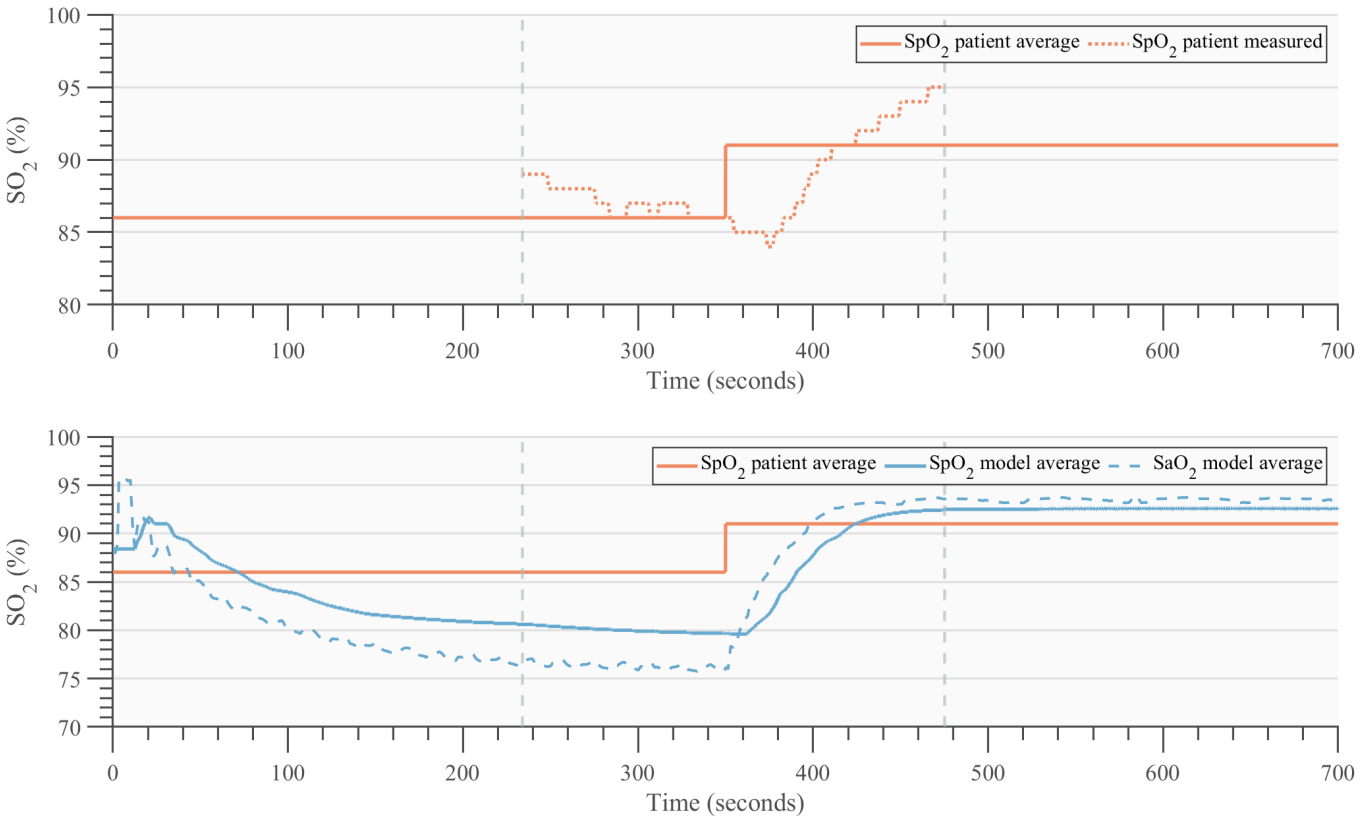

Figure C.5: True and modelled FiO_2-SpO_2 response of uncalibrated increase measurement 2 of patient 2. Measured variable parameters are set for increasing measurement 2 of patient 2. Non-measured variable parameters are set for increasing measurement 1 of patient 1. The FiO_2 changed at time = 350 seconds from 21% to 25%. The upper figure shows the continuous SpO_2 signal extracted from the measured patient data from patient 1. The measured SpO_2 signal was available from 120 seconds before to 120 seconds after the FiO_2 (grey dashed lines). Based on the signal 20 seconds before and 60 to 80 seconds after the FiO_2, the average SpO_2 signal before and after the FiO_2 change was calculated. This average SpO_2 signal was modelled with the complete model. The lower figure shows the SaO_2 output of the MOTP, the SpO_2 output of the SpO_2 sensor system and the average SpO_2 signal of the patient. The sample rate of SaO_2 signal is decreased by a factor of 100 for reduction of the oscillations and clear visualisation.

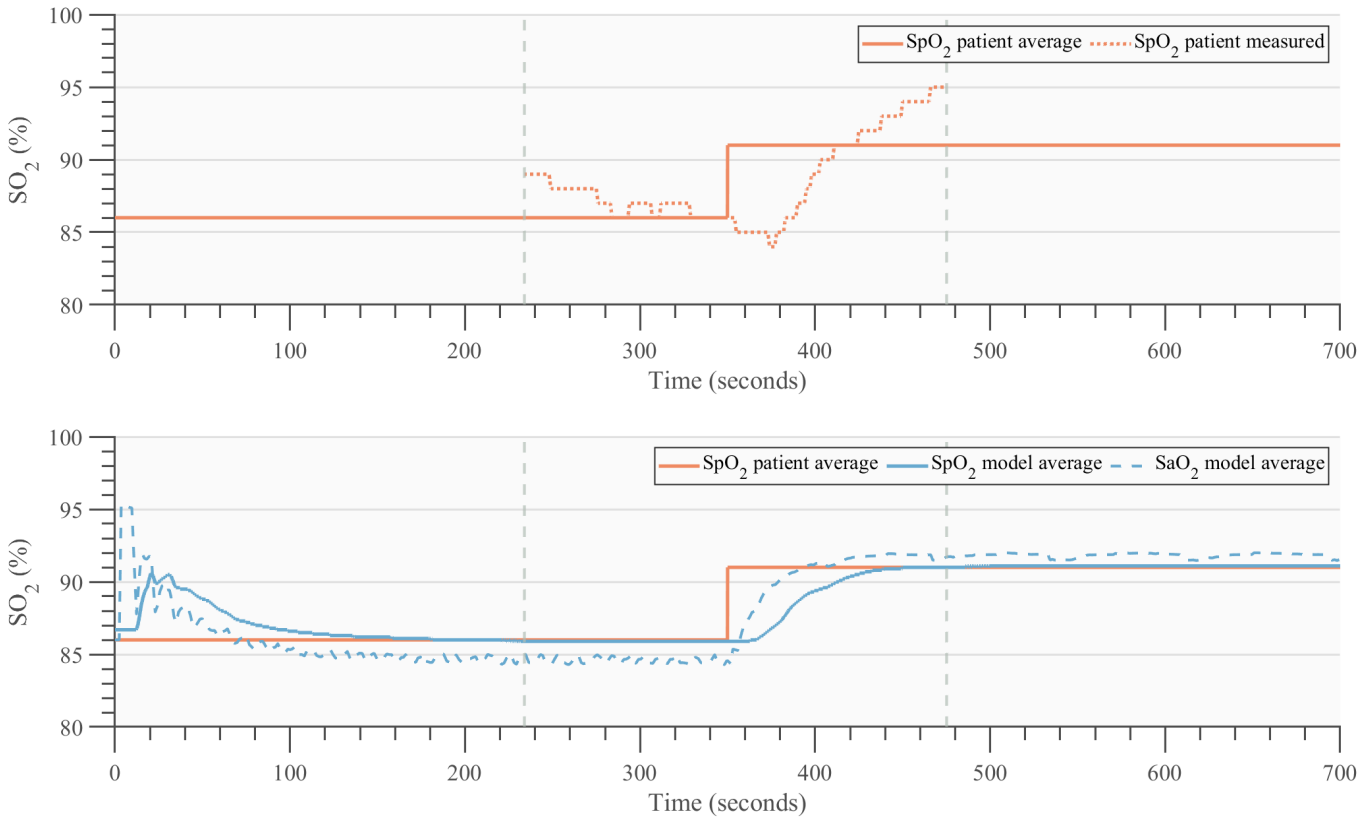

Figure C.6: True and modelled FiO_2-SpO_2 response of calibrated increasing measurement 2 of patient 2. Measured and non-measured variable parameters are set for increasing measurement 2 of patient 2. The FiO_2 changed at time = 350 seconds from 21% to 25%. The upper figure shows the continuous SpO_2 signal extracted from the measured patient data from patient 1. The measured SpO_2 signal was available from 120 seconds before to 120 seconds after the FiO_2 change (grey dashed lines). Based on the signal 20 seconds before and 60 to 80 seconds after the FiO_2 change, the average SpO_2 signal before and after the FiO_2 change was calculated. This average SpO_2 signal was modelled with the complete model. The lower figure shows the SaO_2 output of the MOTP, the SpO_2 output of the SpO_2 sensor system and the average SpO_2 signal of the patient. The sample rate of SaO_2 signal is decreased by a factor of 100 for reduction of the oscillations and clear visualisation.

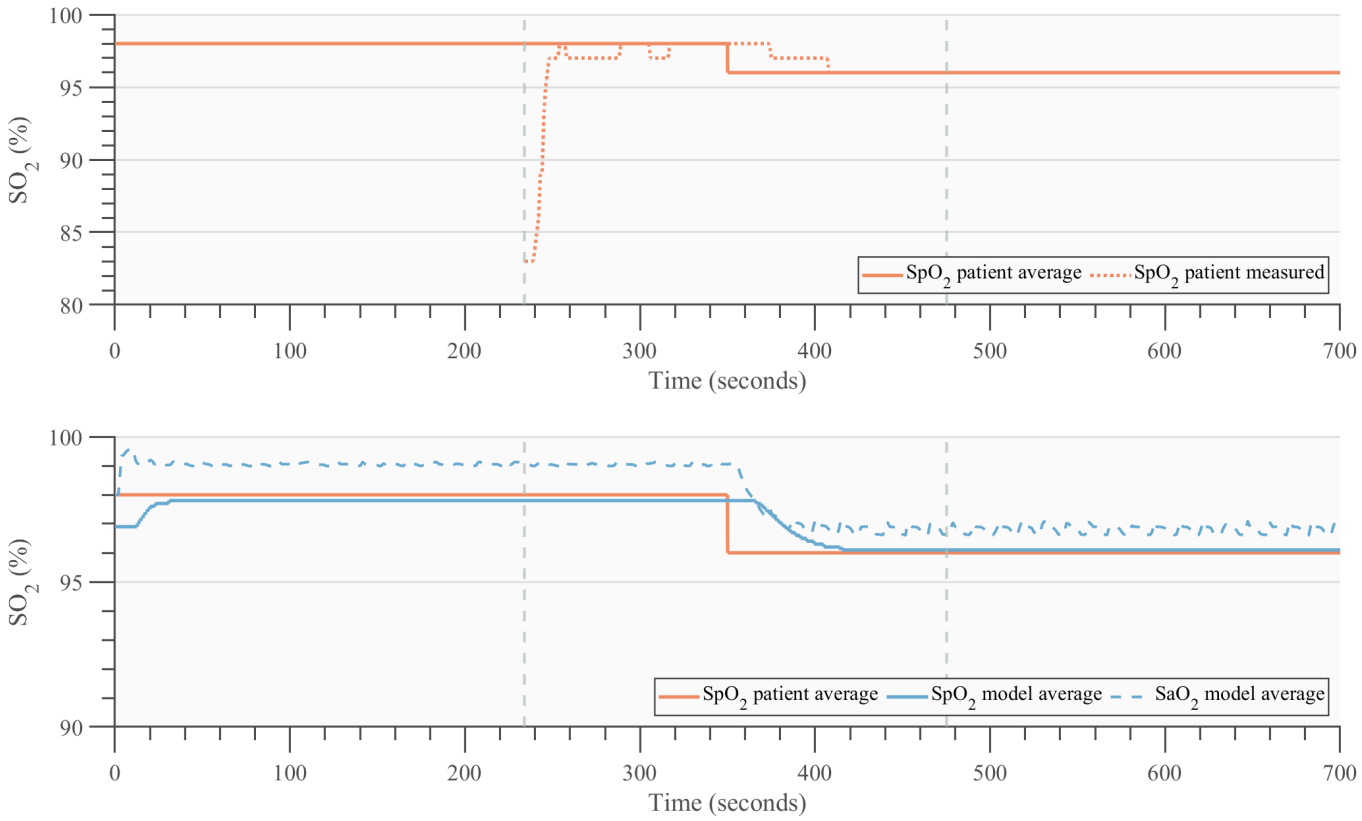

Figure C.7: True and modelled FiO_2-SpO_2 response of calibrated decreasing measurement 1 of patient 2. Measured and non-measured variable parameters are set for decreasing measurement 1 of patient 2. The FiO_2 changed at time = 350 seconds from 27% to 21%. The upper figure shows the continuous SpO_2 signal extracted from the measured patient data from patient 1. The measured SpO_2 signal was available from 120 seconds before to 120 seconds after the FiO_2 change (grey dashed lines). Based on the signal 20 seconds before and 60 to 80 seconds after the FiO_2 change, the average SpO_2 signal before and after the FiO_2 change was calculated. This average SpO_2 signal was modelled with the complete model. The lower figure shows the SaO_2 output of the MOTP, the SpO_2 output of the SpO_2 sensor system and the average SpO_2 signal of the patient. The sample rate of SaO_2 signal is decreased by a factor of 100 for reduction of the oscillations and clear visualisation.

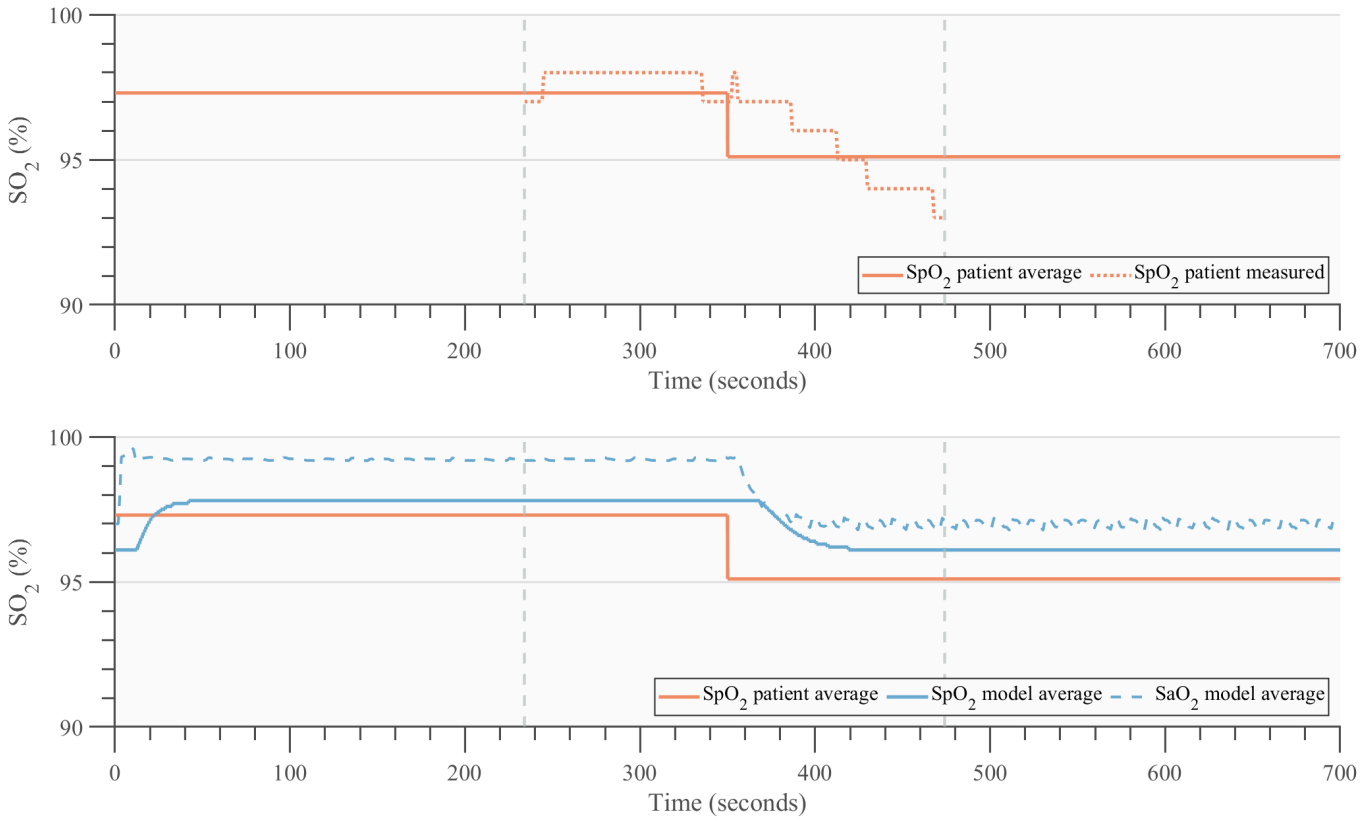

Figure C.8: True and modelled FiO_2-SpO_2 response of uncalibrated decrease measurement 2 of patient 2. Measured variable parameters are set for decreasing measurement 2 of patient 2. Non-measured variable parameters are set for decreasing measurement 1 of patient 1. The FiO_2 changed at time = 350 seconds from 28% to 21%. The upper figure shows the continuous SpO_2 signal extracted from the measured patient data from patient 1. The measured SpO_2 signal was available from 120 seconds before to 120 seconds after the FiO_2 (grey dashed lines). Based on the signal 20 seconds before and 60 to 80 seconds after the FiO_2, the average SpO_2 signal before and after the FiO_2 change was calculated. This average SpO_2 signal was modelled with the complete model. The lower figure shows the SaO_2 output of the MOTP, the SpO_2 output of the SpO_2 sensor system and the average SpO_2 signal of the patient. The sample rate of SaO_2 signal is decreased by a factor of 100 for reduction of the oscillations and clear visualisation.

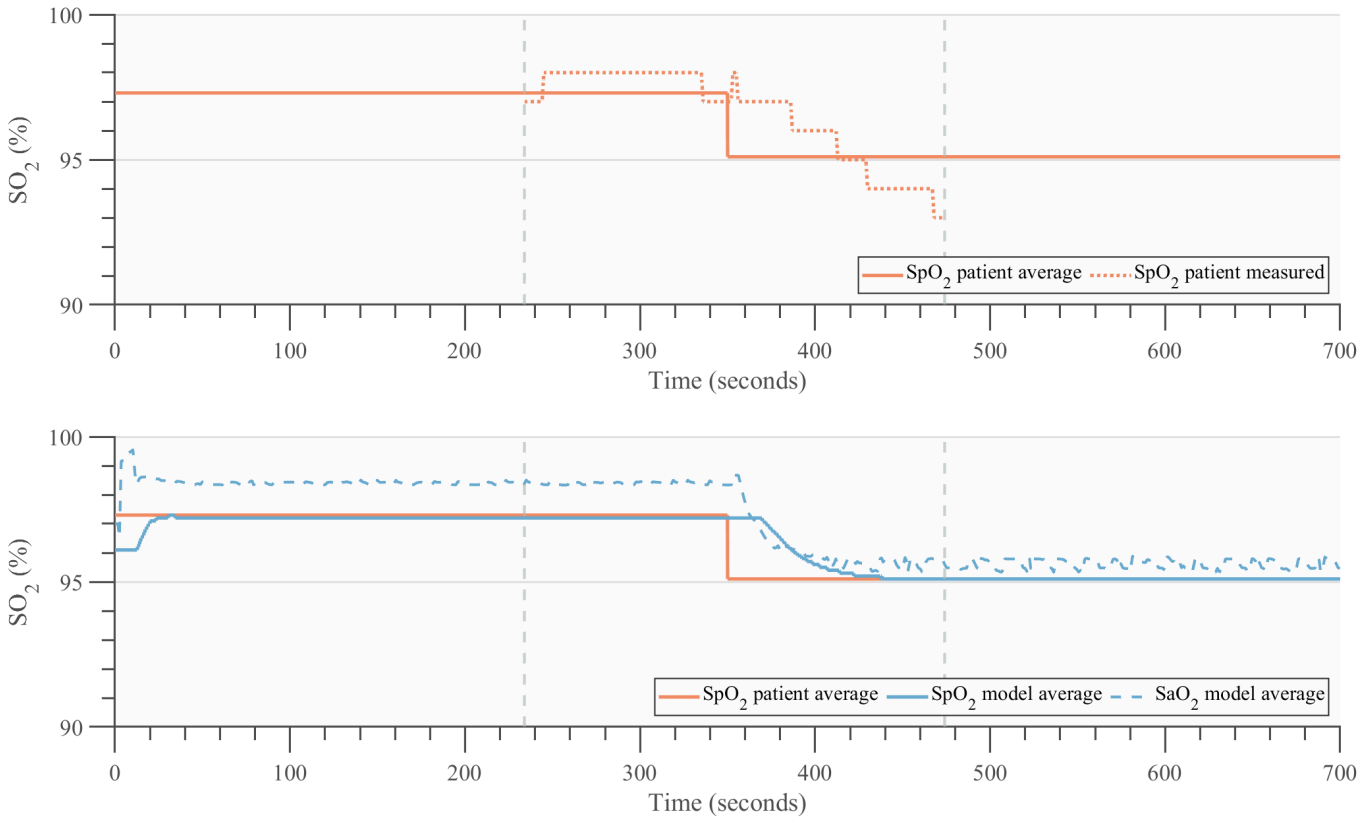

Figure C.9: True and modelled FiO_2-SpO_2 response of calibrated decreasing measurement 2 of patient 2. Measured and non-measured variable parameters are set for decreasing measurement 2 of patient 2. The FiO_2 changed at time = 350 seconds from 28% to 21%. The upper figure shows the continuous SpO_2 signal extracted from the measured patient data from patient 1. The measured SpO_2 signal was available from 120 seconds before to 120 seconds after the FiO_2 change (grey dashed lines). Based on the signal 20 seconds before and 60 to 80 seconds after the FiO_2 change, the average SpO_2 signal before and after the FiO_2 change was calculated. This average SpO_2 signal was modelled with the complete model. The lower figure shows the SaO_2 output of the MOTP, the SpO_2 output of the SpO_2 sensor system and the average SpO_2 signal of the patient. The sample rate of SaO_2 signal is decreased by a factor of 100 for reduction of the oscillations and clear visualisation.

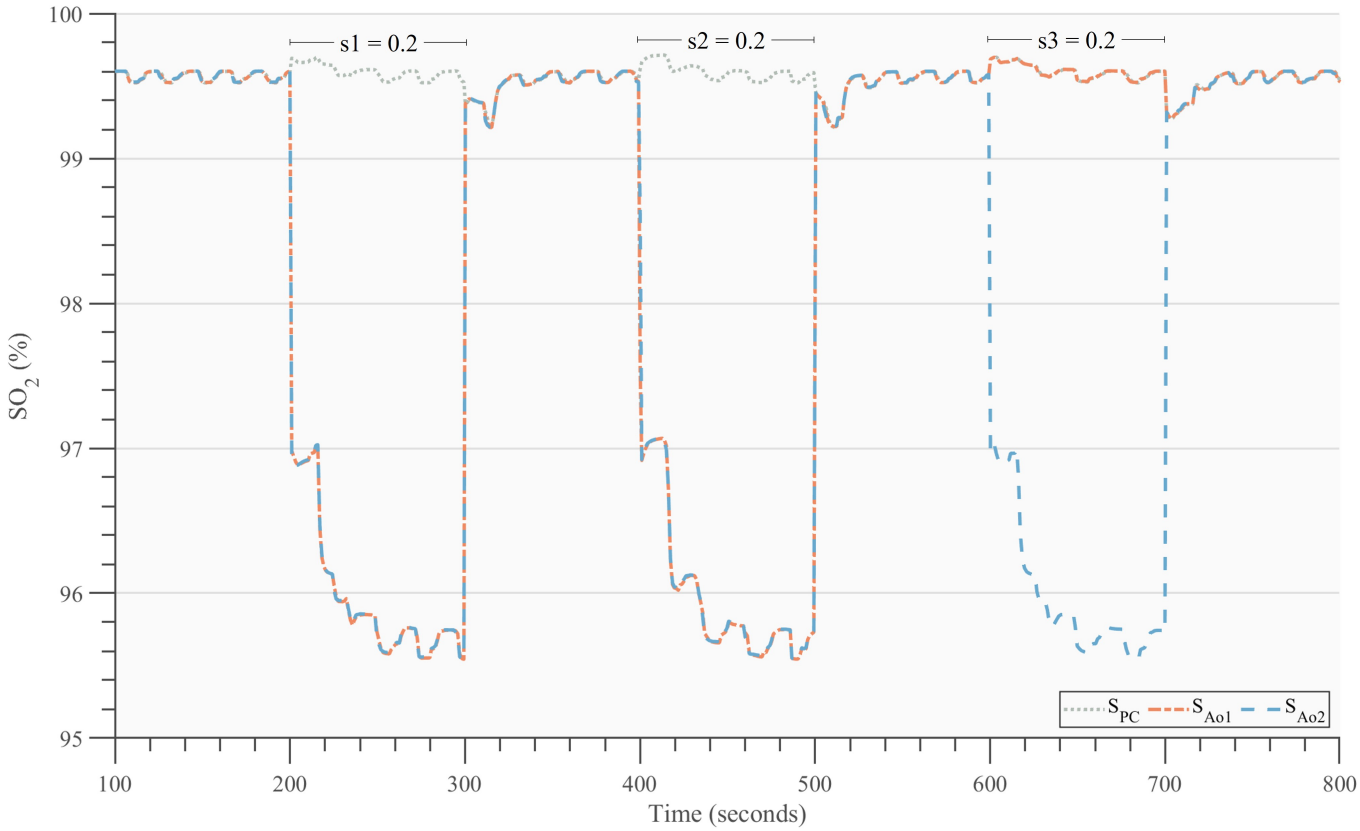

Figure C.10: Demonstration of the effect of $s1$, $s2$, and $s3$ on the oxygen saturations in the pulmonary capillaries, Ao1, and Ao2 (S_{PC}, S_{Ao1}, and S_{Ao2}). The values of $s1$, $s2$, and $s3$ were sequentially modified from 0 to 0.2 and subsequently reset to 0 after 100 seconds. In the absence of all shunts, S_{Ao1} and S_{Ao2} equal S_{PC}. $s1$ and $s2$ affect S_{Ao1} and S_{Ao2}. $s3$ affects S_{Ao2}. The first 100 seconds of the simulation were used for model stabilisation and are removed.

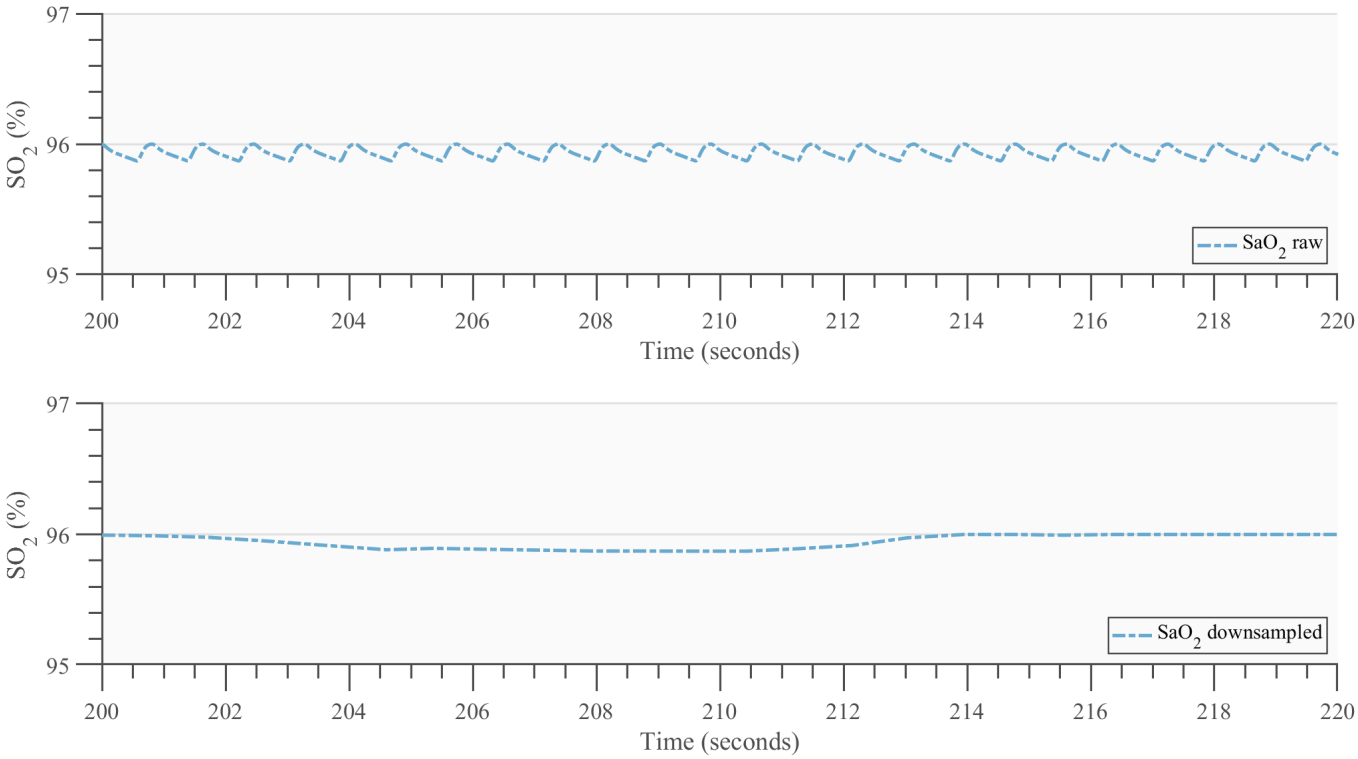

Figure C.11: The upper figure demonstrates the oscillations in the SaO_2 output signal of the MOTP. The frequency of the oscillations corresponds to the breathing frequency. The lower figure demonstrates the effect of downsampling the signal with a factor of 100. Downsampling was used to facilitate better visualisation of the SaO_2 output signal in the results section of this study.